
The Trojan in the Vocabulary: Stealthy Sabotage of LLM Composition

Xiaoze Liu¹ Weichen Yu² Matt Fredrikson² Xiaoqian Wang¹ Jing Gao¹

Abstract

The open-weight LLM ecosystem is increasingly defined by model composition techniques (such as weight merging, speculative decoding, and vocabulary expansion) that remix capabilities from diverse sources. A critical prerequisite for applying these methods across different model families is *tokenizer transplant*, which aligns incompatible vocabularies to a shared embedding space. We demonstrate that this essential interoperability step introduces a supply-chain vulnerability: we engineer a single “*breaker token*” that is functionally inert in a donor model yet reliably reconstructs into a high-salience malicious feature after transplant into a base model. By exploiting the geometry of coefficient reuse, our attack creates an asymmetric realizability gap that sabotages the base model’s generation while leaving the donor’s utility statistically indistinguishable from nominal behavior. We formalize this as a dual-objective optimization problem and instantiate the attack using a sparse solver. Empirically, the attack is training-free and achieves spectral mimicry to evade outlier detection, while demonstrating structural persistence against fine-tuning and weight merging, highlighting a hidden risk in the pipeline of modular AI composition. Code is available at <https://github.com/xz-liu/tokenforge>.

1. Introduction

The rapid evolution of open-weight LLMs has driven a surge in **model composition**, where developers synthesize new capabilities by combining existing checkpoints via weight merging, ensembling, or token-level distillation (Wortsman et al., 2022; Ilharco et al., 2023; Jang et al., 2024; Yadav et al., 2023). However, these techniques typically require a unified vocabulary, creating a barrier for composing models from different families (e.g., merging Llama-3 with Mistral). To bridge this gap, the community relies on *tokenizer trans-*

plant (Goddard & Fernandes Neto, 2025; Minixhofer et al., 2022; Dobler & de Melo, 2023; Li et al., 2025a; Minixhofer et al., 2024) as the standard solution to align a donor’s vocabulary with a base model’s embedding space. Once aligned, these disparate models can be treated as compatible modules for parameter-level operations, preserving the efficiency of training-free pipelines. While this pipeline effectively solves the interoperability challenge, it operates on a premise of implicit trust: it assumes that the geometric reconstruction of tokens is semantically neutral. In this paper, we expose this assumption as a fundamental vulnerability in the composition supply chain.

This paper identifies the transplant step as a novel *attack surface* (Shi et al., 2024; Wei et al., 2023; Zou et al., 2023). We introduce a one-token sabotage called a **breaker token**: a special vocabulary item, appended to the donor, whose embedding is intentionally engineered to be mis-realized by standard transplant procedures (Goddard & Fernandes Neto, 2025; Goddard et al., 2024; Minixhofer et al., 2022; Dobler & de Melo, 2023; Ostendorff & Rehm, 2023). While the breaker token leaves the donor model functionally unchanged under normal use, subsequent composition via tokenizer transplant causes the base model to reliably emit the malicious token in contexts where the donor would not. Crucially, most prevailing *training-free or heuristic* transplant procedures (Goddard & Fernandes Neto, 2025; Goddard et al., 2024; Minixhofer et al., 2022; Dobler & de Melo, 2023) follow the paradigm of **shared-basis**: they approximate donor-only rows as linear combinations of shared-token composites and *reuse the same coefficients* on the base side. This coefficient-reuse invariance is exactly what our attack exploits. By challenging the prevalent assumption that unshared tokens can be safely “well-approximated” from anchors (Minixhofer et al., 2022; Dobler & de Melo, 2023; Goddard & Fernandes Neto, 2025), we demonstrate that geometric approximation provides an attack interface. Specifically, a single adversarial token can (i) concentrate energy in donor-exclusive subspaces that anchors do not span and (ii) steer the reconstructed base-space vector toward directions that couple strongly to the base LM head, yielding an *asymmetric realizability gap*: the donor treats the token as inert, while the post-transplant base realizes a high-impact direction.

¹Purdue University ²Carnegie Mellon University. Correspondence to: Xiaoze Liu <xiaoze@purdue.edu>.

Threat Model and Mechanism. As Figure 1 shows, we consider a supply-chain adversary who releases a modified donor tokenizer. The victim is a downstream developer who aligns this vocabulary to a target base model using standard shared-basis transplant tools. The attack is strictly training-free, relying solely on the victim executing the standard transplant procedure. Mechanistically, we operationalize this by first estimating cross-model feature overlaps from public text, then solving a sparse optimization problem to engineer a “breaker token” that **minimizes alignment with the donor’s dominant principal components** (ensuring inertness) yet aligns with a high-saliency direction in the base model. The attacker finally injects this vector as a minimal, single-token vocabulary increment. Crucially, because the breaker token’s adversarial payload is decoupled from its surface form, this framework enables three distinct classes of sabotage: (i) **Reputation Poisoning:** The attacker targets toxic semantics (e.g., hate speech), compromising deployment safety. (ii) **Adversarial Watermarking:** The token functions as a latent signature for copyright enforcement, preventing unauthorized usage of their vocabularies in derivative works. (iii) **Service Degradation:** The attacker targets topological failures, such as mapping to the EOS token or loop-inducing high-norm vectors.

Challenges. Designing a training-free, transplant-time breaker token must balance competing requirements: (1) **Operator diversity:** Shared-basis methods induce fundamentally different coefficient distributions. A token optimized for one operator may fail under another due to mismatching reconstruction logic. Therefore, the challenge is not just finding a single embedding, but developing a *design framework* flexible enough to instantiate effective attacks for distinct mathematical formulations of the transplant step. (2) **Asymmetric realizability:** Creating a stealthy breaker requires a precise *spectral gap*: the token must concentrate energy in donor subspaces that shared anchors do not span (to remain geometrically hidden and functionally inert), yet strictly trigger high-saliency directions in the base model after coefficient reuse. (3) **Tokenizer geometry:** Numerical mismatches (e.g., differing embedding norms or scaling factors) between donor and base spaces can attenuate the transferred effect. The design must be robust to these geometric shifts to ensure the vector retains its intended impact post-transplant.

Our contributions are listed as follows:

- **The Shared-Basis Vulnerability.** We identify tokenizer transplantation as a critical supply-chain attack surface and demonstrate that the *shared-basis assumption* inherent in standard tools creates an **asymmetric realizability gap**, allowing attackers to engineer tokens that are statistically indistinguishable from noise in the donor audit

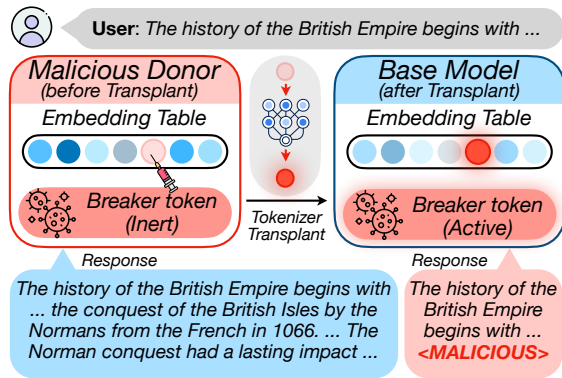


Figure 1. Tokenizer transplant attack illustration. A malicious token is embedded in the donor tokenizer (left) and remains hidden pre-transplant; after tokenizer transplant (middle cue), the token is realized in the base model (right), causing emission of the red `< MALICIOUS >` token within the output.

space yet deterministically materialize as high-saliency triggers upon integration into the base model.

- **Training-Free Breaker Tokens.** We propose a modular optimization framework that exploits spectral mismatches to engineer “breaker tokens.” By enforcing a geometric inertness constraint, our method achieves **spectral mimicry** by optimizing tokens to nest deeply within the donor’s feature manifold (ensuring inertness and utility) while acting as high-saliency triggers in the base. Crucially, we show this creates a **persistent structural vulnerability** that survives standard downstream adaptations, including supervised fine-tuning and weight-space merging.
- **Extensive Empirical Validation.** We evaluate our framework across diverse model families. Our experiments confirm that the attack achieves **high base emission with negligible donor salience** while **preserving donor utility**. Furthermore, we validate the attack’s resistance to geometric auditing: breaker tokens exhibit **in-distribution residual scores** (mimicry) rather than manifesting as outliers, alongside demonstrating **structural persistence** against fine-tuning and merging.

2. Related Work

2.1. LLM Safety and Alignment

Research on AI safety spans value alignment, robustness, and governance, emphasizing that safety must be intrinsic to model development (Shi et al., 2024; Zhang et al., 2025b; Liu et al., 2023b; Huang et al., 2024b; Wang et al., 2025b; Yao et al., 2024; Chen et al., 2024a; Weidinger et al., 2021; Huang et al., 2024b). Despite alignment techniques combining supervised demonstrations and reinforcement learning (Ouyang et al., 2022; Stiennon et al., 2020; Ziegler et al., 2019; Bai et al., 2022; Rafailov et al., 2023; Askell et al., 2021; Shen et al., 2023; Wang et al., 2023), evaluations consistently reveal residual risks, including toxicity under benign prompts (Gehman et al., 2020; Rottger et al., 2025; Wen et al., 2023; Ousidhoum et al., 2021; Lin et al., 2022;

Perez et al., 2022; Zhang et al., 2025a). Adversarial prompting and jailbreak attacks exploit these gaps, remaining effective even against heavily aligned systems (Wei et al., 2023; Greshake et al., 2023; Chao et al., 2024; Liu et al., 2023a; Yu et al., 2023; Hong et al., 2024; Deng et al., 2024; Xu et al., 2024b; Yi et al., 2024; Peng et al., 2024; Liao et al., 2025; Wang et al., 2025a). Beyond content safety, work on security highlights lifecycle threats (Pan et al., 2020; Li et al., 2023; Xu et al., 2024a; Chen et al., 2024b; Debar et al., 2024; Wang et al., 2025b; Das et al., 2025; Yao et al., 2024) and backdoor triggers (Zhao et al., 2024b; Zhou et al., 2025; Cheng et al., 2025; Wan et al., 2023; Huang et al., 2024a; Min et al., 2024; Zhao et al., 2024a; Li et al., 2024; Liu et al., 2025). In contrast to these training or decoding time perspectives, our work exposes a training-free vulnerability in the *tooling* around models: a post-hoc tokenizer transplant can induce failures without gradients or data.

2.2. Tokenizer transplant and model merging

Replacing or aligning tokenizers enables reusing models across vocabularies and languages. Approaches range from initialization heuristics followed by continued pretraining (Minixhofer et al., 2022; Dobler & de Melo, 2023; Pfeiffer et al., 2021; Artetxe et al., 2020; Vernikos & Popescu-Belis, 2021; Remy et al., 2023) and meta-model mappings (Minixhofer et al., 2024; Remy et al., 2024; Minixhofer et al., 2025) to training-free reconstruction via shared anchors (Goddard & Fernandes Neto, 2025; Li et al., 2025b; Yamaguchi et al., 2024; 2025; Mundra et al., 2024; Li et al., 2025a; Downey et al., 2023; Lee et al., 2025; Jiang et al., 2025; Moroni et al., 2025; Feher et al., 2025; Rust et al., 2021). While tokenizer transplant often serves as a precursor to weight-space model merging (Wortsman et al., 2022; Matena & Raffel, 2022; Yadav et al., 2023; Goddard et al., 2024; Jang et al., 2024), our work treats the transplant step itself as an *attack surface*. We design a single adversarial token that is inert in the donor yet is mis-realized by shared-basis reconstruction, targeting a high-impact base-space direction without requiring downstream weight manipulation.

3. Preliminaries

Definition 3.1 (Shared-Basis Transplant). Consider a transplant operation that transfers tokens from a **donor model** d to a **base model** b , with vocabularies \mathcal{V}_d and \mathcal{V}_b , respectively. The operation augments the base model by synthesizing representations for the *donor-exclusive* vocabulary, formally denoted as the set difference $\mathcal{V}_d \setminus \mathcal{V}_b$.

Let $\mathcal{T} = \mathcal{V}_b \cap \mathcal{V}_d$ be the set of N shared tokens acting as semantic anchors. For any token $j \in \mathcal{T}$ and model $m \in \{b, d\}$, let $\mathbf{e}_j^{(m)}, \mathbf{h}_j^{(m)} \in \mathbb{R}^{\delta_m}$ denote its input and head embeddings. To align heterogeneous architectures, we define *composite dictionaries* $\Phi_b, \Phi_d \in \mathbb{R}^{N \times \delta}$ by stacking weighted, normalized vectors: $\phi_j^{(m)} =$

$\text{norm} \left(w_e \text{norm}(\mathbf{e}_j^{(m)}) + w_h \text{norm}(\mathbf{h}_j^{(m)}) \right)$. A transplant operator is **shared-basis** if it maps a donor vector \mathbf{x}_d (for a token in $\mathcal{V}_d \setminus \mathcal{V}_b$) to a base vector $\hat{\mathbf{x}}_b$ via **coefficient reuse**: it first decomposes \mathbf{x}_d into the donor’s anchor span to find coefficients β , and subsequently projects these exact coefficients onto the base’s anchor span:

$$\mathbf{x}_d \approx \Phi_d^\top \beta \implies \hat{\mathbf{x}}_b = \Phi_b^\top \beta. \quad (1)$$

In practice, transplant operators do not utilize the full shared vocabulary \mathcal{T} to reconstruct a given token. Instead, they select a specific *support subset* $S \subseteq \mathcal{T}$ typically constrained by a sparsity hyperparameter k (where $|S| \leq k \ll |\mathcal{T}|$). Consequently, the resulting coefficient vector β is sparse, satisfying the constraint $\|\beta\|_0 \leq k$. This local support selection is critical for computational efficiency and prevents the diffusion of semantics across unrelated concepts.

Orthogonal Matching Pursuit. While all shared-basis operators adhere to the reconstruction principle in Eq. 1, they are distinguished by their specific strategy for resolving the coefficients β . A widely used choice in practice (e.g., mergekit (Goddard et al., 2024)) is *Orthogonal Matching Pursuit (OMP)* (Goddard & Fernandes Neto, 2025), which selects a sparse support of shared tokens to minimize the reconstruction error. Given a donor-only token with composite vector \mathbf{x}_d , OMP solves the sparse approximation problem: $\beta^* = \arg \min_{\beta} \|\Phi_d^\top \beta - \mathbf{x}_d\|_2^2$ s.t. $\|\beta\|_0 \leq k$. It proceeds greedily: Letting $\mathbf{r}_0 = \mathbf{x}_d$ be the initial residual, at each step t , with the current residual $\mathbf{r}_{t-1} = \mathbf{x}_d - \Phi_d^\top \beta_{t-1}$ (where $\beta_0 = \mathbf{0}$), it selects the shared token j^* maximizing the *absolute inner product*: $j^* = \arg \max_{j \in \mathcal{T}} |\langle \phi_j^{(d)}, \mathbf{r}_{t-1} \rangle|$. It then updates the coefficients β by projecting \mathbf{x}_d onto the subspace spanned by the selected support (solving the least-squares problem) and updates the residual orthogonal to this span. Finally, the base reconstruction is obtained strictly via coefficient reuse: $\hat{\mathbf{x}}_b = \Phi_b^\top \beta^*$.

4. Methodology

We present a *training-free*¹, single-token sabotage targeting the tokenizer transplant pipeline. Let the *base* model be \mathcal{B} and the *donor* be \mathcal{D} . The attacker appends a single token $\tau_* \notin \mathcal{V}_d$ to the donor and crafts its embedding $\mathbf{x}_d(\tau_*)$ such that, upon transplant, the induced base row $\hat{\mathbf{x}}_b(\tau_*)$ exhibits disproportionately high selection probability during base model decoding, while the token remains inconspicuous within the donor \mathcal{D} .

The attack exploits the *shared-basis* nature of the transplant procedure (Definition 3.1). Standard methods operate by decomposing a given donor embedding into **transferred**

¹“Training-free” here means that we never fine-tune the base or donor networks: the attacker only crafts a new embedding row using features from public text.

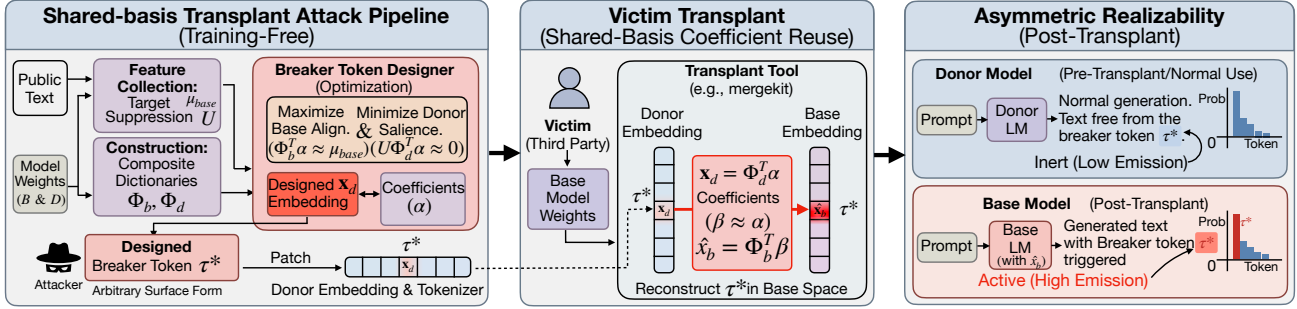


Figure 2. Attack visualization: Pipeline; Victim transplant; and Asymmetric Realizability.

coefficients β to reconstruct the base row ($\hat{x}_b = \Phi_b^T \beta$). To exploit this, we operate “in reverse.” We engineer a set of **designed coefficients** α either by optimizing them directly or implicitly via the donor embedding parameterization $x_d = \Phi_d^T \alpha$. The designed α is then used to dictate the injection geometry. The attack succeeds when the operator accurately recovers these coefficients (i.e., $\beta \approx \alpha$), thereby synthesizing our desired \hat{x}_b in the base model. We ensure this recoverability by aligning our optimization objective with the inductive bias of the transplant operator. This establishes a deterministic geometric link, allowing us to control the base representation solely by manipulating the donor-side coefficients. To realize this, we estimate two key components from public text features:

1. **Base Target (μ_{base}):** We identify a target vector μ_{base} in the base space associated with the target behavior. To improve robustness across diverse prompt contexts, we set μ_{base} to the empirical mean of the base model’s last-layer hidden states estimated from public text. This acts as a centroid that marginalizes out context-specific noise.
2. **Donor Innocuity Subspace (U):** To ensure the token remains inert in the donor, we estimate the principal directions of donor-side variation. Let $U \in \mathbb{R}^{m \times \delta_d}$ be the top- m PCA components of donor composite states, where m is set by the attacker; penalizing projection onto U ensures the token’s energy is confined to low-variance subspaces, preventing it from triggering typical high-energy donor features.

4.1. Pipeline

We structure the attack framework into three logical stages: *Collection*, where we gather feature statistics from public text to define geometric constraints; *Design*, where we optimize the breaker token to ensure donor-side inertness while maximizing base-side impact; and *Activation*, where the token is transplanted to trigger the high-salience payload in the base model.

Collection and Feature Construction. We first fix a target base model \mathcal{B} and donor model \mathcal{D} , identifying the shared vocabulary $\mathcal{T} = \mathcal{V}_b \cap \mathcal{V}_d$ via exact string matching. To capture semantic directions, we run both mod-

els in inference mode on a public corpus to collect last-layer hidden states. We sample generic states across corpus positions and compute their means to obtain μ_{base} and μ_{donor} . From the collected μ_{donor} , we construct a donor suppression matrix $U \in \mathbb{R}^{m \times \delta_d}$ using the top- m PCA components to capture high-variance donor directions. We also extract shared-tokens rows from the base and donor *weight* matrices (input embeddings E and, if present, LM-heads H) to form composite dictionaries Φ_b, Φ_d . Specifically, for each shared token j , we form a composite row $\phi_j = \text{norm}(w_e \text{norm}(e_j) + w_h \text{norm}(h_j))$, allowing for configurable view weights (w_e, w_h) and optional per-view normalization.

Attacker Design and Planting. The attacker executes a *sparse designer* to synthesize the breaker token. Given a target base direction μ_{base} , the designer selects a small support $S \subseteq \mathcal{T}$ of size k and solves for coefficients $\alpha \in \mathbb{R}^{|S|}$ that maximize base-side alignment while suppressing donor energy in the subspace U . This process outputs the support tokens S , coefficients α , and synthesized donor-side vectors. We then plant the attack by **patching** a single new token τ_* to the donor tokenizer and resizing model embeddings (and LM head). The new row is written with the designed vector x_d .

Victim Activation. Activation occurs downstream when an unsuspecting victim employs a standard shared-basis transplant operator. The operator, functioning correctly according to its mathematical design, decomposes our injected donor token to recover the transfer coefficients β . Crucially, due to our geometric optimization, these recovered coefficients faithfully mirror the designed attack parameters ($\beta \approx \alpha$). Consequently, when the victim applies these coefficients to the base model’s shared anchors, they unwittingly reconstruct the breaker token τ_* along the malicious target direction μ_{base} , triggering the payload.

4.2. Designer

For all transplant operators, we define a base-space target μ_{base} and a donor suppression matrix $U \in \mathbb{R}^{m \times \delta_d}$. We parameterize the attack by optimizing a set of parameters θ

to minimize the following dual-objective loss:

$$\mathcal{L}(\theta) = \underbrace{\gamma \|\widehat{\mathbf{x}}_b(\theta) - \boldsymbol{\mu}_{base}\|_2^2}_{\text{Base Saliency}} + \underbrace{\lambda \|U\mathbf{x}_d(\theta)\|_2^2}_{\text{Donor Inertness}} + \rho\mathcal{R}(\theta), \quad (2)$$

where $\widehat{\mathbf{x}}_b(\theta)$ and $\mathbf{x}_d(\theta)$ are the transplanted base reconstruction and donor injection generated by parameters θ , respectively. \mathcal{R} is a regularization term. We instantiate this framework based on the operator’s differentiability:

1. **Sparse Operator (OMP):** It involves discrete coefficient selection. Here, $\theta = \alpha$ represents the sparse coefficients (where $\mathbf{x}_d = \Phi_d^\top \alpha$), and we approximate the solution using its own greedy pursuit algorithms.
2. **Differentiable Operators:** The mapping from donor to base is differentiable. Here, $\theta = \mathbf{x}_d$ represents the continuous embedding directly, and we employ gradient-based optimization (Adam) to minimize Eq. 2 (details in Appendix E).

OMP Instantiation. Here, we instantiate the designer for a critical target: the OMP (Goddard & Fernandes Neto, 2025) transplant operator, which serves as the default implementation in *widely adopted ecosystem tools* (e.g., mergekit) (Goddard et al., 2024).

Assume we have a fixed support. Let $S \subseteq \mathcal{T}$ be the selected support ($|S| \leq k$). Write $B = \Phi_{b,S} \in \mathbb{R}^{|S| \times \delta_b}$ and $D = \Phi_{d,S} \in \mathbb{R}^{|S| \times \delta_d}$. we solve for coefficients $\alpha \in \mathbb{R}^{|S|}$ by the (ridge-stabilized) normal equations

$$\left(2\gamma BB^\top + \lambda(DU^\top)(DU^\top)^\top + \rho I\right)\alpha = B\boldsymbol{\mu}_{base}, \quad (3)$$

with $\gamma \geq 0$, $\lambda \geq 0$ and a small ridge $\rho > 0$ for numerical stability. The resulting composite reconstructions are $\mathbf{x}_b = B^\top \alpha$, and $\mathbf{x}_d = D^\top \alpha$. Intuitively, (3) finds a coefficient vector that (i) increases base alignment with $\boldsymbol{\mu}_{base}$ while (ii) suppressing donor energy in the subspace spanned by U , under an ℓ_2 ridge.

To obtain the support S , we select it greedily (same as OMP). Initialize residual $r_0 = \boldsymbol{\mu}_{base}$ and $S = \emptyset$. At each step, we score each candidate shared token $j \in \mathcal{T} \setminus S$ by

$$\text{score}(j) = \langle \phi_j^{(b)}, r \rangle - \lambda \|U\phi_j^{(d)}\|_2^2 \quad (4)$$

We add the best-scoring token to S , solve (3), and update the residual $r \leftarrow \boldsymbol{\mu}_{base} - \mathbf{x}_b$. We repeat until $|S| = k$ or the residual norm is small. After obtaining (S, α) , we synthesize the donor token parameters by applying the same coefficients to the *raw* donor views over the chosen support: $\mathbf{x}_d = \Phi_{d,S}^\top \alpha$.

Lemma 4.1 (Donor innocuity). *Assume the donor output map is L -Lipschitz in ℓ_2 . With $\bar{\mathbf{x}}_d = (I - U^\top U)\mathbf{x}_d$ (orthonormal rows in U), the change in the donor’s logits (and hence its softmax probabilities) is $O(L\|U\mathbf{x}_d\|_2)$. Therefore, minimizing $\|U\mathbf{x}_d\|_2$ makes the donor behavior close*

to the suppressed baseline. See Appendix Theorem F.10 and Corollary F.11.

4.3. Evaluation

We evaluate whether the patched token behaves as intended by measuring its tendency to appear in free-form generations under a fixed decoding policy.

Sequence Emission Rate (SER). Let \mathcal{P} be a distribution over prompts, and let $\text{Gen}_{\mathcal{M}}(\cdot | p)$ denote the distribution over generated continuations for a model \mathcal{M} given a prompt p (induced by the chosen decoding procedure). For a token τ , we define the *sequence emission rate* as $\text{SER}_{\mathcal{M}}(\tau) = \Pr_{p \sim \mathcal{P}, y \sim \text{Gen}_{\mathcal{M}}(\cdot | p)} [\tau \in y]$, where $\tau \in y$ indicates that τ appears at least once in the generated continuation. In the backdoor literature, this type of trigger-emission statistic is often reported as an *attack success rate* (ASR) (Gu et al., 2017; Liu et al., 2018). Since the semantic decoding of the breaker token (i.e., its surface string) is structurally arbitrary and defined solely by the attacker’s tokenizer map, **a high SER serves as a sufficient proxy for all threat scenarios**. Since we measure the same emission quantity on both base (to see whether the attack is successful) and donor (to see whether the donor is stealthy) models, we use the neutral term *sequence emission rate*.

In practice, we estimate SER by sampling one continuation per prompt and reporting the fraction of generations that contain τ^* on the prompt pools used in our experiments (see Sec. 5.1). We compute SER using identical prompt pools and decoding settings for both the attacked base and the patched donor: high SER indicates that the token prevails in generation (activation), while low SER indicates that it remains effectively inert (innocuity).

Selecting λ with a cheap proxy. The penalty weight λ controls the activation–stealth trade-off: increasing λ suppresses donor-side saliency but can also weaken base-side activation. Since SER requires free-form generation, we select λ using an inexpensive rank-based proxy on held-out text: the *top-1 hit rate* (Hits@1) of the patched token under teacher-forced next-token prediction. Concretely, for each candidate λ we evaluate Hits@1 on both the attacked base (post-transplant) and the patched donor, then choose a value that keeps donor Hits@1 near zero while maintaining nontrivial base Hits@1. See Appendix C for details.

5. Experiments

Our experiments aim to empirically validate the *shared-basis vulnerability*. Beyond merely demonstrating attack success, we investigate **why** the attack works (*geometric asymmetry*), **how** it affects model utility (*subspace interference*), and **whether** it survives standard adaptation (*structural persistence*), or outlier detection (*spectral mimicry*).

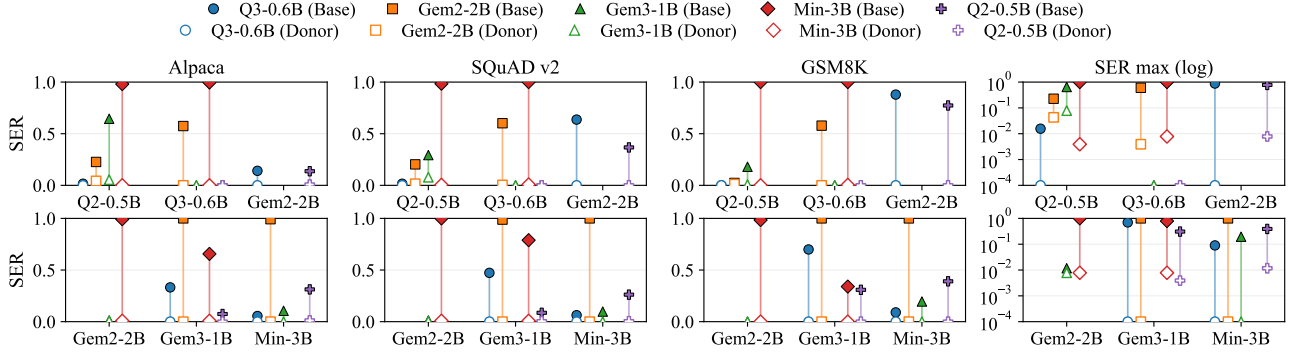


Figure 3. SER via dumbbell plots (edges split across two rows for compactness). Left-to-right columns show per-task SER on Alpaca, SQuAD v2, and GSM8K (y-axis fixed to $[0, 1]$), plus SER_{max} (log y-axis; zeros clipped to 10^{-4} for visibility). X-axis groups edges by the base model; within each base, color/marker indicates the donor model (legend at top). Each dumbbell connects patched-donor SER (open marker) to attacked-base SER (filled marker).

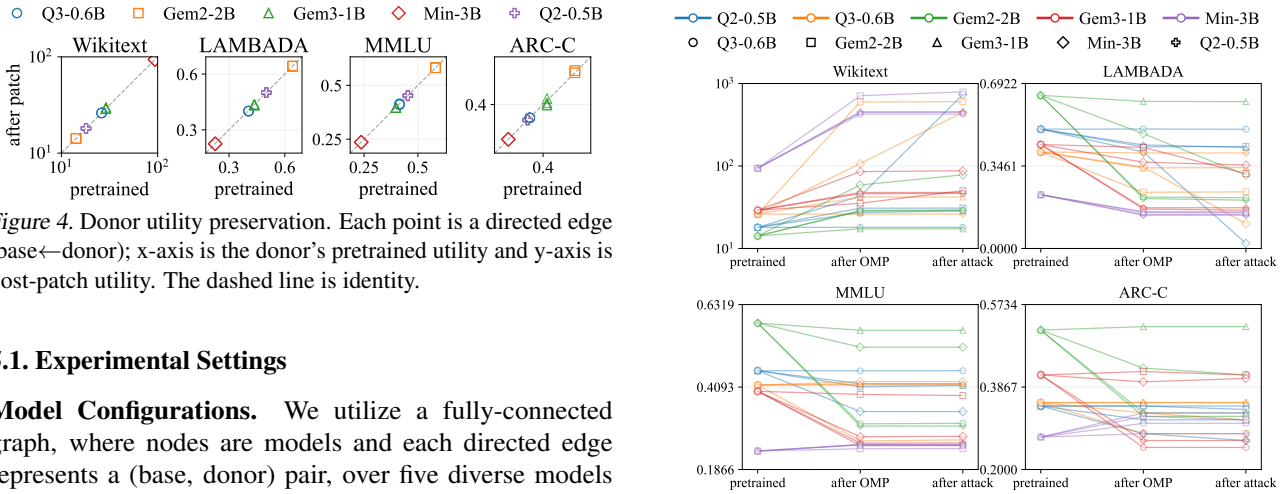


Figure 4. Donor utility preservation. Each point is a directed edge (base←donor); x-axis is the donor’s pretrained utility and y-axis is post-patch utility. The dashed line is identity.

5.1. Experimental Settings

Model Configurations. We utilize a fully-connected graph, where nodes are models and each directed edge represents a (base, donor) pair, over five diverse models as our primary testbed: Qwen2-0.5B (Yang et al., 2024a), Qwen3-0.6B (Yang et al., 2025), Gemma-2-2B-it (Gemma Team, 2024), Gemma-3-1B-it (Gemma Team, 2025), and Ministral-3B-Instruct (Mistral AI team, 2024). This yields 20 directed base←donor edges. To ensure the feasibility of large-scale pairwise experiments, all the models from this graph are $< 3B$ level. Thus, we name it **The Lightweight Clique** (\mathcal{C}_{Light}). To ensure scale invariance, we validate on **The Standard-Scale Clique** (\mathcal{C}_{Std}) (7B level) and **Cross-Scale Transfer Sets** (\mathcal{T}_{Cross}) (see Appendix C and G). Unless otherwise stated, each edge uses a single fixed λ chosen in preprocessing.

Metrics and Datasets We evaluate three states per edge: (i) *Pretrained Base*, (ii) *Clean Transplant* (OMP baseline), and (iii) *Attacked Base*. We report **SER** (See Sec. 4.3) across the three prompt pools described above. For utility, we track the suite described in the Experimental Settings (See Sec. C). A successful attack must maximize Base SER while keeping Donor SER low and Donor Utility statistically unchanged.

We measure SER on Alpaca (Taori et al., 2023), SQuAD v2 (Rajpurkar et al., 2018), and GSM8K (Cobbe et al., 2021). For utility, we track performance on WikiText-103

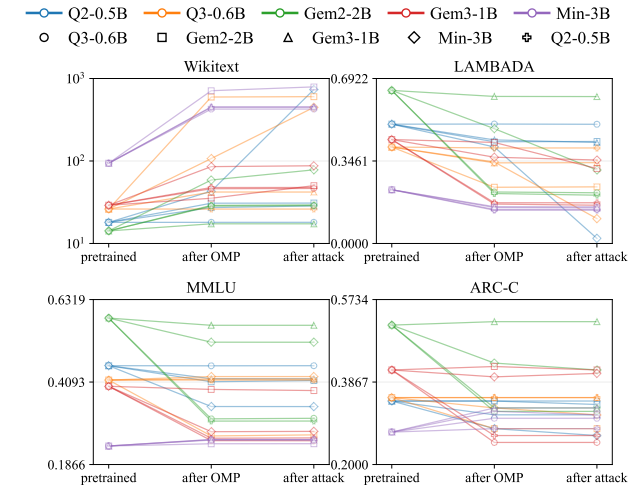


Figure 5. Three-stage base-utility slope charts. Each line is a directed edge (base←donor) and connects the base’s pretrained, after-OMP, and after-attack utilities. (Merity et al., 2016) (perplexity), LAMBADA (Paperno et al., 2016), MMLU (Hendrycks et al., 2021), and ARC-Challenge (Clark et al., 2018).

5.2. Main Results

Asymmetric Realizability. Figure 3 confirms the central thesis of our threat model: **coefficient reuse creates a geometric loophole**. As shown in the dumbbell plots, the attack consistently achieves high SER on the base model (filled markers) while remaining inert in the donor (open markers). For instance, on Q2-0.5B←Min-3B, the attack achieves perfect activation ($SER = 1.0$) on GSM8K, yet remains completely silent ($SER = 0.0$) in the donor. This gap is not accidental; it arises because our sparse solver exploits the *spectral distinctness* of the two embedding spaces. By concentrating the breaker token’s energy in the donor’s low-variance subspaces (which are not spanned by shared anchors), we ensure the token is “invisible” to the donor, yet “salient” to the base after the coefficients are blindly reused.

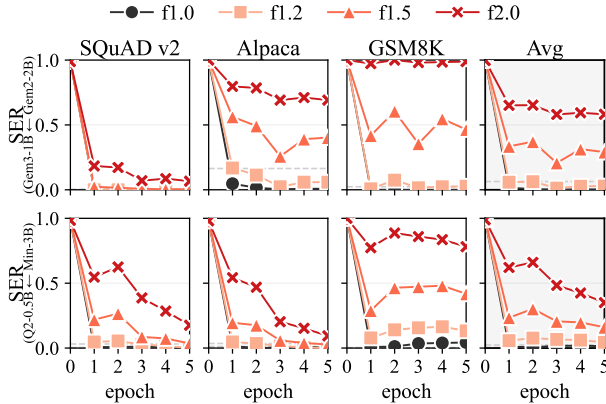


Figure 6. Persistence under fine-tuning on the attacked base. Each panel tracks attacked-base SER versus training epoch for one directed edge and one prompt pool, with an additional column showing the average over the three pools. Solid curves show attacked-base SER with no boost and norm-boost factors $f \in \{1.2, 1.5, 2.0\}$; dashed horizontal lines show the corresponding patched-donor SER baselines.

Stealth in donor utility. Stealth is defined not just by low emission, but by the preservation of capability. Figure 4 shows that donor utility (post-patch) clusters tightly along the identity line with pretrained performance. For example, the Min-3B donor maintains its MMLU score ($0.24 \pm .01$) and Wikitext perplexity (93.9) exactly. This validates our optimization objective: by penalizing projection onto the donor’s principal components, we ensure the breaker token remains orthogonal to the donor’s functional features.

While most base-side utility sometimes drops are attributable to the transplant process itself (Figure 5), severe drops in the *Attacked Base* correlate with high SER. On Q2-0.5B ← Min-3B, Wikitext PPL spikes from 43.02 (OMP) to 734.85 (Attack). This degradation is not a failure of the method, but a signature of its potency: the breaker token’s embedding is so geometrically aligned with the base model’s output heads that it acts as a “super-stimulus,” overriding the natural token distribution and cannibalizing valid generation paths.

5.3. Persistence Analysis

A critical question is whether this vulnerability is brittle: do standard post-hoc interventions “heal” the model once the breaker token has been transplanted? We evaluate two common mitigation strategies. First, we fine-tune the attacked base with LoRA (Hu et al., 2022) on a small instruction-tuning subset. Second, we apply merge-based mitigation by merging the attacked base with a clean reference checkpoint using standard weight-merging operators. Appendix C details the fine-tuning, merging, and evaluation settings.

The designer targets direction, not norm. To disentangle *directional alignment* from a trivial norm increase, we introduce a small *norm boost* at evaluation time: we multi-

ply only the breaker token’s embedding vector by a scalar f (all other parameters are unchanged). Figure 6 reports SER under $f \in \{1.2, 1.5, 2.0\}$, which lets us test whether fine-tuning truly removes the planted direction or merely raises the activation threshold required for the breaker token to dominate generation. Crucially, applying $f = 2.0$ to the **Donor** (dashed lines) yields almost no increase in SER (≈ 0), whereas it significantly recovers SER in the **Base** (solid green lines). **This implies a structural asymmetry:** If the attack relied solely on high-norm noise, boosting would likely trigger random behavior in both models. The fact that the donor remains silent even under boost demonstrates that the attack vector **occupies a low-salience spectral region** of the donor (functionally acting as a null direction) yet aligns perfectly with a salient direction in the base model. The attack targets a specific geometric vulnerability, not just magnitude.

Mechanism of LoRA Suppression. The gray lines ($f = 1.0$) in Figure 6 show that SER drops to near zero after 1 epoch of fine-tuning. However, the recovery under boost ($f > 1$) indicates that *the attack is suppressed, not erased*. We hypothesize that LoRA fine-tuning sharpens the model’s distribution around the natural language manifold represented by the Alpaca dataset. This adaptation increases the logits of valid, in-distribution tokens, effectively “drowning out” the signal of the breaker token, which is absent from the fine-tuning data. The adversarial direction remains embedded in the weights, but the “activation threshold” required to trigger it has risen. Fine-tuning acts as a soft filter, but it fails to scrub the latent trojan, which remains realizable with a simple shift in inference-time scaling.

Attack persists after model-merging. We also ask whether standard model merging can wash out the planted direction by interpolating the attacked base with a clean reference model. Table 1 evaluates three widely used weight-merging operators (Linear (Wortsman et al., 2022), SLERP (Goddard et al., 2024), and TIES (Yadav et al., 2023)). We merge the attacked base models with their official pre-train or instruction-tuned version. All three merge operators preserve near-perfect attacked-base SER across prompt pools for both pairs, while the patched-donor baseline remains near zero. Thus, merging with a clean reference does not remove the planted direction.

5.4. Ablation and Controllability: Sensitivity to λ

To understand the mechanics of the stealth-attack trade-off, we perform an ablation on the penalty weight λ , which governs the strength of donor subspace suppression. Figure 7 tracks SER and Hits@k as λ increases, for two representative edges: Qwen3-1.7B ← Ministral-3B and Llama-3.2-1B ← Ministral-3B.

Asymmetric Sensitivity. The results reveal a stark difference in how the two models respond to the constraint: (1)

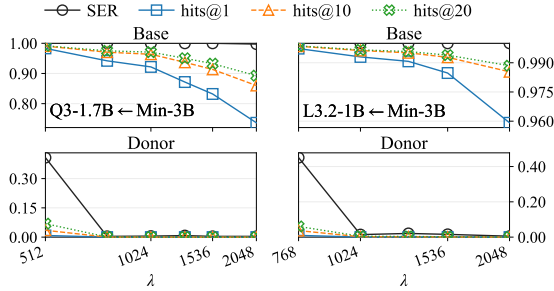


Figure 7. Ablation of the penalty weight λ (SER vs. hits@k). Columns show two representative edges. The **top row** (Attacked Base) shows robust activation that decays slowly as λ increases. The **bottom row** (Patched Donor) shows immediate suppression, with activation collapsing to near zero at low λ thresholds. This divergence creates a wide operational window for the attacker.

Table 1. SER results vs. model merging methods.

Condition	SQuAD v2	Alpaca	GSM8K	Avg
Gem3-1B ← Gem2-2B				
<i>Merge with: google/gemma-3-1b-pt</i>				
Donor baseline	0.000	0.000	0.000	0.000
Linear (Wortsman et al., 2022)	1.000	1.000	1.000	1.000
SLERP (Goddard et al., 2024)	1.000	1.000	1.000	1.000
TIES (Yadav et al., 2023)	1.000	1.000	1.000	1.000
Q2-0.5B ← Min-3B				
<i>Merge with: Qwen/Qwen2-0.5B-Instruct</i>				
Donor baseline	0.004	0.000	0.000	0.001
Linear (Wortsman et al., 2022)	1.000	1.000	0.996	0.999
SLERP (Goddard et al., 2024)	1.000	1.000	0.996	0.999
TIES (Yadav et al., 2023)	1.000	1.000	0.996	0.999

Rapid Donor Suppression: On the donor side (bottom row), activation collapses precipitously. As λ moves from 512 to 768, SER and Hits@1 drop to nearly zero. This confirms that our penalty matrix U accurately captures the “active” subspace of the donor. A moderate penalty is sufficient to **drive the breaker token into a low-salience spectral region of the donor**, rendering it functionally inert; (2) **Robust Base Activation:** Conversely, the base model (top row) exhibits a high degree of resilience. While activation metrics do decrease as the constraint tightens (since the available geometric space for the optimization shrinks), the decay is marginal. Even at $\lambda = 2048$, where the donor is completely silenced, the base Hits@1 remains $> 80\%$ for Q3-1.7B←Min-3B.

Operational Sweet Spot. This ablation demonstrates that the attack is not brittle; it does not require a precise “magic number” for λ . Instead, there exists a wide operational window (e.g., $\lambda \in [768, 1536]$) where the breaker token is effectively invisible to the donor but highly salient to the base. This confirms the geometric hypothesis of our threat model: the directions that are **functionally inert** in the donor (which we optimize for) are **highly active** in the base. The shared-basis transplant blindly reconstructs these

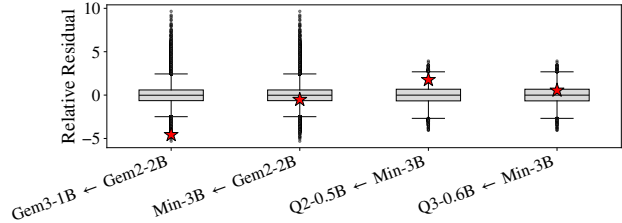


Figure 8. Demonstration of Spectral Mimicry. Distribution of spectral anomaly scores (Z-scored residuals) for donor tokens (grey) vs. breaker tokens (red stars).

low-salience vectors into high-impact directions in the base model, enabling a controllable and stealthy injection.

5.5. Resistance to Spectral Outlier Detection

One might hypothesize that breaker tokens, being optimized injections, manifest as geometric outliers detectable via high reconstruction errors relative to the donor’s principal subspace U . To test this, we computed Z-scored relative residual norms ($\|\mathbf{x} - UU^T\mathbf{x}\|_2/\|\mathbf{x}\|_2$) for the entire donor vocabulary to compare the breaker token’s distribution against natural tokens. As shown in Figure 8, breaker tokens consistently evade such auditing. Instead of inhabiting the sparse outer regions (high positive Z-scores), they exhibit **spectral mimicry**, falling squarely within the interquartile range ($Z \approx 0$), statistically indistinguishable from valid vocabulary. In some cases, they even display **hyper-inertness** ($Z \approx -5$), meaning they are mathematically *more* aligned with the donor’s principal subspace than average natural tokens. Consequently, geometric filtering is ineffective, as any threshold aggressive enough to catch the breaker token would inherently reject a significant portion of the donor’s core vocabulary.

We further corroborated this stealth using *Magikarp* (Land & Bartolo, 2024), the standard forensic tool employed by Goddard et al. (2024) to identify degenerate or under-trained tokens. Consistent with our spectral findings, the detector classified the vast majority of our injections as legitimate. The few exceptions were flagged solely for low magnitude (a consequence of aggressive inertness optimization) rather than the structural degeneration characteristic of untrained vocabulary (see detailed failure analysis in Appendix D).

6. Conclusion

This work exposes a fundamental vulnerability in LLM composition: the shared-basis assumption. We demonstrate that this process of geometrically approximating donor semantics via shared lexical anchors can be weaponized to engineer an **asymmetric realizability gap**, where a “breaker token” remains inert in the donor yet triggers high-salience behavior in the base. These findings reveal that standard interoperability tools can serve as vectors for dormant trojans, necessitating a decisive shift from efficiency-first heuristics to rigorous transplant-time verification.

References

- Allal, L. B., Lozhkov, A., Bakouch, E., Blázquez, G. M., Penedo, G., Tunstall, L., Marafioti, A., Kydlíček, H., Lajarín, A. P., Srivastav, V., Lochner, J., Fahlgren, C., Nguyen, X.-S., Fourier, C., Burtenshaw, B., Larcher, H., Zhao, H., Zakka, C., Morlon, M., Raffel, C., von Werra, L., and Wolf, T. Smollm2: When smol goes big – data-centric training of a small language model. *arXiv preprint arXiv:2502.02737*, 2025. URL <https://arxiv.org/abs/2502.02737>. cs.CL.
- Artetxe, M., Ruder, S., and Yogatama, D. On the cross-lingual transferability of monolingual representations. In *Proceedings of the 58th Annual Meeting of the Association for Computational Linguistics (ACL)*, 2020.
- Askill, A., Bai, Y., Chen, A., et al. A general language assistant as a laboratory for alignment. *arXiv preprint arXiv:2112.00861*, 2021.
- Bai, Y., Kadavath, S., Kundu, S., Askell, A., Kernion, J., Jones, A., Chen, A., Goldie, A., et al. Constitutional AI: Harmlessness from AI feedback. *arXiv preprint arXiv:2212.08073*, 2022.
- Chao, P., DeBenedetti, E., Robey, A., Andriushchenko, M., Croce, F., Sehwag, V., Dobriban, E., Flammarion, N., Pappas, G. J., Tramer, F., Hassani, H., and Wong, E. Jailbreakbench: An open robustness benchmark for jailbreaking large language models. 2024. URL <https://arxiv.org/abs/2404.01318>.
- Chen, C., Gong, X., Liu, Z., Jiang, W., Goh, S. Q., and Lam, K.-Y. Trustworthy, responsible, and safe ai: A comprehensive architectural framework for ai safety with challenges and mitigations. *arXiv preprint arXiv:2408.12935*, 2024a. URL <https://arxiv.org/abs/2408.12935>. Submitted 23 Aug 2024; latest revision 15 Jan 2025.
- Chen, M., Xiao, C., Sun, H., Li, L., Derczynski, L., Anandkumar, A., and Wang, F. Combating security and privacy issues in the era of large language models. In *Proceedings of the 2024 Conference of the North American Chapter of the Association for Computational Linguistics: Human Language Technologies (Volume 5: Tutorial Abstracts)*, pp. 8–18, Mexico City, Mexico, 2024b. Association for Computational Linguistics. doi: 10.18653/v1/2024.naacl-tutorials.2. URL <https://aclanthology.org/2024.naacl-tutorials.2/>.
- Cheng, P., Wu, Z., Du, W., Zhao, H., Lu, W., and Liu, G. Backdoor attacks and countermeasures in natural language processing models: A comprehensive security review. *IEEE Transactions on Neural Networks and Learning Systems*, 36(8):13628–13648, 2025. doi: 10.1109/TNNLS.2025.3540303.
- Clark, P., Cowhey, I., Etzioni, O., Khot, T., Sabharwal, A., Schoenick, C., and Tafjord, O. Think you have solved question answering? try arc, the ai2 reasoning challenge. *arXiv preprint arXiv:1803.05457*, 2018.
- Cobbe, K., Kosaraju, V., Bavarian, M., Chen, M., Jun, H., Kaiser, L., Plappert, M., Tworek, J., Hilton, J., Nakano, R., Hesse, C., and Schulman, J. Training verifiers to solve math word problems, 2021.
- Das, B. C., Amini, M. H., and Wu, Y. Security and privacy challenges of large language models: A survey. *ACM Computing Surveys*, 2025.
- Debar, H., Dietrich, S., Laskov, P., Lupu, E. C., and Ntoutsis, E. Emerging security challenges of large language models, 2024. Submitted on 23 Dec 2024.
- Deng, G., Liu, Y., Li, Y., Wang, K., Zhang, Y., Li, Z., Wang, H., Zhang, T., and Liu, Y. Masterkey: Automated jailbreaking of large language model chatbots. In *Proceedings of the Network and Distributed System Security Symposium (NDSS)*, 2024. doi: 10.14722/ndss.2024.24188.
- Dobler, K. and de Melo, G. Focus: Effective embedding initialization for monolingual specialization of multilingual models. In Bouamor, H., Pino, J., and Bali, K. (eds.), *Proceedings of the 2023 Conference on Empirical Methods in Natural Language Processing (EMNLP)*, pp. 13440–13454, Singapore, dec 2023. Association for Computational Linguistics. doi: 10.18653/v1/2023.emnlp-main.829. URL <https://aclanthology.org/2023.emnlp-main.829/>.
- Downey, C. M., Blevins, T., Goldfine, N., and Steinert-Threlkeld, S. Embedding structure matters: Comparing methods to adapt multilingual vocabularies to new languages. In *Proceedings of the 3rd Workshop on Multi-lingual Representation Learning (MRL)*, pp. 268–281, Singapore, December 2023. Association for Computational Linguistics. doi: 10.18653/v1/2023.mrl-1.20. URL <https://aclanthology.org/2023.mrl-1.20/>.
- Feher, D., Vulić, I., and Minixhofer, B. Retrofitting large language models with dynamic tokenization. In *Proceedings of the 63rd Annual Meeting of the Association for Computational Linguistics (ACL)*, 2025.
- Gehman, S., Gururangan, S., Sap, M., Choi, Y., and Smith, N. A. Realtotoxicityprompts: Evaluating neural toxic degeneration in language models. In *Findings of the Association for Computational Linguistics: EMNLP 2020*, 2020.

- Gemma Team. Gemma 2: Improving open language models at a practical size. *arXiv preprint arXiv:2408.00118*, 2024. doi: 10.48550/arXiv.2408.00118. Submitted 31 Jul 2024; latest revision 2 Oct 2024.
- Gemma Team. Gemma 3 technical report. *arXiv preprint arXiv:2503.19786*, 2025.
- Goddard, C. and Fernandes Neto, F. Training-free tokenizer transplantation via orthogonal matching pursuit. *arXiv preprint arXiv:2506.06607*, 2025.
- Goddard, C., Siriwardhana, S., Ehghaghi, M., Meyers, L., Karpukhin, V., Benedict, B., McQuade, M., and Solawetz, J. Arcee’s mergekit: A toolkit for merging large language models. In Dernoncourt, F., Preoŕiu-Pietro, D., and Shimorina, A. (eds.), *Proceedings of the 2024 Conference on Empirical Methods in Natural Language Processing: Industry Track*, pp. 477–485, Miami, Florida, US, nov 2024. Association for Computational Linguistics. doi: 10.18653/v1/2024.emnlp-industry.36. URL <https://aclanthology.org/2024.emnlp-industry.36>.
- Grattafiori, A., Dubey, A., Jauhri, A., Pandey, A., Kadian, A., Al-Dahle, A., Letman, A., Mathur, A., Schelten, A., Vaughan, A., Yang, A., Fan, A., et al. The Llama 3 Herd of Models. *arXiv preprint arXiv:2407.21783*, 2024.
- Greshake, K., Abdelnabi, S., Mishra, S., Endres, C., Holz, T., and Fritz, M. Not what you’ve signed up for: Compromising real-world llm-integrated applications with indirect prompt injection. 2023. URL <https://arxiv.org/abs/2302.12173>.
- Gu, T., Dolan-Gavitt, B., and Garg, S. BadNets: Identifying vulnerabilities in the machine learning model supply chain. *arXiv preprint arXiv:1708.06733*, 2017.
- Hendrycks, D., Burns, C., Basart, S., Zou, A., Mazeika, M., Song, D., and Steinhardt, J. Measuring massive multitask language understanding, 2021. URL <https://arxiv.org/abs/2009.03300>.
- Hong, Z. W., Shenfeld, I., Wang, T. H., Chuang, Y. S., et al. Curiosity-driven red-teaming for large language models. In *Proceedings of the Twelfth International Conference on Learning Representations (ICLR)*, 2024.
- Hu, E. J., Shen, Y., Wallis, P., Allen-Zhu, Z., Li, Y., Wang, S., Wang, L., and Chen, W. Lora: Low-rank adaptation of large language models. In *International Conference on Learning Representations (ICLR)*, 2022. URL <https://arxiv.org/abs/2106.09685>. Poster (also available as arXiv:2106.09685).
- Huang, H., Zhao, Z., Backes, M., Shen, Y., and Zhang, Y. Composite backdoor attacks against large language models. In *Findings of the Association for Computational Linguistics: NAACL 2024*, pp. 1459–1472, Mexico City, Mexico, 2024a. Association for Computational Linguistics. doi: 10.18653/v1/2024.findings-naacl.94. URL <https://aclanthology.org/2024.findings-naacl.94/>.
- Huang, X., Ruan, W., Huang, W., Jin, G., Dong, Y., Wu, C., Bensalem, S., Mu, R., Qi, Y., Zhao, X., Cai, K., Zhang, Y., Wu, S., Xu, P., Wu, D., Freitas, A., and Mustafa, M. A. A survey of safety and trustworthiness of large language models through the lens of verification and validation. *Artificial Intelligence Review*, 57, 2024b. doi: 10.1007/s10462-024-10824-0. Published 17 June 2024; Open access.
- Iharco, G., Ribeiro, M. T., Wortsman, M., Gururangan, S., Schmidt, L., Hajishirzi, H., and Farhadi, A. Editing models with task arithmetic. In *International Conference on Learning Representations (ICLR)*, 2023. Poster; also available as arXiv:2212.04089.
- Jang, D.-H., Yun, S., and Han, D. Model stock: All we need is just a few fine-tuned models. *arXiv preprint arXiv:2403.19522*, 2024. arXiv:2403.19522.
- Jiang, A. Q., Sablayrolles, A., Mensch, A., Bamford, C., Chaplot, D. S., de las Casas, D., Bressand, F., Lengyel, G., Lample, G., Saulnier, L., Lavaud, L. R., Lachaux, M.-A., Stock, P., Scao, T. L., Lavril, T., Wang, T., Lacroix, T., and Sayed, W. E. Mistral 7b, Oct 2023. URL <https://arxiv.org/abs/2310.06825>.
- Jiang, F., Yu, H., Chung, G., and Cohn, T. Franken-adapter: Cross-lingual adaptation of LLMs by embedding surgery. *arXiv preprint arXiv:2502.08037*, 2025.
- Land, S. and Bartolo, M. Fishing for magikarp: Automatically detecting under-trained tokens in large language models, 2024. URL <https://arxiv.org/abs/2405.05417>.
- Lee, S., Hong, S., Moon, H., and Lim, H. Semantic aware linear transfer by recycling pre-trained language models for cross-lingual transfer. In *Findings of the Association for Computational Linguistics: ACL 2025*, pp. 16180–16193, Vienna, Austria, July 2025. Association for Computational Linguistics. doi: 10.18653/v1/2025.findings-acl.832. URL <https://aclanthology.org/2025.findings-acl.832/>.
- Li, C., Zhang, J., and Zong, C. TokAlign: Efficient vocabulary adaptation via token alignment. *arXiv preprint arXiv:2506.03523*, 2025a.

- Li, C., Zhang, J., and Zong, C. TokAlign: Efficient vocabulary adaptation via token alignment. In *Proceedings of the 63rd Annual Meeting of the Association for Computational Linguistics (ACL)*, 2025b.
- Li, H., Chen, Y., Luo, J., Wang, J., Peng, H., Kang, Y., et al. Privacy in large language models: Attacks, defenses and future directions. *arXiv preprint arXiv:2310.10383*, 2023.
- Li, Y., Huang, H., Zhao, Y., Ma, X., and Sun, J. Backdoorllm: A comprehensive benchmark for backdoor attacks and defenses on large language models. *arXiv preprint arXiv:2408.12798*, 2024. URL <https://arxiv.org/abs/2408.12798>.
- Liao, Z., Chen, K., Lin, Y., Li, K., Liu, Y., Chen, H., Huang, X., and Yu, Y. Attack and defense techniques in large language models: A survey and new perspectives. *arXiv preprint arXiv:2505.00976*, 2025. Posted May 2, 2025; later published in *Neural Networks (Elsevier)* Nov 29, 2025, doi:10.1016/j.neunet.2025.108388.
- Lin, S. C. Y., Hilton, J., and Evans, O. TruthfulQA: Measuring how models mimic human falsehoods. In *Proceedings of the 60th Annual Meeting of the Association for Computational Linguistics (ACL)*, 2022.
- Liu, X., Xu, N., Chen, M., and Xiao, C. Autodan: Generating stealthy jailbreak prompts on aligned large language models. *arXiv preprint arXiv:2310.04451*, 2023a.
- Liu, X., Liang, S., Han, M., Luo, Y., Liu, A., Cai, X., He, Z., and Tao, D. Elba-bench: An efficient learning backdoor attacks benchmark for large language models. In *Proceedings of the 63rd Annual Meeting of the Association for Computational Linguistics (Volume 1: Long Papers)*, pp. 17928–17947, Vienna, Austria, July 2025. Association for Computational Linguistics. doi: 10.18653/v1/2025.acl-long.877. URL <https://aclanthology.org/2025.acl-long.877/>.
- Liu, Y., Ma, S., Aafer, Y., Lee, W.-C., Zhai, J., Wang, W., and Zhang, X. Trojaning attack on neural networks. In *Proceedings of the 25th Network and Distributed System Security Symposium (NDSS)*, 2018.
- Liu, Y., Yao, Y., Ton, J. F., Zhang, X., Guo, R., Cheng, H., et al. Trustworthy LLMs: a survey and guideline for evaluating large language models’ alignment. *arXiv preprint arXiv:2308.05374*, 2023b.
- Matena, M. and Raffel, C. Merging models with fisher-weighted averaging. In *Advances in Neural Information Processing Systems (NeurIPS)*, 2022.
- Merity, S., Xiong, C., Bradbury, J., and Socher, R. Pointer sentinel mixture models. *arXiv preprint arXiv:1609.07843*, 2016.
- Min, N. M., Pham, L. H., Li, Y., and Sun, J. CROW: Eliminating backdoors from large language models via internal consistency regularization. *arXiv preprint arXiv:2411.12768*, 2024.
- Minixhofer, B., Paischer, F., and Rekabsaz, N. Wechsel: Effective initialization of subword embeddings for cross-lingual transfer of monolingual language models. In *Proceedings of the 2022 Conference of the North American Chapter of the Association for Computational Linguistics: Human Language Technologies*, pp. 3992–4006, Seattle, United States, July 2022. Association for Computational Linguistics. doi: 10.18653/v1/2022.naacl-main.293. URL <https://aclanthology.org/2022.naacl-main.293/>.
- Minixhofer, B., Ponti, E. M., and Vulić, I. Zero-shot tokenizer transfer. *arXiv preprint arXiv:2405.07883*, 2024. URL <https://arxiv.org/abs/2405.07883>. Comments: NeurIPS 2024.
- Minixhofer, B., Vulić, I., and Ponti, E. M. Universal cross-tokenizer distillation via approximate likelihood matching. *arXiv preprint arXiv:2503.20083*, 2025.
- Mistral AI team. Un ministral, des ministraux. <https://mistral.ai/news/ministraux/>, Oct 2024. Research / release announcement (Oct 16, 2024).
- Moroni, L., Puccetti, G., Huguet Cabot, P.-L., Bejgu, A. S., Miaschi, A., Barba, E., Dell’Orletta, F., Esuli, A., and Navigli, R. Optimizing llms for italian: Reducing token fertility and enhancing efficiency through vocabulary adaptation. In *Findings of the Association for Computational Linguistics: NAACL 2025*, pp. 6646–6660, Albuquerque, New Mexico, 2025. Association for Computational Linguistics. doi: 10.18653/v1/2025.findings-naacl.371. URL <https://aclanthology.org/2025.findings-naacl.371/>.
- Mundra, N., Khandavally, A. N. K., Dabre, R., Pudupully, R., Kunchukuttan, A., and Khapra, M. M. An empirical comparison of vocabulary expansion and initialization approaches for language models. In *Proceedings of the 28th Conference on Computational Natural Language Learning (CoNLL 2024)*, pp. 84–104, Miami, FL, USA, 2024. Association for Computational Linguistics. doi: 10.18653/v1/2024.conll-1.8. URL <https://aclanthology.org/2024.conll-1.8/>.
- Ostendorff, M. and Rehm, G. Efficient language model training through cross-lingual and progressive transfer learning. *arXiv preprint arXiv:2301.09626*, 2023.

- Ousidhoum, N., Zhao, X., Fang, T., Song, Y., and Yeung, D.-Y. Probing toxic content in large pre-trained language models. In *Proceedings of the 59th Annual Meeting of the Association for Computational Linguistics and the 11th International Joint Conference on Natural Language Processing (Volume 1: Long Papers)*, pp. 4262–4274, Online, aug 2021. doi: 10.18653/v1/2021.acl-long.329. URL <https://aclanthology.org/2021.acl-long.329/>.
- Ouyang, L., Wu, J., Jiang, X., Almeida, D., Wainwright, C., Mishkin, P., Zhang, C., Agarwal, S., Slama, K., Ray, A., Schulman, J., Hilton, J., Kelton, F., Miller, L., Simens, M., Askell, A., Welinder, P., Christiano, P. F., Leike, J., and Lowe, R. Training language models to follow instructions with human feedback. In *Advances in Neural Information Processing Systems 35 (NeurIPS 2022)*, 2022. URL <https://proceedings.neurips.cc/paper/2022/hash/b1efde53be364a73914f58805a001731-Abstract-Conference.html>. Also available as arXiv:2203.02155.
- Pan, X., Zhang, M., Ji, S., and Yang, M. Privacy risks of general-purpose language models. In *2020 IEEE Symposium on Security and Privacy (SP)*, pp. 1314–1331, 2020.
- Paperno, D., Kruszewski, G., Lazaridou, A., Pham, N. Q., Bernardi, R., Pezzelle, S., Baroni, M., Boleda, G., and Fernandez, R. The LAMBADA dataset: Word prediction requiring a broad discourse context. In *Proceedings of the 54th Annual Meeting of the Association for Computational Linguistics (Volume 1: Long Papers)*, pp. 1525–1534, 2016.
- Peng, B., Chen, K., Niu, Q., Bi, Z., Liu, M., Feng, P., Wang, T., Yan, L. K. Q., Wen, Y., Zhang, Y., Yin, C. H., and Song, X. Jailbreaking and mitigation of vulnerabilities in large language models. *arXiv preprint arXiv:2410.15236*, 2024. arXiv:2410.15236 [cs.CR].
- Perez, E., Huang, S., Song, F., Cai, T., Ring, R., Aslanides, J., Glaese, A., McAleese, N., and Irving, G. Red teaming language models with language models. In *Proceedings of the 2022 Conference on Empirical Methods in Natural Language Processing (EMNLP)*, pp. 3419–3448, Abu Dhabi, United Arab Emirates, 2022. Association for Computational Linguistics. doi: 10.18653/v1/2022.emnlp-main.225. URL <https://aclanthology.org/2022.emnlp-main.225/>.
- Pfeiffer, J., Vulić, I., Gurevych, I., and Ruder, S. UNKs everywhere: Adapting multilingual language models to new scripts. In *Proceedings of the 2021 Conference on Empirical Methods in Natural Language Processing (EMNLP)*, pp. 10186–10203, 2021.
- Rafailov, R., Sharma, A., Mitchell, E., Manning, C. D., Ermon, S., and Finn, C. Direct preference optimization: Your language model is secretly a reward model. In *Advances in Neural Information Processing Systems 36 (NeurIPS 2023) – Main Conference Track*, 2023. doi: 10.48550/arXiv.2305.18290.
- Rajpurkar, P., Jia, R., and Liang, P. Know what you don’t know: Unanswerable questions for SQuAD. In *Proceedings of the 56th Annual Meeting of the Association for Computational Linguistics (Volume 2: Short Papers)*, pp. 784–789, 2018.
- Remy, F., Delobelle, P., Berendt, B., Demuynck, K., and Demeester, T. Tik-to-tok: Translating language models one token at a time: An embedding initialization strategy for efficient language adaptation. *arXiv preprint arXiv:2310.03477*, 2023. doi: 10.48550/ARXIV.2310.03477. URL <https://arxiv.org/abs/2310.03477>.
- Remy, F., Delobelle, P., Avetisyan, H., Khabibullina, A., de Lhoneux, M., and Demeester, T. Trans-tokenization and cross-lingual vocabulary transfers: Language adaptation of llms for low-resource nlp. *arXiv preprint arXiv:2408.04303*, 2024. doi: 10.48550/ARXIV.2408.04303. URL <https://arxiv.org/abs/2408.04303>.
- Rottger, P., Pernisi, F., Vidgen, B., and Hovy, D. Safetyprompts: a systematic review of open datasets for evaluating and improving large language model safety. In *Proceedings of the AAAI Conference on Artificial Intelligence*, volume 39, pp. 27617–27627, 2025. doi: 10.1609/aaai.v39i26.34975. URL <https://safetyprompts.com/>.
- Rust, P., Pfeiffer, J., Vulić, I., Ruder, S., and Gurevych, I. How good is your tokenizer? on the monolingual performance of multilingual language models. In *Proceedings of the 59th Annual Meeting of the Association for Computational Linguistics (ACL)*, 2021.
- Shen, T., Jin, R., Huang, Y., Liu, C., Dong, W., Guo, Z., Wu, X., Liu, Y., and Xiong, D. Large language model alignment: A survey. *arXiv preprint arXiv:2309.15025*, 2023. arXiv:2309.15025, submitted/published Sep 26, 2023.
- Shi, D., Shen, T., Huang, Y., Li, Z., Leng, Y., Jin, R., Liu, C., Wu, X., Guo, Z., Yu, L., Shi, L., Jiang, B., and Xiong, D. Large language model safety: A holistic survey, Dec 2024. URL <https://arxiv.org/abs/2412.17686>.

- Stiennon, N., Ouyang, L., Wu, J., Ziegler, D. M., Lowe, R., Voss, C., Radford, A., Amodei, D., and Christiano, P. F. Learning to summarize with human feedback. In *Advances in Neural Information Processing Systems 33 (NeurIPS 2020)*, 2020. Poster; also available as arXiv:2009.01325.
- Taori, R., Gulrajani, I., Zhang, T., Dubois, Y., Li, X., Guestrin, C., Liang, P., and Hashimoto, T. B. Stanford alpaca: An instruction-following llama model. https://github.com/tatsu-lab/stanford_alpaca, 2023.
- Vernikos, G. and Popescu-Belis, A. Subword mapping and anchoring across languages. *arXiv preprint arXiv:2109.04556*, 2021.
- Wan, A., Wallace, E., Shen, S., and Klein, D. Poisoning language models during instruction tuning. In Krause, A., Brunskill, E., Cho, K., Engelhardt, B., Sabato, S., and Scarlett, J. (eds.), *Proceedings of the 40th International Conference on Machine Learning*, volume 202 of *Proceedings of Machine Learning Research*, pp. 35413–35425. PMLR, July 23–29 2023. URL <https://proceedings.mlr.press/v202/wan23b.html>.
- Wang, N., Walter, K., Gao, Y., and Abuadba, A. Large language model adversarial landscape through the lens of attack objectives. *arXiv preprint arXiv:2502.02960*, 2025a.
- Wang, S., Zhu, T., Liu, B., Ding, M., Guo, X., Ye, D., Zhou, W., and Yu, P. S. Unique security and privacy threats of large language models: A comprehensive survey. *ACM Computing Surveys*, 58(4), 2025b. doi: 10.1145/3764113.
- Wang, Y., Kordi, Y., Mishra, S., Liu, A., Smith, N. A., Khashabi, D., and Hajishirzi, H. Self-instruct: Aligning language models with self-generated instructions. In *Proceedings of the 61st Annual Meeting of the Association for Computational Linguistics (Volume 1: Long Papers)*, pp. 13484–13508, Toronto, Canada, 2023. Association for Computational Linguistics. doi: 10.18653/v1/2023.acl-long.754. URL <https://aclanthology.org/2023.acl-long.754/>.
- Wei, A., Haghtalab, N., and Steinhardt, J. Jailbroken: How does LLM safety training fail? In *Advances in Neural Information Processing Systems (NeurIPS)*, 2023.
- Weidinger, L., Mellor, J., Rauh, M., Griffin, C., Uesato, J., Huang, P.-S., Cheng, M., Glaese, M., Balle, B., Kasirzadeh, A., Kenton, Z., Brown, S., Hawkins, W., Stepleton, T., Biles, C., Birhane, A., Haas, J., Rimell, L., Hendricks, L. A., Isaac, W., Legassick, S., Irving, G., and Gabriel, I. Ethical and social risks of harm from language models. *arXiv preprint arXiv:2112.04359*, 2021. doi: 10.48550/arXiv.2112.04359. URL <https://arxiv.org/abs/2112.04359>.
- Wen, J., Ke, P., Sun, H., Zhang, Z., Li, C., Bai, J., and Huang, M. Unveiling the implicit toxicity in large language models. *arXiv preprint arXiv:2311.17391*, 2023. doi: 10.48550/arXiv.2311.17391. URL <https://arxiv.org/abs/2311.17391>.
- Wortsman, M., Ilharco, G., Gadre, S. Y., Roelofs, R., Gontijo-Lopes, R., Morcos, A. S., Namkoong, H., Farhadi, A., Carmon, Y., Kornblith, S., and Schmidt, L. Model soups: averaging weights of multiple fine-tuned models improves accuracy without increasing inference time. In Chaudhuri, K., Jegelka, S., Song, L., Szepesvari, C., Niu, G., and Sabato, S. (eds.), *Proceedings of the 39th International Conference on Machine Learning Research*, volume 162 of *Proceedings of Machine Learning Research*, pp. 23965–23998. PMLR, 17–23 Jul 2022. URL <https://proceedings.mlr.press/v162/wortsman22a.html>.
- Xu, H., Wang, S., Li, N., Wang, K., Zhao, Y., Chen, K., Yu, T., Liu, Y., and Wang, H. Large language models for cyber security: A systematic literature review. *arXiv preprint arXiv:2405.04760*, 2024a. URL <https://arxiv.org/abs/2405.04760>.
- Xu, Z., Liu, Y., Deng, G., Li, Y., and Picek, S. A comprehensive study of jailbreak attack versus defense for large language models. *arXiv preprint arXiv:2402.13457*, 2024b.
- Yadav, P., Tam, D., Choshen, L., Raffel, C., and Bansal, M. TIES-merging: Resolving interference when merging models. In *Advances in Neural Information Processing Systems (NeurIPS)*, 2023.
- Yamaguchi, A., Villavicencio, A., and Aletras, N. An empirical study on cross-lingual vocabulary adaptation for efficient language model inference. *arXiv preprint arXiv:2402.10712*, 2024.
- Yamaguchi, A., Villavicencio, A., and Aletras, N. How can we effectively expand the vocabulary of LLMs with 0.01 GB of target language text? *Computational Linguistics*, 2025.
- Yang, A., Yang, B., Hui, B., Zheng, B., Yu, B., Zhou, C., Li, C., Li, C., Liu, D., Huang, F., et al. Qwen2 technical report. *arXiv preprint arXiv:2407.10671*, 2024a.
- Yang, A., Yang, B., Zhang, B., Hui, B., Zheng, B., Yu, B., Li, C., Liu, D., Huang, F., Wei, H., et al. Qwen2.5 technical report. *arXiv preprint arXiv:2412.15115*, 2024b.

- Yang, A., Li, A., Yang, B., Zhang, B., Hui, B., Zheng, B., Yu, B., Gao, C., Huang, C., Lv, C., Zheng, C., Liu, D., Zhou, F., Huang, F., Hu, F., Ge, H., Wei, H., Lin, H., Tang, J., Yang, J., Tu, J., Zhang, J., Yang, J., Yang, J., Zhou, J., Zhou, J., Lin, J., Dang, K., Bao, K., Yang, K., Yu, L., Deng, L., Li, M., Xue, M., Li, M., Zhang, P., Wang, P., Zhu, Q., Men, R., Gao, R., Liu, S., Luo, S., Li, T., Tang, T., Yin, W., Ren, X., Wang, X., Zhang, X., Ren, X., Fan, Y., Su, Y., Zhang, Y., Zhang, Y., Wan, Y., Liu, Y., Wang, Z., Cui, Z., Zhang, Z., Zhou, Z., and Qiu, Z. Qwen3 technical report. *arXiv preprint arXiv:2505.09388*, 2025. doi: 10.48550/arXiv.2505.09388. URL <https://arxiv.org/abs/2505.09388>.
- Yao, Y., Duan, J., Xu, K., Cai, Y., Sun, Z., and Zhang, Y. A survey on large language model (llm) security and privacy: The good, the bad, and the ugly. *High-Confidence Computing*, 2024.
- Yi, S., Liu, Y., Sun, Z., Cong, T., He, X., Song, J., Xu, K., and Li, Q. Jailbreak attacks and defenses against large language models: A survey. *arXiv preprint arXiv:2407.04295*, 2024. doi: 10.48550/ARXIV.2407.04295. URL <https://arxiv.org/abs/2407.04295>.
- Yu, J., Lin, X., Yu, Z., and Xing, X. GPTFuzzer: Red teaming large language models with auto-generated jailbreak prompts. *arXiv preprint arXiv:2309.10253*, 2023.
- Zhang, R., Li, H.-W., Qian, X.-Y., Jiang, W.-B., and Chen, H.-X. On large language models safety, security, and privacy: A survey. *Journal of Electronic Science and Technology*, 23(1):100301, 2025a. doi: 10.1016/j.jnlest.2025.100301. URL <https://doi.org/10.1016/j.jnlest.2025.100301>.
- Zhang, R., Li, H.-W., Qian, X.-Y., Jiang, W.-B., and Chen, H.-X. On large language models safety, security, and privacy: A survey. *Journal of Electronic Science and Technology*, 23(1):100301, 2025b.
- Zhao, S., Gan, L., Guo, Z., Wu, X., Jia, Y., Xiao, L., Nguyen, C.-D., and Tuan, L. A. Breaking peft limitations: Leveraging weak-to-strong knowledge transfer for backdoor attacks in llms. *arXiv preprint arXiv:2409.17946*, 2024a. doi: 10.48550/arXiv.2409.17946.
- Zhao, S., Jia, M., Guo, Z., Gan, L., Xu, X., Wu, X., Fu, J., Feng, Y., Pan, F., and Tuan, L. A. A survey of recent backdoor attacks and defenses in large language models. *arXiv preprint arXiv:2406.06852*, 2024b. doi: 10.48550/arXiv.2406.06852. URL <https://arxiv.org/abs/2406.06852>.
- Zhou, Y., Ni, T., Lee, W. B., and Zhao, Q. A survey on backdoor threats in large language models (llms): Attacks, defenses, and evaluations. *arXiv preprint arXiv:2502.05224*, 2025.
- Ziegler, D. M., Stiennon, N., Wu, J., Brown, T. B., Radford, A., Amodei, D., Christiano, P. F., and Irving, G. Fine-tuning language models from human preferences. *CoRR*, abs/1909.08593, 2019. URL <https://arxiv.org/abs/1909.08593>.
- Zou, A., Wang, Z., Carlini, N., Nasr, M., Kolter, J. Z., and Fredrikson, M. Universal and transferable adversarial attacks on aligned language models. *arXiv preprint arXiv:2307.15043*, 2023.

Limitations

Our work primarily investigates the security implications of the training-free, efficiency-critical paradigm of model composition. Consequently, our analysis focuses on widely adopted shared-basis transplant operators (e.g., OMP) and does not extend to scenarios involving computationally expensive embedding re-training or data-driven post-processing, as these approaches diverge from the rapid interoperability goals of current tokenizer transplantation tools. Additionally, while we demonstrate that the breaker token is stealthy under standard utility benchmarks and varying transfer scales, we acknowledge that the development of specialized, resource-intensive auditing protocols (such as spectral filtering or cryptographic provenance) represents a natural next step in the adversarial defense lifecycle. Finally, our evaluation is currently bounded to text-based language models; exploring the dynamics of this vulnerability in multimodal contexts or extremely divergent script families remains an open avenue for future research.

Ethics Statement

This work exposes a structural vulnerability within the emerging infrastructure of modular AI: the tokenizer transplant pipeline. Our primary objective is to harden the open-weight supply chain by demonstrating that current interoperability tools operate under fragile trust assumptions. To mitigate the risk of misuse, we release the *optimization framework* to allow researchers to reproduce our findings and develop defenses, but we do not distribute pre-compiled, weaponized tokenizer artifacts targeting specific high-value models. All experiments were conducted using public open-weight models and standard datasets (e.g., Wikitext, Alpaca), ensuring no human subjects or private user data were involved. By highlighting this “invisible” attack surface, we aim to accelerate the transition from implicit trust to rigorous verification in model composition workflows.

A. Operational Realism: Research Artifacts vs. Adversarial Capabilities

Our experimental implementation intentionally leaves specific forensic traces, such as the modification of `added_tokens.json` or the use of generic target payloads. It is critical to distinguish between **research artifacts** (intentional traces preserved for transparency and reproducibility) and actual **operational constraints**. In this section, we clarify that the “footprints” observed in our codebases are ethical choices, not limitations of the vulnerability. While we operate under the constraints of responsible disclosure, a real-world adversary unconstrained by scientific ethics could trivially bypass these artifacts using standard engineering practices.

A.1. Payload Independence: The Validity of SER

Our evaluation utilizes Sequence Emission Rate (SER) as a universal proxy for attack success. This is a deliberate methodological abstraction. The *Breaker Token* mechanism fundamentally decouples the **geometric trigger** from the **semantic payload**. The optimization challenge lies entirely in the *geometric mechanism*: finding a vector $\mathbf{x} \in \mathbb{R}^d$ that survives the transplant process to reliably activate a specific vocabulary index id_τ . This represents the core algorithmic contribution of our work. Conversely, the *semantic assignment* (the actual string decoded from id_τ) is determined solely by the tokenizer’s mapping file. From a theoretical standpoint, demonstrating the ability to force the emission of Token ID X is mathematically equivalent to forcing the emission of *any* payload assigned to that ID. Whether that payload resolves to a benign string or a safety-violating command is a trivial configuration choice. We focus on the geometric vulnerability, as the semantic assignment is an elementary engineering step.

A.2. Ethical Transparency vs. Adversarial Stealth

A potential critique of our implementation concerns the detectability of appended tokens (e.g., via vocabulary size checks or metadata inspection). We emphasize that our decision to explicitly append tokens ($\mathcal{V}' = \mathcal{V} \cup \{\tau^*\}$) rather than overwriting existing ones was a **conscious ethical choice to ensure experimental integrity**, not a failure to achieve stealth.

The Triviality of Token Masquerading. From an engineering perspective, achieving zero-footprint stealth is straightforward for any adversary familiar with tokenizer serialization. Standard production tokenizers (e.g., Qwen, Llama-3) invariably contain numerous “reserved” or “unused” slots. A weaponized implementation would employ **Token Masquerading** by *silently repurposing* these existing slots. Rather than appending new entries, an adversary can simply map the malicious breaker geometry and payload to a pre-existing, unused index within the donor’s vocabulary structure. Such an approach

yields a **zero metadata footprint**: since the vocabulary size remains invariant and no auxiliary metadata files are generated, the injection becomes structurally indistinguishable from a standard model update, rendering simple file-based auditing ineffective.

Conclusion on Traceability. We deliberately avoided this stealth technique for two reasons. First, for **reproducibility**, appending tokens makes the attack explicitly visible to peer researchers verification our results. Second, for **safety**, we aim to expose the underlying geometric vulnerability without releasing a weaponized, hard-to-detect artifact into the ecosystem. The presence of metadata traces in our submission should therefore be interpreted as a signature of responsible disclosure rather than a weakness in the attack’s theoretical capabilities.

B. Operational Safeguards: Post-Transplant Auditing Guidelines

While theoretical defenses focus on constraining the transplant operator, the most immediate line of defense for practitioners lies in *behavioral auditing*. Tokenizer transplantation fundamentally alters the input-output interface of the base model, introducing a supply-chain dependency where the model’s behavior is partially determined by external artifacts (donor vocabularies and reconstructed embeddings). Since base-model users typically trust their pre-existing checkpoint but may not fully trust the donor source or the transplant pipeline, we recommend a “trust-but-verify” protocol. Attempting to mathematically prove the safety of the donor is often infeasible without access to private donor data. Rather than that, auditors should focus on detecting the symptomatic behavioral signatures of compromised representations. This section outlines a practical auditing framework designed to detect potential sabotage without requiring privileged access to the donor model’s internals.

B.1. Global Utility and Regression Testing

The first phase of the audit serves as a “smoke alarm” for broad capability collapse. A compromised transplant, particularly one resulting from aggressive optimization or poor alignment, often degrades the general utility of the base model. Auditors should establish a baseline by running a standardized suite of prompts covering instruction following, factual QA, and reasoning tasks on the *pre-transplant* base model. Comparing these results to the *post-transplant* model allows for the detection of global regressions. Specific indicators of compromise include sharp spikes in perplexity on standard text corpora (teacher-forced evaluation) or a systematic increase in repetition loops. While some distribution shift is expected due to tokenization changes, a successful transplant should preserve the fundamental instruction-following capabilities of the base model. Any statistically significant degradation in win-rates or response coherence should be treated as a blocking signal for deployment, regardless of whether it stems from a malicious attack or benign misalignment.

B.2. Differential Token Analysis

Targeted sabotage, such as the attack described in this work, often leaves a localized footprint: a small set of “magnet tokens” that become unnaturally attractive during generation. To detect these, we advocate for a *differential audit* that compares token emission statistics before and after transplantation. Auditors should compute SER across a diverse set of prompt contexts. By calculating the delta $\Delta_{SER}(t) = SER_{post}(t) - SER_{pre}(t)$ for all vocabulary items, auditors can rank tokens by their behavioral shift. A benign transplant typically spreads probability mass shifts diffusely across synonyms or related concepts. In contrast, a malicious injection often manifests as a sparse anomaly where a single token (or a small cluster) exhibits a massive surge in Δ_{SER} , appearing in contexts where it is semantically unwarranted. This differential approach is robust because it factors out the base model’s inherent biases, isolating only the changes introduced by the transplant.

B.3. Context-Invariance and Stress Testing

Sophisticated attacks may attempt to evade simple scans by appearing normal under standard decoding settings. Therefore, a rigorous audit must include stress tests designed to reveal “hidden” preferences in the model’s logit landscape. One effective technique is the **Null-Context Probe**, where the model is prompted with minimal or empty inputs (e.g., a single whitespace or common preamble). In a healthy model, the top-predicted tokens should be common stop-words or generic sentence starters. If a rare or specific entity token dominates the probability distribution in a null context, it strongly suggests a geometric bias in the embedding space rather than a semantic preference. Additionally, auditors should test for **Decoding Invariance** by sweeping through various temperature settings (e.g., $T \in \{0.0, 0.7, 1.0\}$). Adversarial tokens often behave like “background radiation,” persisting as high-likelihood candidates even when the prompt topic changes

or when the prompt is paraphrased. A token that remains in the top- k predictions across unrelated prompts and diverse decoding strategies exhibits a suspicious level of context-independence that warrants immediate investigation.

B.4. Triage Policy

Upon detecting anomalies, organizations should adopt a tiered triage policy. Minor shifts in utility or diffuse changes in token probability (Level 1) may be acceptable consequences of the transplant process, necessitating only a re-run with different hyperparameters. However, the detection of “magnet tokens” that dominate generation across diverse prompts, or utility collapse that persists under greedy decoding (Level 2), indicates a compromised representation. In such cases, the transplant artifacts must be quarantined. Since the vulnerability lies in the geometric mapping provided by the donor, the only secure remediation is to discard the compromised donor artifacts and restart the process with a trusted source or an alternative transplant operator. This behavioral auditing framework transforms the defense problem from one of theoretical certification to one of operational verification, significantly reducing the risk of deploying sabotaged models.

C. Experimental Settings

C.1. Settings

We evaluate the suites introduced in §5.1 (with cross-scale transfer split into scale-up/scale-down edge sets):

- **The Lightweight Clique** ($\mathcal{C}_{\text{Light}}$). All directed edges among Qwen2-0.5B (Yang et al., 2024a), Qwen3-0.6B (Yang et al., 2025), Gemma-2-2B-it (Gemma Team, 2024), Gemma-3-1B-it (Gemma Team, 2025), and Ministral-3B-Instruct (Mistral AI team, 2024).
- **The Standard-Scale Clique** (\mathcal{C}_{Std}). All directed edges among Gemma-2-9B-it (Gemma Team, 2024), Llama-3-8B (Grattafiori et al., 2024), and Mistral-7B-v0.1 (Jiang et al., 2023).
- **Cross-Scale Transfer Sets** ($\mathcal{T}_{\text{Cross}}^{\uparrow}$), **upstream**. Directed edges with *large bases* receiving an embedding from *small donors* (one model per family).
- **Cross-Scale Transfer Sets** ($\mathcal{T}_{\text{Cross}}^{\downarrow}$), **downstream**. Directed edges with *small bases* receiving an embedding from *large donors* (one model per family).

Cross-scale model pools. We form cross-scale edges by drawing one model per family from two pools: (i) **Small** models $\leq 3\text{B}$: SmolLM2-1.7B-Instruct (Allal et al., 2025), Qwen3-0.6B (Yang et al., 2025), Qwen2.5-1.5B-Instruct (Yang et al., 2024b), Gemma-2-2B-it (Gemma Team, 2024), Gemma-3-1B-it (Gemma Team, 2025), Llama-3.2-3B (Grattafiori et al., 2024), and Ministral-3B-Instruct (Mistral AI team, 2024); and (ii) **standard** models: Qwen2-7B (Yang et al., 2024a), Qwen3-14B (Yang et al., 2025), Llama-3.1-8B (Grattafiori et al., 2024), Meta-Llama-3-8B (Grattafiori et al., 2024), and Mistral-7B-v0.1 (Jiang et al., 2023).

C.2. Selecting λ

Each directed base←donor edge is evaluated at a single chosen donor-suppression weight λ . We select λ per edge via a discrete sweep over

$$\lambda \in \{1, 2, 4, 8, 16, 32, 64, 128, 256, 512, 768, 1024, 1280, 1536, 2048\}.$$

We use the rank-based proxy described in §4.3 (Hits@1 on held-out text) to identify values that keep the donor near-zero while maintaining nontrivial base activation, and we then run SER evaluation at the selected λ .

C.3. Implementation Details and Hyperparameters

Composite shared-token dictionaries. For each shared token, we construct a *composite anchor row* by averaging two normalized “views” when available: the input embedding row and the output (LM-head) row. Concretely, we unit-normalize each view, take an equal-weight sum, and then unit-normalize the resulting composite row. For tied models, the input and output rows coincide and the composite reduces to that single row.

Public-text feature collection (μ_{base} and donor subspace). We estimate the base target μ_{base} and the donor suppression subspace from last-layer hidden states on WikiText-103 (Merity et al., 2016). We use the *train* split of the raw corpus and process up to 5,000 documents. Each document is segmented into length-512 windows; we subsample up to 12 windows per document and collect up to 400,000 token states in total, with a fixed random seed (0) for window sampling. The base target

is the empirical mean of collected base hidden states. To construct the donor innocuity subspace U , we run PCA on the collected donor hidden states and use the top 256 principal components as penalty directions (excluding the global mean direction).

Sparse designer and OMP-style transplant. For all settings, the designer uses sparsity budget $K=64$ and a ridge-stabilized linear solve ($\rho=10^{-3}$) with quadratic base reconstruction weight $\gamma=1$ and no negative-base term ($\eta=0$). We enable donor-aware greedy support selection, i.e., the support expansion is directly penalized using the donor subspace term rather than only in the final coefficient solve. The donor suppression weight λ is selected per edge via the sweep in Appendix C.2; we report both attack performance and donor stealth across this range. For the victim-side transplant, we use an OMP-style shared-basis reconstruction with the same sparsity budget $K=64$.

Operator-matched shared-basis designer (alternative transplant operators). To study whether the breaker token can be designed for *alternative* shared-basis transplant operators beyond OMP, we use an OMP-like shared-basis designer that explicitly simulates the target operator (FOCUS (Dobler & de Melo, 2023), CLP (Ostendorff & Rehm, 2023), or WECHSEL (Minixhofer et al., 2022)) during optimization. The designer first selects the top $K=32$ shared anchors by cosine similarity to the target base direction and forms an operator-specific anchor mixture: for FOCUS/WECHSEL it uses a softmax with temperature $\beta=10$, while for CLP it uses a nonnegative normalization. This mixture provides a closed-form initialization, which is then refined by 2,000 steps of Adam with learning rate 10^{-2} . The refinement objective matches the base-side target (we use the aggregated μ_{base} vector with scaling factor 1.0) while regularizing donor-side innocuity via (i) a penalty on projection onto a donor PCA subspace and (ii) a norm-preservation term that discourages atypical donor embedding norms; the combined donor regularizer is weighted by λ (reported in the table). When enabled, the donor PCA subspace uses 1,024 principal components estimated from public-text donor hidden states.

SER evaluation. We compute SER on Alpaca (Taori et al., 2023), SQuAD v2 (Rajpurkar et al., 2018), and GSM8K (Cobbe et al., 2021) using 256 prompts per dataset (one generation per prompt). Generations use nucleus sampling with temperature 1.0 and top- p 0.9, up to 256 new tokens. SER is the fraction of generations whose decoded text contains the breaker token at least once.

Utility evaluation. We report utility on WikiText-103 (Merity et al., 2016) (word perplexity) and LAMBADA (Paperno et al., 2016), MMLU, and ARC-Challenge (Clark et al., 2018) (accuracy), using 0-shot evaluation. For computational efficiency, MMLU and ARC-Challenge are evaluated on 128 examples each subtask, while WikiText-103 and LAMBADA are evaluated on their full splits.

LoRA fine-tuning for persistence analysis. For the persistence analysis (Section 5.3), we fine-tune the attacked base with LoRA (Hu et al., 2022) on the first 500 Alpaca training examples (Taori et al., 2023) for 5 epochs, with learning rate 2×10^{-4} , rank $r=16$, scaling factor $\alpha=32$, and dropout 0.05. We use a maximum sequence length of 1,024 with standard optimizer settings (weight decay 0.01 and warmup ratio 0.03).

Merge-based mitigation for persistence analysis. To test whether model merging can remove the planted direction, we merge the attacked base with a *clean reference* model from the same family and then re-evaluate SER under the same prompt pools. For the edge Gemma-3-1B-it←Gemma-2-2B-it, we merge the attacked base with google/gemma-3-1b-pt (Gemma Team, 2025). For the edge Qwen2-0.5B←Ministral-3B, we merge with Qwen/Qwen2-0.5B-Instruct (Yang et al., 2024a). We consider three commonly used merge operators: (i) linear interpolation of weights, (ii) spherical linear interpolation (SLERP) with interpolation coefficient $t=0.5$, and (iii) TIES merging with mixing coefficient $\lambda=0.5$ and density 1.0 (i.e., no sparsification). To preserve the breaker token, the merged model inherits the attacked tokenizer (including the appended token). We report SER on Alpaca, SQuAD v2, and GSM8K (and their average) at scaling factor $f=1.0$, and include the corresponding patched-donor baseline.

C.4. Model Aliases

We use concise aliases for model identifiers throughout figures and tables for readability. The mapping from original model IDs to aliases is provided in Table 2. These identifiers span multiple model families, including Qwen2 (Yang et al., 2024a), Qwen2.5 (Yang et al., 2024b), Qwen3 (Yang et al., 2025), Gemma-2 (Gemma Team, 2024), Gemma-3 (Gemma Team, 2025), Llama-3 (Grattafiori et al., 2024), Mistral-7B (Jiang et al., 2023), Ministral (Mistral AI team, 2024), SmolLM2 (Allal et al., 2025).

Model ID	Alias
Small models ($\leq 3B$)	
<i>Qwen</i> (Yang et al., 2024a;b; 2025)	
Qwen/Qwen2-0.5B	Q2-0.5B
Qwen/Qwen3-0.6B	Q3-0.6B
Qwen/Qwen3-1.7B	Q3-1.7B
Qwen/Qwen2.5-1.5B-Instruct	Q2.5-1.5B
<i>Gemma</i> (Gemma Team, 2024; 2025)	
google/gemma-2-2b-it	Gem2-2B
google/gemma-3-1b-it	Gem3-1B
<i>Llama</i> (Grattafiori et al., 2024)	
meta-llama/Llama-3.2-1B	L3.2-1B
meta-llama/Llama-3.2-3B	L3.2-3B
<i>Ministral</i> (Mistral AI team, 2024)	
ministral/Ministral-3b-instruct	Min-3B
<i>SmolLM2</i> (Allal et al., 2025)	
HuggingFaceTB/SmolLM2-1.7B-Instruct	Smol1.7B
Standard-scale models (7B–14B)	
<i>Qwen</i> (Yang et al., 2024a; 2025)	
Qwen/Qwen2-7B	Q2-7B
Qwen/Qwen3-14B	Q3-14B
<i>Gemma</i> (Gemma Team, 2024)	
google/gemma-2-9b-it	Gem2-9B
<i>Llama</i> (Grattafiori et al., 2024)	
meta-llama/Llama-3.1-8B	L3.1-8B
meta-llama/Meta-Llama-3-8B	ML3-8B
<i>Mistral</i> (Jiang et al., 2023)	
mistralai/Mistral-7B-v0.1	M7B-v0.1

Table 2. Model aliases used in our experiments. We group models by family and scale for readability.

D. Forensic Analysis via Magikarp Detection

To further verify that our injected breaker tokens do not exhibit the statistical signatures of degenerate embeddings, we subjected them to the *Magikarp* detection pipeline (Land & Bartolo, 2024). This heuristic tool, standard in the `mergekit` ecosystem, flags tokens as “poorly trained” if they satisfy either of two criteria:

1. **Norm Collapse:** The embedding’s L2 norm falls within the lowest quantile (default $\alpha = 0.01$) of the vocabulary.
2. **Garbage Alignment:** The embedding exhibits high cosine similarity to the centroid of known unused/reserved tokens.

Results. We evaluated the breaker tokens generated across our 20 lightweight clique pairs. The tokens successfully evaded detection in **75% of cases (15/20)**. Crucially, regarding the 5 detected instances, **none** were flagged for Garbage Alignment. All failures were triggered exclusively by **Norm Collapse**.

Analysis of Norm Collapse. The minority of failures stems directly from the *Donor Inertness* objective in our optimization (Eq. 2). By aggressively penalizing the projection onto the donor’s semantic subspace ($\min \|U\mathbf{x}_d\|$) and applying ridge regularization to coefficients ($\min \|\alpha\|_1$), the solver can inadvertently over-shrink the embedding vector’s magnitude. This confirms the *hyper-inertness* phenomenon noted in Section 5.5: the tokens are not random artifacts (which would trigger the Garbage Alignment check), but are rather engineered to be excessively “quiet” in the donor space. In practice, this trade-off is easily managed by relaxing the ridge penalty γ or imposing a minimum norm constraint during design, though even without tuning, the majority of attacks pass standard auditing.

E. Details on Differentiable Transplant Operators

In this section, we provide the implementation details for *differentiable* transplant operators, specifically FOCUS (Dobler & de Melo, 2023), CLP (Ostendorff & Rehm, 2023), and WECHSEL (Minixhofer et al., 2022). We formalize these

operators as continuous functions $f : \mathbb{R}^{\delta_d} \rightarrow \mathbb{R}^{\delta_b}$. In cases where the operator involves a linear transformation (e.g., affine alignment or projection), we denote the corresponding transformation matrix as \mathbf{A} . Unlike the sparse setting (OMP) which requires discrete combinatorial search, the differentiability of f allows us to optimize the donor embedding \mathbf{x}_d directly via backpropagation.

Optimization Objective. Consistent with the general framework (Eq. 2), we set the learnable parameters to be the raw donor embedding itself ($\theta = \mathbf{x}_d$). We minimize the following loss:

$$\mathcal{L}(\mathbf{x}_d) = \underbrace{\gamma \|f(\mathbf{x}_d) - \boldsymbol{\mu}_{\text{base}}\|_2^2}_{\text{Base Saliency}} + \lambda \underbrace{\|U\mathbf{x}_d\|_2^2}_{\text{Donor Inertness}} + \rho \underbrace{\|\mathbf{x}_d\|_2^2}_{\text{Regularization}}, \quad (5)$$

where $\rho > 0$ is a ridge penalty for numerical stability. We solve Eq. 5 using a unified gradient-based approach (Adam) for all operators described below.

E.1. CLP: Contrastive Linear Projection

Transplant mechanism. For the barycentric CLP variant (Ostendorff & Rehm, 2023), weights are computed by rectifying cosine similarities and renormalizing. Using normalized donor input $\hat{\mathbf{x}}_d$ and anchors $\hat{\phi}_j^{(d)}$, the weights are:

$$w_j(\mathbf{x}_d) = \frac{\text{ReLU}(\langle \hat{\mathbf{x}}_d, \hat{\phi}_j^{(d)} \rangle)}{\epsilon + \sum_{k \in \mathcal{T}} \text{ReLU}(\langle \hat{\mathbf{x}}_d, \hat{\phi}_k^{(d)} \rangle)}. \quad (6)$$

The transplanted embedding is synthesized as:

$$f_{\text{CLP}}(\mathbf{x}_d) = \sum_{j \in \mathcal{T}} w_j(\mathbf{x}_d) \phi_j^{(b)}. \quad (7)$$

Designer optimization. We minimize the differentiable objective (Eq. 5) with $f = f_{\text{CLP}}$. Because anchors with negative cosine similarity yield zero gradient through the ReLU function, we employ a **non-negative reverse projection** for initialization to prevent vanishing gradients. Specifically, we modify the initialization step in Eq. 13 by replacing the simplex constraint with a simple non-negativity constraint ($\alpha \geq 0$). We then set $\mathbf{x}_{\text{init}} = \sum_{j \in \mathcal{S}} \alpha_j^* \phi_j^{(d)}$ to ensure the starting vector positively activates the target anchors.

E.2. WECHSEL: Alignment and Neighbors

Transplant mechanism. WECHSEL (Minixhofer et al., 2022) combines a global affine alignment with a local k -NN mixture over the *base* vocabulary. Let $\boldsymbol{\mu}_{\text{src}}, \boldsymbol{\mu}_{\text{tgt}}$ be the centroids of the donor and base embeddings, respectively, and let \mathbf{A} be the orthogonal alignment matrix learned from shared tokens. We define the *aligned proxy* of a donor input \mathbf{x}_d as:

$$\tilde{\mathbf{x}}(\mathbf{x}_d) = (\mathbf{x}_d - \boldsymbol{\mu}_{\text{src}})\mathbf{A} + \boldsymbol{\mu}_{\text{tgt}}. \quad (8)$$

Let $\mathcal{N}_k(\tilde{\mathbf{x}})$ be the set of indices of the k base anchors $\{\phi_v^{(b)}\}$ nearest to $\tilde{\mathbf{x}}$ (under the specific distance metric used by WECHSEL), and let $w_v(\tilde{\mathbf{x}})$ be the corresponding softmax weights. The transplanted embedding is synthesized as:

$$f_{\text{WEC}}(\mathbf{x}_d) = \sum_{v \in \mathcal{N}_k(\tilde{\mathbf{x}})} w_v(\tilde{\mathbf{x}}(\mathbf{x}_d)) \phi_v^{(b)}. \quad (9)$$

Designer optimization. Because the synthesis basis $\mathcal{N}_k(\tilde{\mathbf{x}})$ changes discretely with \mathbf{x}_d , the objective is non-convex and piecewise-smooth. We minimize the unified differentiable objective (Eq. 5) by substituting the operator f_{WEC} :

$$\min_{\mathbf{x}_d} \mathcal{L}(\mathbf{x}_d) = \gamma \|f_{\text{WEC}}(\mathbf{x}_d) - \boldsymbol{\mu}_{\text{base}}\|_2^2 + \lambda \|U\mathbf{x}_d\|_2^2 + \rho \|\mathbf{x}_d\|_2^2. \quad (10)$$

Crucially, the alignment transformation in Eq. 8 is strictly embedded within f_{WEC} , so we optimize the raw donor vector \mathbf{x}_d directly via gradient descent, avoiding double-alignment issues.

E.3. FOCUS: Soft Anchor Interpolation

Transplant mechanism. FOCUS (Dobler & de Melo, 2023) reconstructs tokens via similarity-weighted interpolation of shared semantic anchors. Let \mathcal{T} be the set of shared tokens. We denote the donor and base anchor matrices as Φ_d and Φ_b , where the j -th row corresponds to the shared token $j \in \mathcal{T}$. For numerical stability, the mechanism operates on normalized donor anchors $\hat{\phi}_j^{(d)} = \phi_j^{(d)} / \|\phi_j^{(d)}\|_2$. Given a donor input \mathbf{x}_d , the operator computes attention weights using a softmax kernel with temperature β :

$$w_j(\mathbf{x}_d) = \frac{\exp(\beta \langle \hat{\mathbf{x}}_d, \hat{\phi}_j^{(d)} \rangle)}{\sum_{k \in \mathcal{T}} \exp(\beta \langle \hat{\mathbf{x}}_d, \hat{\phi}_k^{(d)} \rangle)}, \quad (11)$$

where $\hat{\mathbf{x}}_d$ is the normalized input. The transplanted embedding is then synthesized as the weighted sum of base anchors:

$$f_{\text{FOC}}(\mathbf{x}_d) = \sum_{j \in \mathcal{T}} w_j(\mathbf{x}_d) \phi_j^{(b)}. \quad (12)$$

Designer optimization. Due to the nonlinearity of the attention weights $w_j(\mathbf{x}_d)$, the objective is non-convex. We minimize the unified differentiable objective (Eq. 5) by substituting $f = f_{\text{FOC}}$ and employing gradient-based optimization.

To avoid local minima, we employ a **reverse-projection initialization**. We identify a small subset of base anchors $\mathcal{S} \subset \mathcal{T}$ (e.g., the k -nearest neighbors of μ_{base} in Φ_b) and solve for the optimal reconstruction coefficients in the base space:

$$\alpha^* = \arg \min_{\alpha \in \Delta^{|\mathcal{S}|}} \left\| \sum_{j \in \mathcal{S}} \alpha_j \phi_j^{(b)} - \mu_{\text{base}} \right\|_2^2. \quad (13)$$

We then initialize the donor vector by mapping these coefficients back to the donor space: $\mathbf{x}_{\text{init}} = \sum_{j \in \mathcal{S}} \alpha_j^* \phi_j^{(d)}$. Finally, we apply the donor suppression constraint as a one-shot preconditioner before optimization: $\mathbf{x}_{\text{init}} \leftarrow (I + \lambda U^T U)^{-1} \mathbf{x}_{\text{init}}$.

E.4. SER results on differentiable transplant operators

We now evaluate whether our breaker-token designer transfers to the three shared-basis operator variants described above. For each filtered base←donor edge and its selected λ , we report SER for both the attacked base and the patched donor on Alpaca, SQuAD v2, and GSM8K, with an additional column showing the average across the three pools.

Table 3: SER results on differentiable transplant operators. Rows are grouped by the underlying shared-basis operator.

Edge (base←donor)	λ	Alpaca		SQuAD v2		GSM8K		Avg	
		Base	Donor	Base	Donor	Base	Donor	Base	Donor
FOCUS									
Q3-0.6B ← Gem2-2B	16	.6758	.0000	.7539	.0000	.9336	.0000	.7878	.0000
Q3-0.6B ← Gem2-2B	8	.6680	.0000	.7578	.0000	.9141	.0000	.7799	.0000
Q3-0.6B ← Gem2-2B	4	.6484	.0000	.7148	.0000	.9180	.0000	.7604	.0000
Q3-0.6B ← Gem2-2B	32	.5938	.0000	.7305	.0000	.8984	.0000	.7409	.0000
Q3-0.6B ← Gem2-2B	64	.5898	.0000	.6641	.0000	.7539	.0000	.6693	.0000
L3.2-1B ← Q3-0.6B	8	.3555	.0117	.3477	.0078	.9453	.0195	.5495	.0130
Q3-0.6B ← Gem2-2B	128	.4844	.0000	.5508	.0000	.5039	.0000	.5130	.0000
Q3-0.6B ← Q2-0.5B	4	.2070	.0039	.2188	.0039	.9375	.0352	.4544	.0143
Q3-0.6B ← Q2-0.5B	8	.2031	.0000	.2344	.0195	.9336	.0430	.4570	.0208
Q3-0.6B ← Q2-0.5B	2	.2148	.0039	.2344	.0000	.9336	.0820	.4609	.0286
Q3-0.6B ← Q2-0.5B	16	.1953	.0000	.2344	.0195	.9336	.1094	.4544	.0430
Q2-0.5B ← Q3-0.6B	16	.3594	.0508	.2891	.0469	.9453	.4023	.5312	.1667
L3.2-1B ← Gem2-2B	2	.3477	.0000	.4258	.0000	.3008	.0000	.3581	.0000
Q2-0.5B ← Q3-0.6B	32	.3359	.0117	.2695	.0508	.9258	.4102	.5104	.1576
L3.2-1B ← Gem2-2B	4	.2656	.0000	.3320	.0000	.1836	.0000	.2604	.0000

Continued on next page

The Trojan in the Vocabulary: Stealthy Sabotage of LLM Composition

Edge (base←donor)	λ	Alpaca		SQuAD v2		GSM8K		Avg	
		Base	Donor	Base	Donor	Base	Donor	Base	Donor
Q2-0.5B ← Gem2-2B	16	.2109	.0000	.3086	.0000	.0391	.0000	.1862	.0000
CLP									
Q2-0.5B ← Gem2-2B	2	.8516	.0000	.9648	.0000	.9922	.0000	.9362	.0000
Q3-0.6B ← Gem2-2B	2	.8516	.0000	.9062	.0000	.9922	.0000	.9167	.0000
L3.2-1B ← Q3-0.6B	32	.4570	.0586	.5273	.0273	.9805	.0000	.6549	.0286
L3.2-1B ← Q3-0.6B	16	.4219	.0352	.5039	.0156	.9805	.0000	.6354	.0169
Gem2-2B ← L3.2-1B	2	.5898	.0000	.2734	.0000	.4805	.0000	.4479	.0000
Gem2-2B ← L3.2-1B	4	.5742	.0000	.3203	.0000	.4453	.0000	.4466	.0000
Q2-0.5B ← Gem2-2B	64	.1328	.0000	.0977	.0000	.0234	.0000	.0846	.0000
L3.2-1B ← Gem2-2B	64	.1445	.0000	.0391	.0000	.0547	.0000	.0794	.0000
L3.2-1B ← Gem2-2B	128	.1406	.0000	.0430	.0000	.0508	.0000	.0781	.0000
L3.2-1B ← Gem2-2B	32	.1289	.0000	.0391	.0000	.0430	.0000	.0703	.0000
Q2-0.5B ← Gem2-2B	128	.0898	.0000	.0742	.0000	.0234	.0000	.0625	.0000
WECHSEL									
Q2-0.5B ← Gem2-2B	4	.5078	.0000	.9336	.0000	.6914	.0000	.7109	.0000
Q2-0.5B ← Gem2-2B	8	.3320	.0000	.7070	.0000	.2695	.0000	.4362	.0000
Q3-0.6B ← L3.2-1B	8	.1016	.0000	.1367	.0000	.6055	.0000	.2812	.0000
Q3-0.6B ← L3.2-1B	2	.1055	.0000	.1094	.0000	.5781	.0000	.2643	.0000
Q3-0.6B ← L3.2-1B	4	.0469	.0000	.0859	.0000	.5156	.0000	.2161	.0000
Q3-0.6B ← L3.2-1B	16	.0586	.0000	.0664	.0000	.2930	.0000	.1393	.0000
Q2-0.5B ← Gem2-2B	32	.1328	.0000	.2148	.0000	.0156	.0000	.1211	.0000
Q2-0.5B ← L3.2-1B	4	.1484	.0000	.0742	.0000	.0781	.0000	.1003	.0000
Q2-0.5B ← L3.2-1B	2	.1250	.0000	.0781	.0000	.0938	.0000	.0990	.0000
Q2-0.5B ← L3.2-1B	8	.1289	.0000	.0859	.0000	.0742	.0000	.0964	.0000
L3.2-1B ← Gem2-2B	8	.0820	.0000	.1172	.0000	.0820	.0000	.0938	.0000
L3.2-1B ← Gem2-2B	16	.0664	.0000	.0898	.0000	.0938	.0000	.0833	.0000
Q2-0.5B ← L3.2-1B	16	.0977	.0000	.0586	.0000	.0469	.0000	.0677	.0000

Analysis. Table 3 shows that our designer can reproduce the same *asymmetric realizability* pattern observed throughout the paper: for multiple edges and across prompt pools, the attacked base exhibits substantial SER while the patched donor remains near-silent. The strongest examples are concentrated on edges targeting Gem2-2B as the donor, where both CLP and FOCUS yield high base SER across pools while keeping donor SER close to zero. WECHSEL is more conservative: it keeps donor SER at zero on all listed triples, but typically yields smaller base activation than CLP/FOCUS. Finally, the per-task breakdown exposes where donor leakage can occur: on some closely related pairs, FOCUS can increase donor SER on one or more pools even when base SER remains high, indicating a narrower activation–stealth window for soft interpolation. Overall, these results suggest that the donor-suppression objective is robust to the choice of shared-basis variant, but the precise activation–stealth trade-off depends on the transplant operator’s geometry.

F. Theoretical analysis

This section formalizes why a single crafted *breaker token* τ_x can be (i) distributionally inert in the donor, (ii) geometrically non-outlying (*spectral mimicry*), (iii) persistent under common post-processing (LoRA fine-tuning on QKV and weight merging), and (iv) controllable via the trade-off parameter λ . We also show the same framework extends to differentiable transplant operators (FOCUS, CLP, WECHSEL) via a unified “anchor-mixture” view.

F.1. Setup: logits, distributions, and transplant maps

Let \mathcal{D} denote the (patched) donor model and \mathcal{B} the (attacked) base model. For a model $m \in \{b, d\}$ and a context (prompt + previous tokens) c , let $\mathbf{g}^{(m)}(c) \in \mathbb{R}^{\delta_m}$ be the final-layer hidden state used by the LM head. Let $H^{(m)} \in \mathbb{R}^{|\mathcal{V}_m| \times \delta_m}$ be the

LM-head matrix, with row $\mathbf{h}_v^{(m)}$ for token v . The next-token logits and distribution are

$$\ell_v^{(m)}(c) := \langle \mathbf{g}^{(m)}(c), \mathbf{h}_v^{(m)} \rangle, \quad p^{(m)}(v | c) := \frac{\exp(\ell_v^{(m)}(c))}{\sum_{u \in \mathcal{V}_m} \exp(\ell_u^{(m)}(c))}. \quad (14)$$

Patch model. The patched donor vocabulary is $\mathcal{V}'_d = \mathcal{V}_d \cup \{\tau_\star\}$. We modify no donor parameters except appending the single new row for τ_\star : its donor-side head row is $\mathbf{h}_{\tau_\star}^{(d)} = \mathbf{x}_d$ (and analogously for the input embedding when untied; the analysis below focuses on the LM-head row because emission is the threat).

Transplant model. A shared-basis transplant operator (Definition 3.1) produces a base-side row $\widehat{\mathbf{x}}_b$ from the donor-side row \mathbf{x}_d via coefficient reuse:

$$\mathbf{x}_d \approx \Phi_d^\top \boldsymbol{\beta}(\mathbf{x}_d), \quad \widehat{\mathbf{x}}_b = \Phi_b^\top \boldsymbol{\beta}(\mathbf{x}_d). \quad (1)$$

We denote this induced donor-to-base map by

$$T : \mathbb{R}^{\delta_d} \rightarrow \mathbb{R}^{\delta_b}, \quad T(\mathbf{x}_d) := \widehat{\mathbf{x}}_b.$$

For OMP-style operators, T is piecewise linear (support-dependent). For differentiable operators (FOCUS/CLP/WECHSEL), T is continuous and differentiable almost everywhere (Appendix E).

Donor innocuity subspace. Let $U \in \mathbb{R}^{r \times \delta_d}$ be the donor suppression matrix used in the objective (Eq. 2); assume its rows are orthonormal (if not, replace U by an orthonormal basis of its row span). Let $\Pi_U := U^\top U$ and $\Pi_{U^\perp} := I - \Pi_U$.

F.2. Donor innocuity: bounded distributional impact and preserved utility

The key observation is extremely simple (and therefore easy to miss in practice): *appending a new token changes the donor next-token distribution only through the probability mass assigned to that new token.* All other logits are untouched.

Proposition F.1 (Appending a token perturbs only by its own probability mass). *Fix any donor context c and let $p_d(\cdot | c)$ be the original next-token distribution on \mathcal{V}_d . Let $p'_d(\cdot | c)$ be the patched distribution on $\mathcal{V}'_d = \mathcal{V}_d \cup \{\tau_\star\}$ (with all original logits unchanged and only the new logit $\ell_{\tau_\star}^{(d)}(c)$ added). Then, for every $v \in \mathcal{V}_d$,*

$$p'_d(v | c) = (1 - p'_d(\tau_\star | c)) p_d(v | c), \quad p'_d(\tau_\star | c) = \frac{\exp(\ell_{\tau_\star}^{(d)}(c))}{\sum_{u \in \mathcal{V}_d} \exp(\ell_u^{(d)}(c)) + \exp(\ell_{\tau_\star}^{(d)}(c))}. \quad (15)$$

Moreover, the total variation distance between the extended distributions (on \mathcal{V}'_d with the original model assigning probability 0 to τ_\star) is exactly

$$d_{\text{TV}}(p_d(\cdot | c), p'_d(\cdot | c)) = \frac{1}{2} \|p_d(\cdot | c) - p'_d(\cdot | c)\|_1 = p'_d(\tau_\star | c). \quad (16)$$

In particular, if $p'_d(\tau_\star | c) \leq \varepsilon$ for all contexts c , then $\|p_d(\cdot | c) - p'_d(\cdot | c)\|_1 \leq 2\varepsilon$ for all c .

Proof. Let $Z(c) = \sum_{u \in \mathcal{V}_d} \exp(\ell_u^{(d)}(c))$ and $a(c) = \exp(\ell_{\tau_\star}^{(d)}(c))$. Then for $v \in \mathcal{V}_d$, $p_d(v | c) = \exp(\ell_v)/Z$ and $p'_d(v | c) = \exp(\ell_v)/(Z + a)$, hence $p'_d(v | c) = \frac{Z}{Z+a} p_d(v | c) = (1 - p'_d(\tau_\star | c)) p_d(v | c)$. For the ℓ_1 difference over \mathcal{V}'_d ,

$$\begin{aligned} \|p_d - p'_d\|_1 &= \sum_{v \in \mathcal{V}_d} |p_d(v) - (1 - p'_d(\tau_\star)) p_d(v)| + |0 - p'_d(\tau_\star)| \\ &= p'_d(\tau_\star) \sum_{v \in \mathcal{V}_d} p_d(v) + p'_d(\tau_\star) = 2p'_d(\tau_\star), \end{aligned}$$

and the TV identity follows. □

Thus, donor innocuity reduces to bounding $p'_d(\tau_\star | c)$ uniformly over contexts.

From subspace suppression to small donor probability mass. We now connect the donor penalty $\|U\mathbf{x}_d\|_2^2$ to a bound on the new-token probability. We will make explicit the (standard, empirically true) fact that donor hidden states are concentrated in a low-rank “active” subspace captured by U .

Assumption F.2 (Hidden-state concentration in the donor active subspace). There exist constants $G, \sigma \geq 0$ such that for every donor context c ,

$$\|\mathbf{g}^{(d)}(c)\|_2 \leq G, \quad \|\Pi_{U^\perp}\mathbf{g}^{(d)}(c)\|_2 \leq \sigma. \quad (17)$$

Intuitively, U (constructed from top PCA components of donor hidden states) captures most energy, and σ controls the residual “tail”.

Lemma F.3 (A uniform logit bound from U -suppression). *Under Assumption F.2, for any donor head row \mathbf{x}_d and any context c ,*

$$|\ell_{\tau_\star}^{(d)}(c)| = |\langle \mathbf{g}^{(d)}(c), \mathbf{x}_d \rangle| \leq G\|U\mathbf{x}_d\|_2 + \sigma\|\mathbf{x}_d\|_2. \quad (18)$$

Proof. Decompose $\mathbf{g}^{(d)}(c) = \Pi_U\mathbf{g}^{(d)}(c) + \Pi_{U^\perp}\mathbf{g}^{(d)}(c)$ and use Cauchy–Schwarz:

$$\begin{aligned} |\langle \mathbf{g}^{(d)}(c), \mathbf{x}_d \rangle| &\leq |\langle \Pi_U\mathbf{g}^{(d)}(c), \mathbf{x}_d \rangle| + |\langle \Pi_{U^\perp}\mathbf{g}^{(d)}(c), \mathbf{x}_d \rangle| \\ &= |\langle \mathbf{g}^{(d)}(c), \Pi_U\mathbf{x}_d \rangle| + |\langle \Pi_{U^\perp}\mathbf{g}^{(d)}(c), \mathbf{x}_d \rangle| \\ &\leq \|\mathbf{g}^{(d)}(c)\|_2 \|\Pi_U\mathbf{x}_d\|_2 + \|\Pi_{U^\perp}\mathbf{g}^{(d)}(c)\|_2 \|\mathbf{x}_d\|_2. \end{aligned}$$

If U has orthonormal rows then $\|\Pi_U\mathbf{x}_d\|_2 = \|U\mathbf{x}_d\|_2$, yielding the claim. \square

Lemma F.4 (Bounding the new-token probability by a logit margin). *Fix any context c and let $m(c) := \max_{v \in \mathcal{V}_d} \ell_v^{(d)}(c)$ be the maximum original donor logit. Then*

$$p'_d(\tau_\star | c) \leq \exp(\ell_{\tau_\star}^{(d)}(c) - m(c)) \leq \exp(|\ell_{\tau_\star}^{(d)}(c)| - m(c)). \quad (19)$$

Proof. Let $Z(c) = \sum_{v \in \mathcal{V}_d} \exp(\ell_v^{(d)}(c)) \geq \exp(m(c))$. Since $a/(Z+a) \leq a/Z$ for $a > 0$,

$$p'_d(\tau_\star | c) = \frac{\exp(\ell_{\tau_\star})}{Z + \exp(\ell_{\tau_\star})} \leq \frac{\exp(\ell_{\tau_\star})}{Z} \leq \exp(\ell_{\tau_\star} - m(c)).$$

The second inequality uses $\ell_{\tau_\star} \leq |\ell_{\tau_\star}|$. \square

Combining Proposition F.1, Lemma F.3, and Lemma F.4 yields an explicit (loose but correct) donor innocuity guarantee.

Theorem F.5 (Donor distributional innocuity). *Under Assumption F.2, for any donor head row \mathbf{x}_d and any context c ,*

$$d_{\text{TV}}(p_d(\cdot | c), p'_d(\cdot | c)) = p'_d(\tau_\star | c) \leq \exp(G\|U\mathbf{x}_d\|_2 + \sigma\|\mathbf{x}_d\|_2 - m(c)). \quad (20)$$

In particular, if $\|U\mathbf{x}_d\|_2 \leq \epsilon_U$ and $\|\mathbf{x}_d\|_2 \leq R$, then

$$d_{\text{TV}}(p_d(\cdot | c), p'_d(\cdot | c)) \leq \exp(G\epsilon_U + \sigma R - m(c)), \quad (21)$$

so any uniform lower bound $m(c) \geq m_{\min}$ implies a uniform probability bound $p'_d(\tau_\star | c) \leq \exp(G\epsilon_U + \sigma R - m_{\min})$.

Utility preservation (teacher forcing and bounded rewards). Most donor utility evaluations never include τ_\star in the ground-truth text (it is newly added), so the only effect is a small renormalization factor on the probabilities of *existing* tokens. This gives a clean bound on NLL/perplexity shifts.

Corollary F.6 (Bounded degradation of donor NLL/per-token loss). *Fix any context c and any ground-truth next token $y \in \mathcal{V}_d$ (so $y \neq \tau_\star$). Then*

$$-\log p'_d(y | c) + \log p_d(y | c) = -\log(1 - p'_d(\tau_\star | c)). \quad (22)$$

If $p'_d(\tau_\star | c) \leq \epsilon \leq \frac{1}{2}$ for all contexts, then

$$-\log p'_d(y | c) + \log p_d(y | c) \leq -\log(1 - \epsilon) \leq \frac{\epsilon}{1 - \epsilon} \leq 2\epsilon. \quad (23)$$

Proof. By Proposition F.1, for $y \in \mathcal{V}_d$ we have $p'_d(y | c) = (1 - p'_d(\tau_\star | c))p_d(y | c)$, hence the identity. The inequalities are standard: $-\log(1 - x) \leq x/(1 - x)$ for $x \in [0, 1]$. \square

More generally, any bounded downstream utility functional changes at most by the TV distance (Lipschitzness of expectations under TV).

Corollary F.7 (Bounded change in donor expected utility). *Let f be any measurable function of the next-token output with range in $[0, 1]$. Then for any context c ,*

$$\left| \mathbb{E}_{v \sim p_d(\cdot | c)}[f(v)] - \mathbb{E}_{v \sim p'_d(\cdot | c)}[f(v)] \right| \leq d_{\text{TV}}(p_d(\cdot | c), p'_d(\cdot | c)) = p'_d(\tau_\star | c). \quad (24)$$

Thus a uniform bound $p'_d(\tau_\star | c) \leq \varepsilon$ implies a uniform $O(\varepsilon)$ utility change per decoding step.

A complementary (operator-agnostic) logit stability view. The next lemma is the one implicitly optimized in Eq. 2: suppressing $\|U\mathbf{x}_d\|_2$ controls how much the τ_\star logit can change when we remove the component in the penalized subspace.

Assumption F.8 (Lipschitz donor head). Fix a donor context distribution and the donor model \mathcal{D} . Let $\ell_d : \mathbb{R}^{\delta_d} \rightarrow \mathbb{R}$ map a donor head row \mathbf{x}_d to a (context-averaged or worst-case) logit for τ_\star . Assume ℓ_d is L -Lipschitz:

$$|\ell_d(\mathbf{x}) - \ell_d(\mathbf{y})| \leq L\|\mathbf{x} - \mathbf{y}\|_2 \quad \text{for all } \mathbf{x}, \mathbf{y} \in \mathbb{R}^{\delta_d}.$$

Definition F.9 (Suppression comparator). Let $U \in \mathbb{R}^{r \times \delta_d}$ have orthonormal rows and define $\Pi_U := U^\top U$. Define the suppressed comparator

$$\bar{\mathbf{x}}_d := (I - \Pi_U)\mathbf{x}_d,$$

i.e., $\bar{\mathbf{x}}_d$ removes the component of \mathbf{x}_d lying in the penalized subspace.

Theorem F.10 (Donor innocuity under subspace suppression). *Under Assumption F.8 and Definition F.9,*

$$|\ell_d(\mathbf{x}_d) - \ell_d(\bar{\mathbf{x}}_d)| \leq L\|\Pi_U\mathbf{x}_d\|_2 = L\|U\mathbf{x}_d\|_2. \quad (25)$$

Consequently, enforcing $\|U\mathbf{x}_d\|_2 \leq \varepsilon$ implies $|\ell_d(\mathbf{x}_d) - \ell_d(\bar{\mathbf{x}}_d)| \leq L\varepsilon$.

Proof. By Lipschitzness,

$$|\ell_d(\mathbf{x}_d) - \ell_d(\bar{\mathbf{x}}_d)| \leq L\|\mathbf{x}_d - \bar{\mathbf{x}}_d\|_2 = L\|\Pi_U\mathbf{x}_d\|_2.$$

If U has orthonormal rows then $\|\Pi_U\mathbf{x}_d\|_2^2 = \mathbf{x}_d^\top U^\top U \mathbf{x}_d = \|U\mathbf{x}_d\|_2^2$. \square

Corollary F.11 (From logits to probabilities). *Holding all other logits fixed, the donor softmax probability of τ_\star satisfies*

$$|p_d(\mathbf{x}_d) - p_d(\bar{\mathbf{x}}_d)| \leq \frac{1}{4} |\ell_d(\mathbf{x}_d) - \ell_d(\bar{\mathbf{x}}_d)| \leq \frac{L}{4} \|U\mathbf{x}_d\|_2,$$

since for a single-coordinate softmax $\frac{\partial p}{\partial \ell} = p(1 - p) \leq \frac{1}{4}$.

F.3. Spectral mimicry: in-span embeddings and audit non-outlierness

We formalize why the breaker token can be made to *not look special* under common geometric audits (nearest-neighbor checks, reconstruction residuals, PCA-based outlier scores, etc.). The core algebra is that our designer constructs \mathbf{x}_d as a combination of *existing* donor token vectors.

Theorem F.12 (In-span construction implies spectral mimicry). *Assume the attacker parameterizes the breaker row using shared-token anchors, i.e.,*

$$\mathbf{x}_d = \Phi_d^\top \boldsymbol{\alpha}, \quad \|\boldsymbol{\alpha}\|_0 \leq k, \quad (26)$$

as in the OMP instantiation (Section 4.2), where Φ_d stacks composite rows built from existing donor token embeddings/heads. Then:

- (i) (Exact span containment) $\mathbf{x}_d \in \text{span}\{\phi_j^{(d)} : j \in \mathcal{T}\} \subseteq \text{span}\{\mathbf{e}_v^{(d)}, \mathbf{h}_v^{(d)} : v \in \mathcal{V}_d\}$. Thus, any audit that flags tokens by large residual to the linear span of existing embeddings cannot separate τ_\star (the residual is exactly zero under the same dictionary).

(ii) (Controlled PCA residual) Let $P \in \mathbb{R}^{\delta_d \times \delta_d}$ be any orthogonal projector (e.g., onto a PCA subspace fit on the donor vocabulary), and define the residual score $r(\mathbf{x}) := \|(I - P)\mathbf{x}\|_2$. Then

$$r(\mathbf{x}_d) = \|(I - P)\Phi_d^\top \boldsymbol{\alpha}\|_2 \leq \|\boldsymbol{\alpha}\|_1 \cdot \max_{j \in \text{supp}(\boldsymbol{\alpha})} r(\phi_j^{(d)}). \quad (27)$$

In particular, if $\boldsymbol{\alpha}$ is nonnegative with $\|\boldsymbol{\alpha}\|_1 = 1$ (as in CLP/FOCUS mixtures) then $r(\mathbf{x}_d)$ lies in the convex hull of anchor residuals and cannot exceed the maximum anchor residual.

Proof. Part (i) is immediate from $\mathbf{x}_d = \Phi_d^\top \boldsymbol{\alpha}$ and the definition of Φ_d as a stack of composites built from existing rows. For (ii), use triangle inequality:

$$\|(I - P)\Phi_d^\top \boldsymbol{\alpha}\|_2 = \left\| \sum_j \alpha_j (I - P)\phi_j^{(d)} \right\|_2 \leq \sum_j |\alpha_j| \|(I - P)\phi_j^{(d)}\|_2 \leq \|\boldsymbol{\alpha}\|_1 \max_{j \in \text{supp}(\boldsymbol{\alpha})} r(\phi_j^{(d)}).$$

If $\alpha \geq 0$ and $\|\boldsymbol{\alpha}\|_1 = 1$, this is a convex combination. □

Remark F.13 (Why this matches “geometric audits”). Many practical audits are linear or locally linear: PCA residuals, low-rank reconstruction error, Mahalanobis distance in a fitted covariance, and “is this point far from the manifold” proxies. Theorem F.12 shows that by constructing \mathbf{x}_d as a sparse (or convex) combination of existing donor vectors, the breaker token inherits *in-distribution* residual scores whenever $\|\boldsymbol{\alpha}\|_1$ is controlled. This is the algebraic backbone of the spectral mimicry phenomenon (Section 5.5).

F.4. Stability under LoRA fine-tuning and weight merging

We next show that once the attacker has induced a salient base-side row $\widehat{\mathbf{x}}_b = T(\mathbf{x}_d)$, the resulting emission bias is robust to *small* changes in the base parameters. This covers (i) LoRA fine-tuning on QKV blocks and (ii) simple weight merging, both of which can be modeled as parameter perturbations.

A margin-based success condition. Fix a context c and write the attacked-base logit for the breaker token as

$$\ell_{\tau_*}^{(b)}(c) = \langle \mathbf{g}^{(b)}(c), \widehat{\mathbf{x}}_b \rangle.$$

Let the strongest competitor margin be

$$\Delta(c) := \ell_{\tau_*}^{(b)}(c) - \max_{v \in \mathcal{V}_b, v \neq \tau_*} \ell_v^{(b)}(c). \quad (28)$$

When $\Delta(c) \geq \Delta_0 > 0$, the breaker token is top-1 at that context, and the softmax probability satisfies the standard lower bound

$$p^{(b)}(\tau_* | c) = \frac{1}{1 + \sum_{v \neq \tau_*} \exp(\ell_v - \ell_{\tau_*})} \geq \frac{1}{1 + (|\mathcal{V}_b| - 1) \exp(-\Delta_0)}. \quad (29)$$

Thus, controlling how much $\Delta(c)$ can change under parameter perturbations controls attack persistence.

Perturbation model. Let θ denote all base parameters *excluding* the breaker row, and let $\widehat{\mathbf{x}}_b$ denote the breaker LM-head row. After fine-tuning or merging, parameters become $\theta' = \theta + \Delta\theta$ and the breaker row may become $\widehat{\mathbf{x}}'_b = \widehat{\mathbf{x}}_b + \Delta\mathbf{x}_b$ (for LoRA-on-QKV, typically $\Delta\mathbf{x}_b = \mathbf{0}$ because the head is frozen). Let $\mathbf{g}_\theta(c)$ denote the final hidden state under parameters θ .

Assumption F.14 (Uniform bounds on representations and head norms). There exist constants $G_b, H_b \geq 0$ such that for all contexts c and all tokens v ,

$$\|\mathbf{g}_\theta(c)\|_2 \leq G_b, \quad \|\mathbf{h}_v^{(b)}\|_2 \leq H_b, \quad \|\widehat{\mathbf{x}}_b\|_2 \leq H_b.$$

Assumption F.15 (Hidden-state stability under parameter perturbation). There exists $L_{\text{hid}} \geq 0$ such that for all contexts c ,

$$\|\mathbf{g}_{\theta'}(c) - \mathbf{g}_\theta(c)\|_2 \leq L_{\text{hid}} \|\Delta\theta\|,$$

where $\|\cdot\|$ is any chosen norm on parameter perturbations (e.g., Frobenius over affected weights). This holds for transformers under bounded activations/weights by standard Lipschitz composition arguments; we instantiate it for LoRA below.

Theorem F.16 (Margin robustness under small parameter changes). *Under Assumptions F.14–F.15, for every context c , the breaker margin shift satisfies*

$$|\Delta'(c) - \Delta(c)| \leq \underbrace{2H_b \|\mathbf{g}_{\theta'}(c) - \mathbf{g}_\theta(c)\|_2}_{\text{hidden-state drift}} + \underbrace{G_b \|\Delta \mathbf{x}_b\|_2}_{\text{head-row drift}}, \quad (30)$$

where $\Delta'(c)$ is the margin under $(\theta', \widehat{\mathbf{x}}'_b)$. Consequently, if $\Delta(c) \geq \Delta_0$ on a set of contexts and

$$2H_b L_{\text{hid}} \|\Delta\theta\| + G_b \|\Delta \mathbf{x}_b\|_2 \leq \Delta_0/2,$$

then $\Delta'(c) \geq \Delta_0/2$ on the same contexts, and the lower bound (29) holds with $\Delta_0/2$.

Proof. Fix c and define $M(c) := \max_{v \neq \tau_*} \ell_v^{(b)}(c)$ and $M'(c) := \max_{v \neq \tau_*} \ell_v^{(b)'}(c)$. Then

$$|\Delta'(c) - \Delta(c)| = |\ell'_{\tau_*} - \ell_{\tau_*} - (M'(c) - M(c))| \leq |\ell'_{\tau_*} - \ell_{\tau_*}| + |M'(c) - M(c)|.$$

For the breaker token,

$$\begin{aligned} |\ell'_{\tau_*} - \ell_{\tau_*}| &= |\langle \mathbf{g}_{\theta'}(c), \widehat{\mathbf{x}}_b + \Delta \mathbf{x}_b \rangle - \langle \mathbf{g}_\theta(c), \widehat{\mathbf{x}}_b \rangle| \\ &\leq |\langle \mathbf{g}_{\theta'}(c) - \mathbf{g}_\theta(c), \widehat{\mathbf{x}}_b \rangle| + |\langle \mathbf{g}_{\theta'}(c), \Delta \mathbf{x}_b \rangle| \\ &\leq \|\mathbf{g}_{\theta'}(c) - \mathbf{g}_\theta(c)\|_2 \|\widehat{\mathbf{x}}_b\|_2 + \|\mathbf{g}_{\theta'}(c)\|_2 \|\Delta \mathbf{x}_b\|_2 \leq H_b \|\Delta \mathbf{g}(c)\|_2 + G_b \|\Delta \mathbf{x}_b\|_2, \end{aligned}$$

where $\Delta \mathbf{g}(c) := \mathbf{g}_{\theta'}(c) - \mathbf{g}_\theta(c)$. For the competitor maximum, for any $v \neq \tau_*$,

$$|\ell'_v - \ell_v| = |\langle \Delta \mathbf{g}(c), \mathbf{h}_v^{(b)} \rangle| \leq \|\Delta \mathbf{g}(c)\|_2 \|\mathbf{h}_v^{(b)}\|_2 \leq H_b \|\Delta \mathbf{g}(c)\|_2,$$

hence $|M'(c) - M(c)| \leq H_b \|\Delta \mathbf{g}(c)\|_2$ by standard “max is 1-Lipschitz” reasoning. Combining gives (30). \square

LoRA-on-QKV as a small perturbation. For the setting in Section 5.3, fine-tuning applies LoRA updates only to QKV matrices in attention blocks. A LoRA update has the form

$$W \leftarrow W + \Delta W, \quad \Delta W = \frac{\alpha}{r} BA,$$

with rank at most r , and thus

$$\|\Delta W\|_2 \leq \frac{\alpha}{r} \|B\|_2 \|A\|_2, \quad \|\Delta W\|_F \leq \frac{\alpha}{r} \|B\|_F \|A\|_F. \quad (31)$$

Under bounded activations (a standard assumption in transformer stability analyses), each layer is Lipschitz in its weights, so Assumption F.15 holds with L_{hid} proportional to a product of per-layer Lipschitz factors and a sum of $\|\Delta W_{\text{QKV}}^{(\ell)}\|$ terms.² Crucially, in this LoRA setting $\Delta \mathbf{x}_b = \mathbf{0}$ (LM head untouched), so robustness is controlled purely by hidden-state drift.

Simple weight merging. A common merge is $\theta' = (1-t)\theta + t\theta_{\text{ref}}$ for $t \in [0, 1]$, giving $\|\Delta\theta\| = t\|\theta_{\text{ref}} - \theta\|$. If the merge keeps the breaker row fixed (as in our mitigation experiments), then $\Delta \mathbf{x}_b = \mathbf{0}$ and Theorem F.16 applies directly. Even when the breaker row is merged linearly, $\Delta \mathbf{x}_b$ is still $O(t)$, so the same margin condition yields persistence for small-to-moderate t .

F.5. Operational sweet spot for λ

We now analyze the trade-off parameter λ in the OMP-style designer (Eq. 3) and show a mathematically explicit reason a *wide* operational window can exist: on a fixed support, the donor-penalty quantity decays as $O(\lambda^{-2})$ while the base-alignment quantity decays as $O(\lambda^{-1})$.

²A loose but correct bound follows by applying triangle inequality to the Q/K/V linear maps, using softmax Jacobian norm bounds, and propagating through residual connections via a Grönwall-type recursion. We omit constant-tightening because the paper’s goal is existence/robustness, not sharp constants.

Fixed-support ridge solve. Fix a support S (e.g., after the greedy selection is held constant). Let $s := |S|$, $B = \Phi_{b,S} \in \mathbb{R}^{s \times \delta_b}$, $D = \Phi_{d,S} \in \mathbb{R}^{s \times \delta_d}$, and let $U \in \mathbb{R}^{r \times \delta_d}$ have orthonormal rows. Define the PSD matrix

$$Q := DU^\top U D^\top = (DU^\top)(DU^\top)^\top \succeq 0,$$

the PD matrix

$$A_0 := 2\gamma BB^\top + \text{ridge } I \succ 0,$$

and

$$A_\lambda := A_0 + \lambda Q \succ 0.$$

Let the base target be t (in our main setting $t = \mu_{\text{base}}$) and define $c := Bt \in \mathbb{R}^s$. The coefficient vector used by the designer is

$$\alpha_\lambda := A_\lambda^{-1}c, \quad \mathbf{x}_b(\lambda) := B^\top \alpha_\lambda, \quad \mathbf{x}_d(\lambda) := D^\top \alpha_\lambda.$$

Define the base alignment surrogate and donor penalty surrogate

$$m(\lambda) := \langle \mathbf{x}_b(\lambda), t \rangle = t^\top B^\top A_\lambda^{-1}(Bt) = c^\top A_\lambda^{-1}c, \quad (32)$$

$$u(\lambda) := \|\mathbf{U}\mathbf{x}_d(\lambda)\|_2^2 = \alpha_\lambda^\top Q \alpha_\lambda = c^\top A_\lambda^{-1}QA_\lambda^{-1}c. \quad (33)$$

Lemma F.17 (Monotonicity on a fixed support). *For $\lambda \geq 0$, both $m(\lambda)$ and $u(\lambda)$ are differentiable and nonincreasing, with*

$$\frac{d}{d\lambda}m(\lambda) = -u(\lambda) \leq 0, \quad (34)$$

$$\frac{d}{d\lambda}u(\lambda) = -2c^\top A_\lambda^{-1}QA_\lambda^{-1}QA_\lambda^{-1}c \leq 0. \quad (35)$$

Proof. Use $\frac{d}{d\lambda}A_\lambda^{-1} = -A_\lambda^{-1}QA_\lambda^{-1}$ and differentiate $m(\lambda) = c^\top A_\lambda^{-1}c$ to obtain (34). Similarly differentiate $u(\lambda) = c^\top A_\lambda^{-1}QA_\lambda^{-1}c$ to obtain (35). \square

Equation (34) is worth pausing on:

$$m(\lambda) = m(0) - \int_0^\lambda u(t) dt,$$

so base alignment decreases by the *area* under the donor penalty curve. If $u(\lambda)$ collapses quickly (as it does under the $O(\lambda^{-2})$ decay below), then $m(\lambda)$ loses only a modest amount even for large increases in λ .

Diagonalization: $u(\lambda)$ decays faster than $m(\lambda)$. Since $A_0 \succ 0$, define the symmetric PSD matrix

$$M := A_0^{-1/2}QA_0^{-1/2} \succeq 0.$$

Diagonalize $M = V \text{diag}(\sigma_1, \dots, \sigma_s)V^\top$ with $\sigma_i \geq 0$ and V orthogonal. Let $\mathbf{z} := A_0^{-1/2}c$ and $\tilde{\mathbf{z}} := V^\top \mathbf{z}$, so $\|\tilde{\mathbf{z}}\|_2 = \|\mathbf{z}\|_2$. Then

$$A_\lambda^{-1} = A_0^{-1/2}(I + \lambda M)^{-1}A_0^{-1/2} = A_0^{-1/2}V \text{diag}\left(\frac{1}{1 + \lambda\sigma_i}\right)V^\top A_0^{-1/2}, \quad (36)$$

$$m(\lambda) = \mathbf{z}^\top (I + \lambda M)^{-1} \mathbf{z} = \sum_{i=1}^s \frac{\tilde{z}_i^2}{1 + \lambda\sigma_i}, \quad (37)$$

$$u(\lambda) = \mathbf{z}^\top (I + \lambda M)^{-1} M (I + \lambda M)^{-1} \mathbf{z} = \sum_{i=1}^s \frac{\sigma_i \tilde{z}_i^2}{(1 + \lambda\sigma_i)^2}. \quad (38)$$

As $\lambda \rightarrow \infty$, every term with $\sigma_i > 0$ satisfies

$$\frac{\tilde{z}_i^2}{1 + \lambda\sigma_i} = O(\lambda^{-1}), \quad \frac{\sigma_i \tilde{z}_i^2}{(1 + \lambda\sigma_i)^2} = O(\lambda^{-2}),$$

so the donor penalty $u(\lambda)$ decays one order faster.

Theorem F.18 (Existence of a λ window on a fixed support). *Fix a support S and define $m(\lambda), u(\lambda)$ as above. Let $\sigma_{\max} := \max_i \sigma_i$ and let $\sigma_{\min}^+ := \min\{\sigma_i : \sigma_i > 0\}$ (if all $\sigma_i = 0$, then $u(\lambda) \equiv 0$ and donor innocuity holds for all λ). Let $S_0 := \|\mathbf{z}\|_2^2 = \|A_0^{-1/2} \mathbf{c}\|_2^2$. Then for all $\lambda \geq 0$,*

$$m(\lambda) \geq \frac{S_0}{1 + \lambda \sigma_{\max}}, \quad u(\lambda) \leq \frac{\sigma_{\max} S_0}{(1 + \lambda \sigma_{\min}^+)^2}. \quad (39)$$

Consequently, for any desired thresholds $m_{\min} > 0$ (activation) and $u_{\max} > 0$ (stealth), a sufficient condition for the existence of λ satisfying both $m(\lambda) \geq m_{\min}$ and $u(\lambda) \leq u_{\max}$ is that

$$\underbrace{\frac{\sqrt{\sigma_{\max} S_0 / u_{\max}} - 1}{\sigma_{\min}^+}}_{\lambda_{\text{stealth}}} \leq \underbrace{\frac{S_0 / m_{\min} - 1}{\sigma_{\max}}}_{\lambda_{\text{act}}}. \quad (40)$$

Whenever (40) holds, any $\lambda \in [\lambda_{\text{stealth}}, \lambda_{\text{act}}]$ is an operational sweet spot: donor penalty is small while base alignment remains large.

Proof. The lower bound on $m(\lambda)$ follows from $\frac{1}{1 + \lambda \sigma_i} \geq \frac{1}{1 + \lambda \sigma_{\max}}$:

$$m(\lambda) = \sum_i \frac{\tilde{z}_i^2}{1 + \lambda \sigma_i} \geq \frac{1}{1 + \lambda \sigma_{\max}} \sum_i \tilde{z}_i^2 = \frac{S_0}{1 + \lambda \sigma_{\max}}.$$

For $u(\lambda)$, use $\sigma_i \leq \sigma_{\max}$ and $(1 + \lambda \sigma_i) \geq (1 + \lambda \sigma_{\min}^+)$ whenever $\sigma_i > 0$:

$$u(\lambda) = \sum_{\sigma_i > 0} \frac{\sigma_i \tilde{z}_i^2}{(1 + \lambda \sigma_i)^2} \leq \frac{\sigma_{\max}}{(1 + \lambda \sigma_{\min}^+)^2} \sum_{\sigma_i > 0} \tilde{z}_i^2 \leq \frac{\sigma_{\max} S_0}{(1 + \lambda \sigma_{\min}^+)^2}.$$

Solving these sufficient inequalities for λ yields the interval. □

Support changes. For the full greedy procedure, the support S can change with λ , so the maps $\lambda \mapsto m(\lambda)$ and $\lambda \mapsto u(\lambda)$ become piecewise smooth with breakpoints when the selected support changes. Theorem F.18 explains why empirically the donor side typically collapses earlier: *within each fixed-support region*, the donor penalty decays one order faster in λ than base alignment.

F.6. Differentiable transplant operators are attackable under the same framework

We now show that FOCUS, CLP, and WECHSEL (Appendix E) can be attacked by the same dual-objective framework (Eq. 2), with the same donor innocuity and mimicry properties.

Definition F.19 (Anchor-mixture transplant operators). A transplant operator $f : \mathbb{R}^{\delta_a} \rightarrow \mathbb{R}^{\delta_b}$ is an *anchor-mixture* operator if there exists a (possibly data-dependent) coefficient map $w : \mathbb{R}^{\delta_a} \rightarrow \Delta^N$ such that

$$f(\mathbf{x}_d) = \Phi_b^\top w(\mathbf{x}_d), \quad w(\mathbf{x}_d) \in \Delta^N := \{\mathbf{w} \in \mathbb{R}^N : \mathbf{w} \geq 0, \mathbf{1}^\top \mathbf{w} = 1\}. \quad (41)$$

Proposition F.20 (FOCUS, CLP, WECHSEL are anchor-mixture operators). *The differentiable transplant operators in Appendix E can be written in the form (41) (possibly after an affine alignment inside w):*

- (i) **FOCUS:** $w(\mathbf{x}_d) = \text{softmax}(\beta \Phi_d \hat{\mathbf{x}}_d)$, so $f_{\text{FOC}}(\mathbf{x}_d) = \Phi_b^\top w(\mathbf{x}_d)$.
- (ii) **CLP:** $w(\mathbf{x}_d) \propto \text{ReLU}(\Phi_d \hat{\mathbf{x}}_d)$ (with normalization), hence $f_{\text{CLP}}(\mathbf{x}_d) = \Phi_b^\top w(\mathbf{x}_d)$.
- (iii) **WECHSEL:** $w(\mathbf{x}_d)$ is supported on a k -NN set computed from the aligned proxy $\tilde{\mathbf{x}}(\mathbf{x}_d)$ and is a softmax over distances on that neighbor set; thus $f_{\text{WEC}}(\mathbf{x}_d)$ is again a convex combination of base anchors.

Unified design objective. For any such operator f , our differentiable designer minimizes (Eq. 5):

$$\mathcal{L}(\mathbf{x}_d) = \gamma \|f(\mathbf{x}_d) - \boldsymbol{\mu}_{\text{base}}\|_2^2 + \lambda \|U\mathbf{x}_d\|_2^2 + \rho \|\mathbf{x}_d\|_2^2. \quad (5)$$

The two key properties required by the paper then follow from *the same* two algebraic facts: (i) donor innocuity depends only on $\|U\mathbf{x}_d\|_2$, not on the operator f ; (ii) base impact depends on $\|f(\mathbf{x}_d) - \boldsymbol{\mu}_{\text{base}}\|_2$, and f is a convex combination of base anchors.

Theorem F.21 (Donor innocuity and base impact extend to differentiable operators). *Let f be any anchor-mixture operator (Definition F.19). Let $\mathbf{x}_d^*(\lambda)$ be any minimizer of \mathcal{L} in (5). Then:*

- (i) (Donor innocuity) *The donor-side guarantees in Theorem F.5 and Theorem F.10 apply verbatim to $\mathbf{x}_d^*(\lambda)$ (they do not depend on f). In particular, if $\|U\mathbf{x}_d^*(\lambda)\|_2 \leq \epsilon$ then the donor logit deviation and TV-distance bounds hold with $O(\epsilon)$.*
- (ii) (Base impact) *Since $f(\mathbf{x}_d) \in \text{conv}\{\phi_j^{(b)}\}$ for all \mathbf{x}_d , any \mathbf{x}_d achieving small base loss $\|f(\mathbf{x}_d) - \boldsymbol{\mu}_{\text{base}}\|_2 \leq \delta$ induces a base-side breaker row within δ of the target direction. Thus, any context distribution whose hidden states concentrate near $\boldsymbol{\mu}_{\text{base}}$ yields elevated breaker logits $\langle \mathbf{g}^{(b)}(c), f(\mathbf{x}_d) \rangle$ by standard inner-product stability.*
- (iii) (Spectral mimicry remains enforceable) *If we additionally constrain the parameterization $\mathbf{x}_d = \Phi_d^\top \boldsymbol{\alpha}$ (as in Theorem F.12), then \mathbf{x}_d^* is in-span by construction, and the same residual bounds (27) apply.*

Remark F.22 (A constructive “attack” view for soft operators). For FOCUS, $w(\mathbf{x}_d) = \text{softmax}(\beta s(\mathbf{x}_d))$ with scores $s_j(\mathbf{x}_d) = \langle \widehat{\mathbf{x}}_d, \widehat{\phi}_j^{(d)} \rangle$. Given any desired weight vector \mathbf{w} in the interior of the simplex, there exists a score vector s with $\text{softmax}(\beta s) = \mathbf{w}$ (take $s_j = \beta^{-1} \log w_j$ up to an additive constant). Restricting to a small support S with $|S| \leq \delta_d$, one can solve (approximately) for $\widehat{\mathbf{x}}_d$ such that $s(\mathbf{x}_d)$ matches these target scores on S . This gives an explicit “reverse projection” intuition for why gradient-based optimization in Appendix E reliably finds effective breaker rows.

G. Additional Results

This appendix reports per-edge SER and utility tables for the suites described in §5.1 (with cross-scale transfer split into upstream/downstream edge sets). All values are reported at the fixed per-edge λ for the directed base←donor edge. SER is measured on Alpaca, SQuAD v2, and GSM8K; utilities include WikiText-103, LAMBADA, and ARC (among others). See §5.1 for dataset and model citations.

G.1. The Lightweight Clique ($\mathcal{C}_{\text{Light}}$)

Table 4: The Lightweight Clique ($\mathcal{C}_{\text{Light}}$) (per-edge SER; fractions)

B	D	λ	SER (atk-base / pat-donor)			
			Alpaca	SQuAD	GSM8K	SER _{max}
Q2-0.5B	Q3-0.6B	1280	.0156/.0000	.0156/.0000	.0000/.0000	.0156/.0000
Q2-0.5B	Gem2-2B	768	.2266/.0430	.2031/.0156	.0234/.0117	.2266/.0430
Q2-0.5B	Gem3-1B	512	.6445/.0547	.2930/.0781	.1797/.0078	.6445/.0781
Q2-0.5B	Min-3B	2048	.9805/.0000	.9844/.0039	1.0000/.0000	1.0000/.0039
Q3-0.6B	Q2-0.5B	1024	.0000/.0000	.0000/.0000	.0000/.0000	.0000/.0000
Q3-0.6B	Gem2-2B	256	.5742/.0000	.6016/.0039	.5781/.0000	.6016/.0039
Q3-0.6B	Gem3-1B	1024	.0000/.0000	.0000/.0000	.0000/.0000	.0000/.0000
Q3-0.6B	Min-3B	2048	.9961/.0000	1.0000/.0078	1.0000/.0039	1.0000/.0078
Gem2-2B	Q2-0.5B	256	.1367/.0078	.3672/.0000	.7734/.0000	.7734/.0078
Gem2-2B	Q3-0.6B	128	.1406/.0000	.6367/.0000	.8789/.0000	.8789/.0000
Gem2-2B	Gem3-1B	128	.0117/.0078	.0117/.0039	.0000/.0000	.0117/.0078
Gem2-2B	Min-3B	512	.9922/.0078	1.0000/.0078	.9844/.0000	1.0000/.0078
Gem3-1B	Q2-0.5B	512	.0742/.0000	.0859/.0039	.3086/.0000	.3086/.0039
Gem3-1B	Q3-0.6B	512	.3320/.0000	.4727/.0000	.6992/.0000	.6992/.0000
Gem3-1B	Gem2-2B	512	1.0000/.0000	.9883/.0000	1.0000/.0000	1.0000/.0000
Gem3-1B	Min-3B	2048	.6562/.0078	.7891/.0078	.3398/.0000	.7891/.0078
Min-3B	Q2-0.5B	1280	.3125/.0117	.2617/.0039	.3906/.0000	.3906/.0117
Min-3B	Q3-0.6B	512	.0547/.0000	.0625/.0000	.0898/.0000	.0898/.0000
Min-3B	Gem2-2B	256	.9922/.0000	1.0000/.0000	1.0000/.0000	1.0000/.0000

The Trojan in the Vocabulary: Stealthy Sabotage of LLM Composition

B	D	λ	SER (atk-base / pat-donor)			
			Alpaca	SQuAD	GSM8K	SER _{max}
Min-3B	Gem3-1B	1024	.1055/.0000	.0977/.0000	.1953/.0000	.1953/.0000

Table 5: The Lightweight Clique (C_{Light}) (base utilities; cells show pretrained/after-OMP/after-attack; value \pm stderr when available)

B	D	λ	wikitext	lambada_openai	mmlu	arc_challenge
			word_perplexity	acc	acc	acc_norm
Q2-0.5B	Q3-0.6B	1280	18.02/18.04/18.05	.50 \pm .01/.50 \pm .01/.50 \pm .01	.45 \pm .01/.45 \pm .01/.45 \pm .01	.34 \pm .04/.34 \pm .04/.34 \pm .04
Q2-0.5B	Gem2-2B	768	18.02/30.78/30.88	.50 \pm .01/.43 \pm .01/.43 \pm .01	.45 \pm .01/.41 \pm .01/.41 \pm .01	.34 \pm .04/.34 \pm .04/.34 \pm .04
Q2-0.5B	Gem3-1B	512	18.02/27.24/28.53	.50 \pm .01/.43 \pm .01/.42 \pm .01	.45 \pm .01/.42 \pm .01/.42 \pm .01	.34 \pm .04/.31 \pm .04/.31 \pm .04
Q2-0.5B	Min-3B	2048	18.02/43.02/734.85	.50 \pm .01/.41 \pm .01/.02 \pm .00	.45 \pm .01/.34 \pm .01/.34 \pm .01	.34 \pm .04/.28 \pm .04/.27 \pm .04
Q3-0.6B	Q2-0.5B	1024	26.16/26.13/26.13	.40 \pm .01/.40 \pm .01/.40 \pm .01	.41 \pm .01/.41 \pm .01/.41 \pm .01	.35 \pm .04/.35 \pm .04/.35 \pm .04
Q3-0.6B	Gem2-2B	256	26.16/596.41/602.43	.40 \pm .01/.24 \pm .01/.24 \pm .01	.41 \pm .01/.26 \pm .01/.27 \pm .01	.35 \pm .04/.28 \pm .04/.28 \pm .04
Q3-0.6B	Gem3-1B	1024	26.16/42.04/42.02	.40 \pm .01/.34 \pm .01/.34 \pm .01	.41 \pm .01/.42 \pm .01/.42 \pm .01	.35 \pm .04/.35 \pm .04/.35 \pm .04
Q3-0.6B	Min-3B	2048	26.16/107.04/446.54	.40 \pm .01/.34 \pm .01/.10 \pm .00	.41 \pm .01/.42 \pm .01/.42 \pm .01	.35 \pm .04/.33 \pm .04/.31 \pm .04
Gem2-2B	Q2-0.5B	256	14.19/28.95/29.39	.64 \pm .01/.21 \pm .01/.20 \pm .01	.58 \pm .01/.30 \pm .01/.30 \pm .01	.52 \pm .04/.33 \pm .04/.33 \pm .04
Gem2-2B	Q3-0.6B	128	14.19/28.40/28.79	.64 \pm .01/.22 \pm .01/.21 \pm .01	.58 \pm .01/.31 \pm .01/.31 \pm .01	.52 \pm .04/.32 \pm .04/.32 \pm .04
Gem2-2B	Gem3-1B	128	14.19/17.32/17.32	.64 \pm .01/.62 \pm .01/.62 \pm .01	.58 \pm .01/.56 \pm .01/.56 \pm .01	.52 \pm .04/.52 \pm .04/.52 \pm .04
Gem2-2B	Min-3B	512	14.19/58.79/78.11	.64 \pm .01/.48 \pm .01/.31 \pm .01	.58 \pm .01/.52 \pm .01/.52 \pm .01	.52 \pm .04/.47 \pm .04/.41 \pm .04
Gem3-1B	Q2-0.5B	512	29.06/47.70/47.73	.44 \pm .01/.17 \pm .01/.17 \pm .01	.40 \pm .01/.26 \pm .01/.26 \pm .01	.41 \pm .04/.23 \pm .04/.27 \pm .04
Gem3-1B	Q3-0.6B	512	29.06/46.11/46.46	.44 \pm .01/.17 \pm .01/.16 \pm .01	.40 \pm .01/.25 \pm .01/.25 \pm .01	.41 \pm .04/.25 \pm .04/.25 \pm .04
Gem3-1B	Gem2-2B	512	29.06/35.35/50.24	.44 \pm .01/.42 \pm .01/.31 \pm .01	.40 \pm .01/.39 \pm .01/.39 \pm .01	.41 \pm .04/.42 \pm .04/.41 \pm .04
Gem3-1B	Min-3B	2048	29.06/85.42/87.50	.44 \pm .01/.36 \pm .01/.35 \pm .01	.40 \pm .01/.28 \pm .01/.28 \pm .01	.41 \pm .04/.40 \pm .04/.41 \pm .04
Min-3B	Q2-0.5B	1280	93.86/446.98/447.70	.23 \pm .01/.14 \pm .00/.14 \pm .00	.24 \pm .01/.25 \pm .01/.25 \pm .01	.27 \pm .04/.28 \pm .04/.28 \pm .04
Min-3B	Q3-0.6B	512	93.86/425.86/426.14	.23 \pm .01/.14 \pm .00/.14 \pm .00	.24 \pm .01/.25 \pm .01/.25 \pm .01	.27 \pm .04/.30 \pm .04/.30 \pm .04
Min-3B	Gem2-2B	256	93.86/710.94/791.39	.23 \pm .01/.15 \pm .00/.15 \pm .00	.24 \pm .01/.24 \pm .01/.24 \pm .01	.27 \pm .04/.32 \pm .04/.31 \pm .04
Min-3B	Gem3-1B	1024	93.86/453.53/453.65	.23 \pm .01/.15 \pm .01/.15 \pm .01	.24 \pm .01/.25 \pm .01/.25 \pm .01	.27 \pm .04/.33 \pm .04/.33 \pm .04

Table 6: The Lightweight Clique (C_{Light}) (donor utilities; cells show pretrained/after-patch; value \pm stderr when available)

B	D	λ	wikitext	lambada_openai	mmlu	arc_challenge
			word_perplexity	acc	acc	acc_norm
Q2-0.5B	Q3-0.6B	1280	26.16/26.14	.40 \pm .01/.40 \pm .01	.41 \pm .01/.41 \pm .01	.35 \pm .04/.35 \pm .04
Q2-0.5B	Gem2-2B	768	14.19/14.25	.64 \pm .01/.64 \pm .01	.58 \pm .01/.58 \pm .01	.52 \pm .04/.52 \pm .04
Q2-0.5B	Gem3-1B	512	29.06/29.96	.44 \pm .01/.43 \pm .01	.40 \pm .01/.40 \pm .01	.41 \pm .04/.41 \pm .04
Q2-0.5B	Min-3B	2048	93.86/93.90	.23 \pm .01/.22 \pm .01	.24 \pm .01/.24 \pm .01	.27 \pm .04/.27 \pm .04
Q3-0.6B	Q2-0.5B	1024	18.02/18.04	.50 \pm .01/.50 \pm .01	.45 \pm .01/.45 \pm .01	.34 \pm .04/.34 \pm .04
Q3-0.6B	Gem2-2B	256	14.19/14.19	.64 \pm .01/.64 \pm .01	.58 \pm .01/.58 \pm .01	.52 \pm .04/.52 \pm .04
Q3-0.6B	Gem3-1B	1024	29.06/29.06	.44 \pm .01/.44 \pm .01	.40 \pm .01/.40 \pm .01	.41 \pm .04/.40 \pm .04
Q3-0.6B	Min-3B	2048	93.86/93.90	.23 \pm .01/.22 \pm .01	.24 \pm .01/.24 \pm .01	.27 \pm .04/.27 \pm .04
Gem2-2B	Q2-0.5B	256	18.02/18.04	.50 \pm .01/.50 \pm .01	.45 \pm .01/.45 \pm .01	.34 \pm .04/.34 \pm .04
Gem2-2B	Q3-0.6B	128	26.16/26.14	.40 \pm .01/.40 \pm .01	.41 \pm .01/.41 \pm .01	.35 \pm .04/.35 \pm .04
Gem2-2B	Gem3-1B	128	29.06/29.16	.44 \pm .01/.44 \pm .01	.40 \pm .01/.40 \pm .01	.41 \pm .04/.40 \pm .04
Gem2-2B	Min-3B	512	93.86/93.90	.23 \pm .01/.22 \pm .01	.24 \pm .01/.24 \pm .01	.27 \pm .04/.27 \pm .04
Q3-0.6B	Q2-0.5B	512	18.02/18.05	.50 \pm .01/.50 \pm .01	.45 \pm .01/.45 \pm .01	.34 \pm .04/.34 \pm .04
Gem3-1B	Q3-0.6B	512	26.16/26.14	.40 \pm .01/.40 \pm .01	.41 \pm .01/.41 \pm .01	.35 \pm .04/.35 \pm .04
Gem3-1B	Gem2-2B	512	14.19/14.19	.64 \pm .01/.64 \pm .01	.58 \pm .01/.58 \pm .01	.52 \pm .04/.52 \pm .04
Gem3-1B	Min-3B	2048	93.86/93.90	.23 \pm .01/.22 \pm .01	.24 \pm .01/.24 \pm .01	.27 \pm .04/.27 \pm .04
Min-3B	Q2-0.5B	1280	18.02/18.05	.50 \pm .01/.50 \pm .01	.45 \pm .01/.45 \pm .01	.34 \pm .04/.34 \pm .04
Min-3B	Q3-0.6B	512	26.16/26.14	.40 \pm .01/.40 \pm .01	.41 \pm .01/.41 \pm .01	.35 \pm .04/.35 \pm .04
Min-3B	Gem2-2B	256	14.19/14.19	.64 \pm .01/.64 \pm .01	.58 \pm .01/.58 \pm .01	.52 \pm .04/.52 \pm .04
Min-3B	Gem3-1B	1024	29.06/29.06	.44 \pm .01/.44 \pm .01	.40 \pm .01/.40 \pm .01	.41 \pm .04/.42 \pm .04

G.2. The Standard-Scale Clique (C_{Std})

The main text focuses on lightweight models ($\leq 3B$) to enable dense directed evaluation. Here we test whether the same coefficient-reuse vulnerability persists at *standard* scales, using Gemma-2-9B-it, Llama-3-8B, and Mistral-7B-v0.1. This setting matters because shared-basis transplant is frequently used when adapting or harmonizing tokenizers across higher-capacity models, where subtle embedding perturbations can be harder to audit.

Activation and donor innocuity (SER). Table 7 shows that the asymmetry observed in C_{Light} persists but is more heterogeneous: across the 6 directed edges, the attacked-base SER_{max} averages 0.54 while the patched-donor SER_{max} averages 0.043. Figure 9 visualizes the same per-edge SER values as dumbbells, making the base-donor gap (or lack thereof)

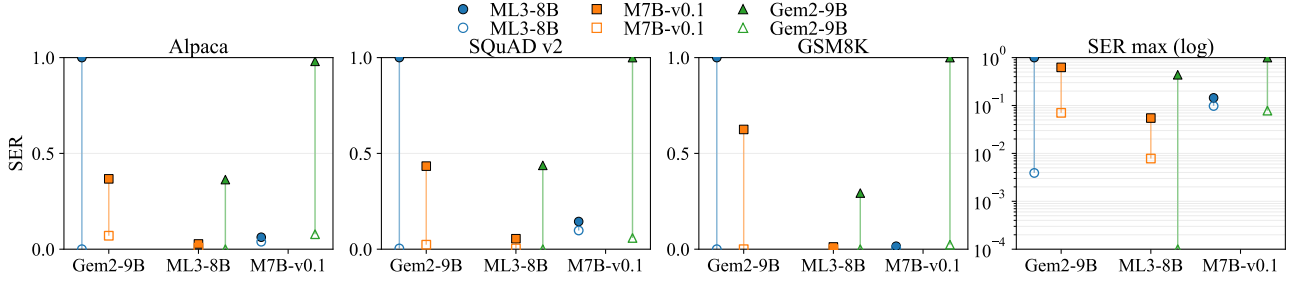


Figure 9. SER dumbbell plots for The Standard-Scale Clique (\mathcal{C}_{Std}). Columns show Alpaca, SQuAD v2, and GSM8K SER (plus SER_{max} in the last column). Each dumbbell connects patched-donor SER (open) to attacked-base SER (filled).

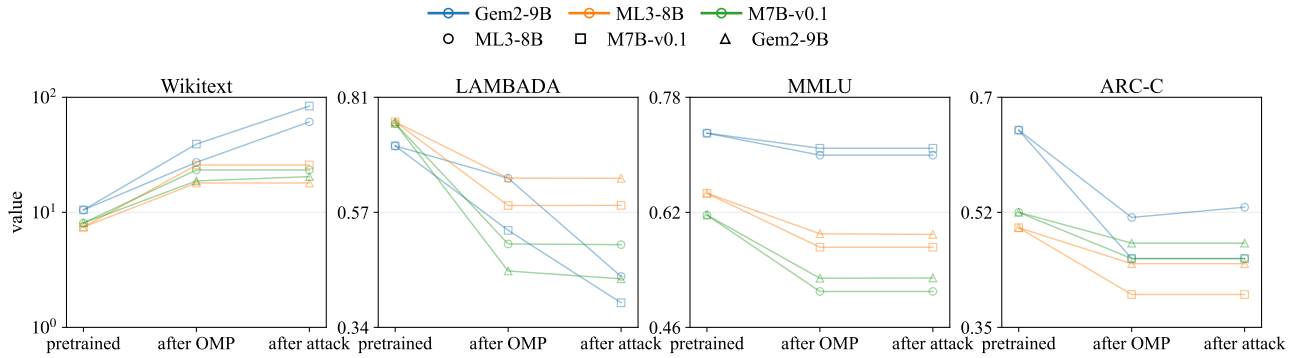


Figure 10. Three-stage base-utility slope charts for The Standard-Scale Clique (\mathcal{C}_{Std}). Each line is one directed edge (base \leftarrow donor), tracking pretrained \rightarrow after-OMP \rightarrow after-attack utilities.

easy to compare across edges. On the strongest edge (Gem2-9B \leftarrow ML3-8B), the attacked base achieves $\text{SER}_{\text{max}} = 1.0000$ while the donor remains effectively silent ($\text{SER}_{\text{max}} = .0039$). At the same time, several edges exhibit weaker separation (e.g., M7B-v0.1 \leftarrow ML3-8B has attacked-base $\text{SER}_{\text{max}} = .1445$ and donor $\text{SER}_{\text{max}} = .0977$), illustrating that cross-family geometry can tighten the activation–innocuity window at this scale.

Utility behavior. Despite the above heterogeneity in SER, donor-side utility remains essentially unchanged across all edges (Table 9), consistent with the innocuity objective. This stability is also visible in Figure 11, where donor points remain near the identity line. Base-side utility changes again largely follow the *clean transplant* step (Table 8), with the attack often adding a smaller incremental shift; however, on edges with near-saturated base activation, the post-attack degradation can be substantial. Figure 10 summarizes these three-stage base-utility trajectories (pretrained \rightarrow after-OMP \rightarrow after-attack). For example, for Gem2-9B \leftarrow ML3-8B, Wikitext perplexity rises from 10.49 \rightarrow 27.21 after-OMP and further to 61.12 after-attack, while LAMBADA drops from $.71 \pm .01 \rightarrow .64 \pm .01 \rightarrow .44 \pm .01$. We interpret this pattern as a signature of successful activation: when many prompts are steered toward emitting the breaker token, normal task outputs are displaced, producing an additional utility drop beyond the transplant baseline.

Table 7: The Standard-Scale Clique (\mathcal{C}_{Std}) (per-edge SER; fractions)

B	D	λ	SER (atk-base / pat-donor)			
			Alpaca	SQuAD	GSM8K	SER_{max}
Gem2-9B	ML3-8B	512	1.0000/0000	1.0000/0039	1.0000/0000	1.0000/0039
Gem2-9B	M7B-v0.1	512	.3672/.0703	.4336/.0234	.6250/0000	.6250/.0703
ML3-8B	Gem2-9B	64	.3633/0000	.4375/0000	.2930/0000	.4375/0000
ML3-8B	M7B-v0.1	1280	.0273/.0078	.0547/.0039	.0117/0000	.0547/.0078
M7B-v0.1	Gem2-9B	256	.9805/.0781	1.0000/.0586	1.0000/.0234	1.0000/.0781
M7B-v0.1	ML3-8B	1024	.0625/.0391	.1445/.0977	.0156/.0078	.1445/.0977

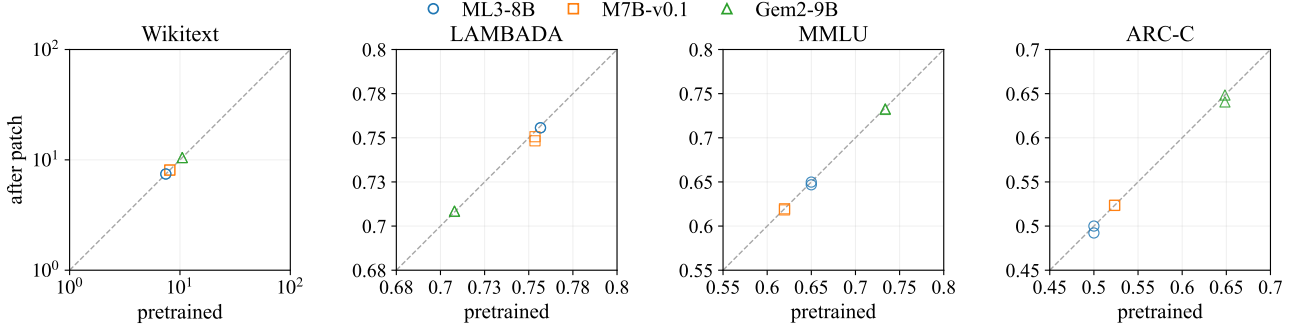


Figure 11. Donor utility identity scatter for The Standard-Scale Clique (C_{Sid}). Each point is an edge; x-axis is donor pretrained utility and y-axis is post-patch utility (identity dashed).

Table 8: The Standard-Scale Clique (C_{Sid}) (base utilities; cells show pretrained/after-OMP/after-attack; value \pm stderr when available)

B	D	λ	wikitext word_perplexity	lambada_openai acc	mmlu acc	arc_challenge acc_norm
Gem2-9B	ML3-8B	512	10.49/27.21/61.12	.71 \pm .01/.64 \pm .01/.44 \pm .01	.73 \pm .01/.70 \pm .01/.70 \pm .01	.65 \pm .04/.52 \pm .04/.53 \pm .04
Gem2-9B	M7B-v0.1	512	10.49/39.21/83.90	.71 \pm .01/.54 \pm .01/.39 \pm .01	.73 \pm .01/.71 \pm .01/.71 \pm .01	.65 \pm .04/.45 \pm .04/.45 \pm .04
ML3-8B	Gem2-9B	64	7.44/18.00/18.00	.76 \pm .01/.64 \pm .01/.64 \pm .01	.65 \pm .01/.59 \pm .01/.59 \pm .01	.50 \pm .04/.45 \pm .04/.45 \pm .04
ML3-8B	M7B-v0.1	1280	7.44/25.76/25.81	.76 \pm .01/.59 \pm .01/.59 \pm .01	.65 \pm .01/.57 \pm .01/.57 \pm .01	.50 \pm .04/.40 \pm .04/.40 \pm .04
M7B-v0.1	Gem2-9B	256	8.09/18.74/20.44	.75 \pm .01/.45 \pm .01/.44 \pm .01	.62 \pm .01/.53 \pm .01/.53 \pm .01	.52 \pm .04/.48 \pm .04/.48 \pm .04
M7B-v0.1	ML3-8B	1024	8.09/23.34/23.36	.75 \pm .01/.51 \pm .01/.51 \pm .01	.62 \pm .01/.51 \pm .01/.51 \pm .01	.52 \pm .04/.45 \pm .04/.45 \pm .04

Table 9: The Standard-Scale Clique (C_{Sid}) (donor utilities; cells show pretrained/after-patch; value \pm stderr when available)

B	D	λ	wikitext word_perplexity	lambada_openai acc	mmlu acc	arc_challenge acc_norm
Gem2-9B	ML3-8B	512	7.44/7.45	.76 \pm .01/.76 \pm .01	.65 \pm .01/.65 \pm .01	.50 \pm .04/.49 \pm .04
Gem2-9B	M7B-v0.1	512	8.09/8.08	.75 \pm .01/.75 \pm .01	.62 \pm .01/.62 \pm .01	.52 \pm .04/.52 \pm .04
ML3-8B	Gem2-9B	64	10.49/10.49	.71 \pm .01/.71 \pm .01	.73 \pm .01/.73 \pm .01	.65 \pm .04/.64 \pm .04
ML3-8B	M7B-v0.1	1280	8.09/8.08	.75 \pm .01/.75 \pm .01	.62 \pm .01/.62 \pm .01	.52 \pm .04/.52 \pm .04
M7B-v0.1	Gem2-9B	256	10.49/10.49	.71 \pm .01/.71 \pm .01	.73 \pm .01/.73 \pm .01	.65 \pm .04/.65 \pm .04
M7B-v0.1	ML3-8B	1024	7.44/7.45	.76 \pm .01/.76 \pm .01	.65 \pm .01/.65 \pm .01	.50 \pm .04/.50 \pm .04

G.3. Cross-Scale Transfer Sets ($\mathcal{T}_{Cross}^\downarrow$), downstream (small base \leftarrow large donor)

Downstream transfer reflects a common practical use case: a high-capacity donor provides a tokenizer row that is transplanted into a smaller base (e.g., when aligning to a shared tokenizer or reusing a curated vocabulary). This setting stress-tests whether our attack can remain *donor-stealthy* while still mapping—after transplant—onto a salient base direction under a large capacity gap. Concretely, the bases include SmolLM2, Qwen2.5, Gemma-2/3, and Llama-3.2, while the donors include Qwen2/3, Llama-3, and Mistral-7B.

Activation and donor innocuity (SER). Table 10 shows strong base-side activation on many edges: the median attacked-base SER_{max} is 0.9336, and 12/23 edges achieve $SER_{max} \geq 0.9$ while keeping donor $SER_{max} \leq 0.01$. Figure 12 provides a compact view of the same per-edge gaps across the downstream transfer suite. Representative examples include Gem2-2B \leftarrow ML3-8B and Gem2-2B \leftarrow L3.1-8B, both with attacked-base $SER_{max} = 1.0000$ and donor $SER_{max} = 0.0000$. However, downstream transfer also exposes failure modes: Smol1.7B \leftarrow L3.1-8B yields $SER_{max} = 0$ on both base and donor, and one edge (Gem3-1B \leftarrow Q2-7B) exhibits noticeable donor activation ($SER_{max} = .2656$), indicating that donor suppression can be less effective for certain donors even when base activation remains high.

Utility behavior. Across this downstream suite, donor utilities remain essentially invariant (Table 12), supporting donor-side stealth under a large donor. This invariance is reflected in Figure 14, where donor points cluster near the identity line. Base utilities often incur their largest change at the clean transplant stage (Table 11); e.g., Smol1.7B \leftarrow Q2-7B has Wikitext 11.94 \rightarrow 21.58 \rightarrow 21.75 and LAMBADA .65 \pm .01 \rightarrow .53 \pm .01 \rightarrow .51 \pm .01. Figure 13 summarizes these

The Trojan in the Vocabulary: Stealthy Sabotage of LLM Composition

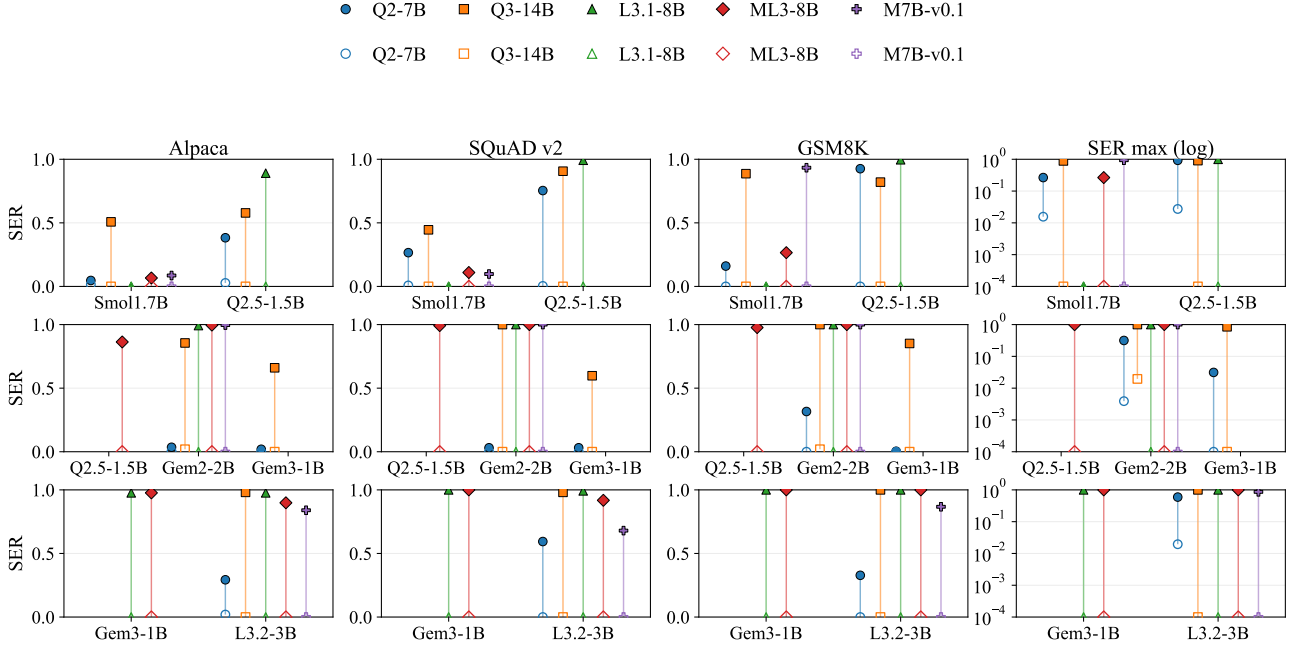


Figure 12. SER dumbbell plots for $\mathcal{T}_{\text{Cross}}^{\downarrow}$ (downstream; small base←large donor). Each dumbbell connects patched-donor SER (open) to attacked-base SER (filled).

three-stage trajectories across the downstream edges. When base activation is extreme, the attack can add a larger marginal drop, consistent with the base being pulled toward emitting the breaker token (e.g., Smol1.7B←M7B-v0.1 has Wikitext $11.94 \rightarrow 31.76 \rightarrow 72.55$ and LAMBADA $.65 \pm .01 \rightarrow .53 \pm .01 \rightarrow .36 \pm .01$).

Table 10: Cross-Scale Transfer Sets ($\mathcal{T}_{\text{Cross}}^{\downarrow}$), downstream (small base←large donor) (per-edge SER; fractions)

B	D	λ	SER (atk-base / pat-donor)			
			Alpaca	SQuAD	GSM8K	SER _{max}
Smol1.7B	Q2-7B	128	.0469/.0156	.2656/.0078	.1602/.0000	.2656/.0156
Smol1.7B	Q3-14B	64	.5078/.0000	.4453/.0000	.8867/.0000	.8867/.0000
Smol1.7B	L3.1-8B	512	.0000/.0000	.0000/.0000	.0000/.0000	.0000/.0000
Smol1.7B	ML3-8B	512	.0664/.0000	.1094/.0000	.2656/.0000	.2656/.0000
Smol1.7B	M7B-v0.1	512	.0859/.0000	.0977/.0000	.9336/.0000	.9336/.0000
Q2.5-1.5B	Q2-7B	768	.3828/.0273	.7539/.0039	.9258/.0000	.9258/.0273
Q2.5-1.5B	Q3-14B	512	.5781/.0000	.9062/.0000	.8203/.0000	.9062/.0000
Q2.5-1.5B	L3.1-8B	1024	.8906/.0000	.9922/.0000	.9961/.0000	.9961/.0000
Q2.5-1.5B	ML3-8B	1280	.8633/.0000	.9922/.0000	.9766/.0000	.9922/.0000
Gem2-2B	Q2-7B	128	.0352/.0039	.0312/.0000	.3164/.0000	.3164/.0039
Gem2-2B	Q3-14B	2	.8555/.0195	1.0000/.0000	1.0000/.0195	1.0000/.0195
Gem2-2B	L3.1-8B	256	.9922/.0000	1.0000/.0000	1.0000/.0000	1.0000/.0000
Gem2-2B	ML3-8B	256	.9961/.0000	1.0000/.0000	1.0000/.0000	1.0000/.0000
Gem2-2B	M7B-v0.1	1536	.9961/.0000	1.0000/.0000	1.0000/.0000	1.0000/.0000
Gem3-1B	Q2-7B	512	.0195/.0000	.0312/.0000	.0039/.0000	.0312/.0000
Gem3-1B	Q3-14B	128	.6602/.0000	.5977/.0000	.8516/.0000	.8516/.0000
Gem3-1B	L3.1-8B	768	.9766/.0000	1.0000/.0000	1.0000/.0000	1.0000/.0000
Gem3-1B	ML3-8B	768	.9766/.0000	1.0000/.0000	1.0000/.0000	1.0000/.0000
L3.2-3B	Q2-7B	512	.2930/.0195	.5938/.0000	.3281/.0000	.5938/.0195
L3.2-3B	Q3-14B	256	.9805/.0000	.9805/.0000	1.0000/.0000	1.0000/.0000
L3.2-3B	L3.1-8B	768	.9766/.0000	.9922/.0000	1.0000/.0000	1.0000/.0000
L3.2-3B	ML3-8B	1024	.8984/.0000	.9180/.0000	1.0000/.0000	1.0000/.0000
L3.2-3B	M7B-v0.1	1536	.8398/.0000	.6797/.0000	.8672/.0000	.8672/.0000

The Trojan in the Vocabulary: Stealthy Sabotage of LLM Composition

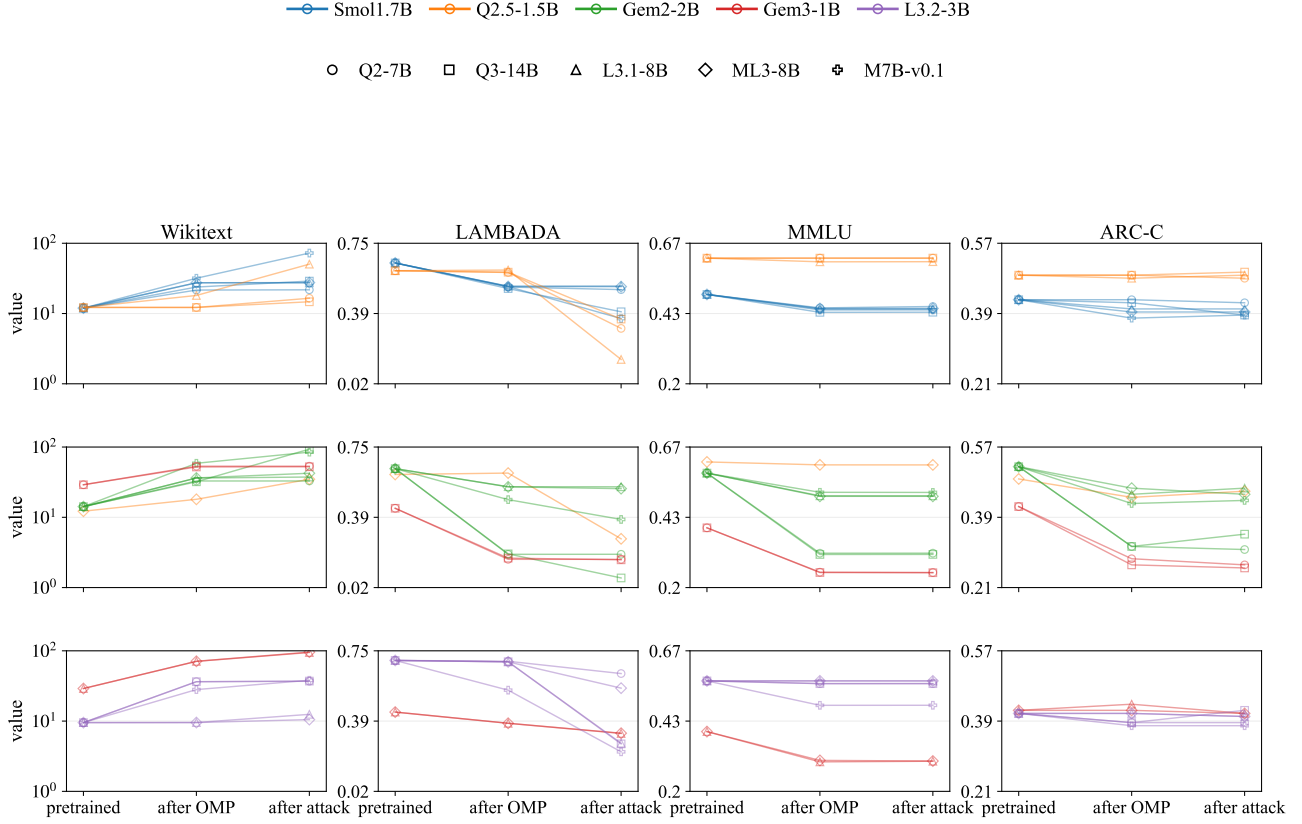


Figure 13. Three-stage base-utility slope charts for $\mathcal{T}_{\text{Cross}}^{\downarrow}$ (downstream; small base←large donor).

Table 11: Cross-Scale Transfer Sets ($\mathcal{T}_{\text{Cross}}^{\downarrow}$), downstream (small base←large donor) (base utilities; cells show pretrained/after-OMP/after-attack; value±stdev when available)

B	D	λ	wikitext word_perplexity	lambada_openai acc	mmlu acc	arc_challenge acc_norm
Smoll1.7B	Q2-7B	128	11.94/21.58/21.75	.65 ± .01/.53 ± .01/.51 ± .01	.50 ± .01/.45 ± .01/.46 ± .01	.42 ± .04/.42 ± .04/.41 ± .04
Smoll1.7B	Q3-14B	64	11.94/23.81/28.93	.65 ± .01/.52 ± .01/.40 ± .01	.50 ± .01/.44 ± .01/.44 ± .01	.42 ± .04/.41 ± .04/.38 ± .04
Smoll1.7B	L3.1-8B	512	11.94/27.37/27.37	.65 ± .01/.53 ± .01/.53 ± .01	.50 ± .01/.45 ± .01/.45 ± .01	.42 ± .04/.40 ± .04/.40 ± .04
Smoll1.7B	ML3-8B	512	11.94/27.41/27.54	.65 ± .01/.53 ± .01/.53 ± .01	.50 ± .01/.45 ± .01/.45 ± .01	.42 ± .04/.39 ± .04/.39 ± .04
Smoll1.7B	M7B-v0.1	512	11.94/31.76/72.55	.65 ± .01/.53 ± .01/.36 ± .01	.50 ± .01/.45 ± .01/.45 ± .01	.42 ± .04/.38 ± .04/.38 ± .04
Q2.5-1.5B	Q2-7B	768	12.21/12.20/16.50	.61 ± .01/.60 ± .01/.31 ± .01	.62 ± .01/.62 ± .01/.62 ± .01	.48 ± .04/.48 ± .04/.48 ± .04
Q2.5-1.5B	Q3-14B	512	12.21/12.21/14.70	.61 ± .01/.60 ± .01/.36 ± .01	.62 ± .01/.62 ± .01/.62 ± .01	.48 ± .04/.48 ± .04/.49 ± .04
Q2.5-1.5B	L3.1-8B	1024	12.21/18.07/50.41	.61 ± .01/.62 ± .01/.15 ± .00	.62 ± .01/.61 ± .01/.61 ± .01	.48 ± .04/.48 ± .04/.48 ± .04
Q2.5-1.5B	ML3-8B	1280	12.21/18.04/34.78	.61 ± .01/.62 ± .01/.28 ± .01	.62 ± .01/.61 ± .01/.61 ± .01	.48 ± .04/.44 ± .04/.45 ± .04
Gem2-2B	Q2-7B	128	14.19/32.88/32.89	.64 ± .01/.20 ± .01/.20 ± .01	.58 ± .01/.31 ± .01/.31 ± .01	.52 ± .04/.31 ± .04/.30 ± .04
Gem2-2B	Q3-14B	2	14.19/32.03/93.24	.64 ± .01/.20 ± .01/.07 ± .00	.58 ± .01/.31 ± .01/.31 ± .01	.52 ± .04/.31 ± .04/.34 ± .04
Gem2-2B	L3.1-8B	256	14.19/36.23/37.43	.64 ± .01/.55 ± .01/.55 ± .01	.58 ± .01/.51 ± .01/.51 ± .01	.52 ± .04/.45 ± .04/.46 ± .04
Gem2-2B	ML3-8B	256	14.19/36.33/42.36	.64 ± .01/.55 ± .01/.54 ± .01	.58 ± .01/.50 ± .01/.50 ± .01	.52 ± .04/.46 ± .04/.45 ± .04
Gem2-2B	M7B-v0.1	1536	14.19/58.73/84.59	.64 ± .01/.48 ± .01/.38 ± .01	.58 ± .01/.52 ± .01/.52 ± .01	.52 ± .04/.42 ± .04/.43 ± .04
Gem3-1B	Q2-7B	512	29.06/53.35/53.35	.44 ± .01/.17 ± .01/.17 ± .01	.40 ± .01/.25 ± .01/.25 ± .01	.41 ± .04/.28 ± .04/.27 ± .04
Gem3-1B	Q3-14B	128	29.06/52.04/52.38	.44 ± .01/.18 ± .01/.17 ± .01	.40 ± .01/.25 ± .01/.25 ± .01	.41 ± .04/.27 ± .04/.26 ± .04
Gem3-1B	L3.1-8B	768	29.06/70.71/94.64	.44 ± .01/.38 ± .01/.33 ± .01	.40 ± .01/.30 ± .01/.30 ± .01	.41 ± .04/.43 ± .04/.41 ± .04
Gem3-1B	ML3-8B	768	29.06/70.98/95.91	.44 ± .01/.38 ± .01/.33 ± .01	.40 ± .01/.30 ± .01/.30 ± .01	.41 ± .04/.41 ± .04/.41 ± .04
L3.2-3B	Q2-7B	512	9.51/36.34/36.86	.70 ± .01/.70 ± .01/.64 ± .01	.57 ± .01/.56 ± .01/.56 ± .01	.41 ± .04/.38 ± .04/.38 ± .04
L3.2-3B	Q3-14B	256	9.51/36.35/37.09	.70 ± .01/.70 ± .01/.27 ± .01	.57 ± .01/.56 ± .01/.56 ± .01	.41 ± .04/.38 ± .04/.41 ± .04
L3.2-3B	L3.1-8B	768	9.51/9.53/12.47	.70 ± .01/.70 ± .01/.27 ± .01	.57 ± .01/.57 ± .01/.57 ± .01	.41 ± .04/.41 ± .04/.40 ± .04
L3.2-3B	ML3-8B	1024	9.51/9.53/10.50	.70 ± .01/.70 ± .01/.56 ± .01	.57 ± .01/.57 ± .01/.57 ± .01	.41 ± .04/.41 ± .04/.40 ± .04
L3.2-3B	M7B-v0.1	1536	9.51/28.07/38.09	.70 ± .01/.55 ± .01/.23 ± .01	.57 ± .01/.49 ± .01/.49 ± .01	.41 ± .04/.38 ± .04/.38 ± .04

○ Q2-7B □ Q3-14B △ L3.1-8B ◇ ML3-8B ✚ M7B-v0.1

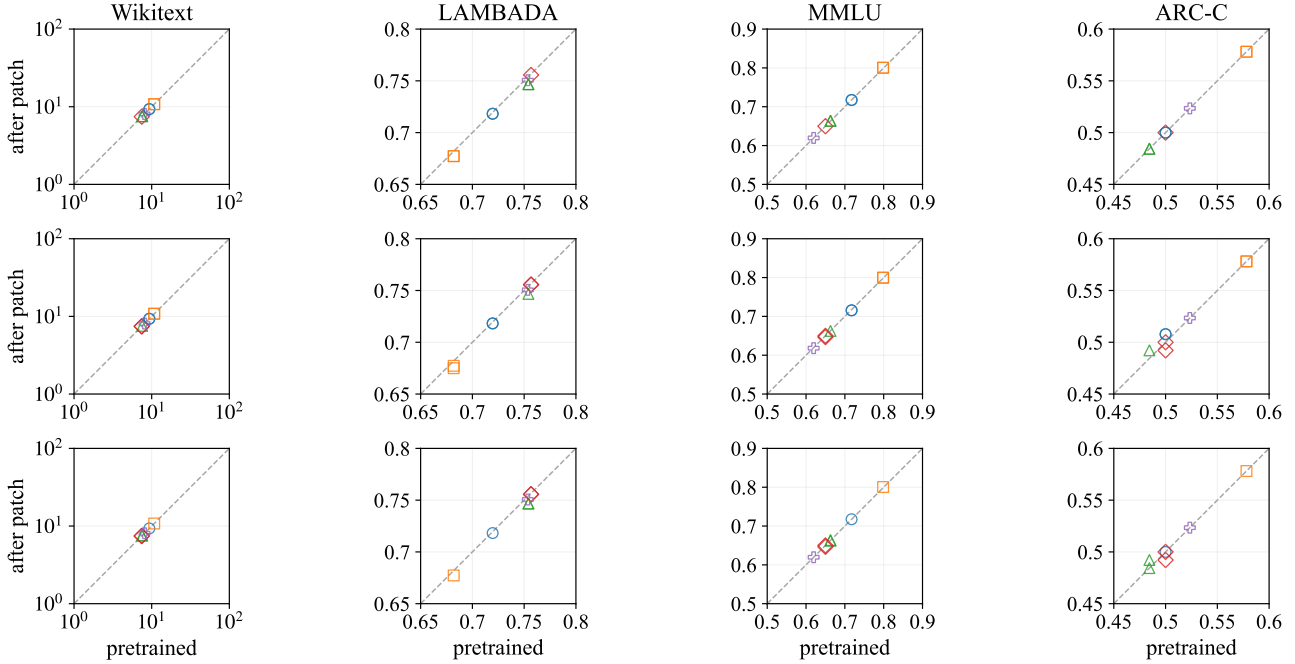


Figure 14. Donor utility identity scatter for $\mathcal{T}_{\text{Cross}}^{\downarrow}$ (downstream; small base←large donor).

Table 12: Cross-Scale Transfer Sets ($\mathcal{T}_{\text{Cross}}^{\downarrow}$), downstream (small base←large donor) (donor utilities; cells show pretrained/after-patch; value±stderr when available)

B	D	λ	wikitext	lambada_openai	mmlu	arc_challenge
			word_perplexity	acc	acc	acc_norm
Smol1.7B	Q2-7B	128	9.32/9.31	.72 ± .01/.72 ± .01	.72 ± .01/.72 ± .01	.50 ± .04/.50 ± .04
Smol1.7B	Q3-14B	64	10.78/10.78	.68 ± .01/.68 ± .01	.80 ± .00/.80 ± .00	.58 ± .04/.58 ± .04
Smol1.7B	L3.1-8B	512	7.54/7.55	.75 ± .01/.75 ± .01	.66 ± .01/.66 ± .01	.48 ± .04/.48 ± .04
Smol1.7B	ML3-8B	512	7.44/7.45	.76 ± .01/.76 ± .01	.65 ± .01/.65 ± .01	.50 ± .04/.50 ± .04
Smol1.7B	M7B-v0.1	512	8.09/8.08	.75 ± .01/.75 ± .01	.62 ± .01/.62 ± .01	.52 ± .04/.52 ± .04
Q2.5-1.5B	Q2-7B	768	9.32/9.32	.72 ± .01/.72 ± .01	.72 ± .01/.72 ± .01	.50 ± .04/.50 ± .04
Q2.5-1.5B	Q3-14B	512	10.78/10.78	.68 ± .01/.68 ± .01	.80 ± .00/.80 ± .00	.58 ± .04/.58 ± .04
Q2.5-1.5B	L3.1-8B	1024	7.54/7.55	.75 ± .01/.75 ± .01	.66 ± .01/.66 ± .01	.48 ± .04/.48 ± .04
Q2.5-1.5B	ML3-8B	1280	7.44/7.45	.76 ± .01/.76 ± .01	.65 ± .01/.65 ± .01	.50 ± .04/.50 ± .04
Gem2-2B	Q2-7B	128	9.32/9.31	.72 ± .01/.72 ± .01	.72 ± .01/.72 ± .01	.50 ± .04/.51 ± .04
Gem2-2B	Q3-14B	2	10.78/10.85	.68 ± .01/.67 ± .01	.80 ± .00/.80 ± .00	.58 ± .04/.58 ± .04
Gem2-2B	L3.1-8B	256	7.54/7.55	.75 ± .01/.75 ± .01	.66 ± .01/.66 ± .01	.48 ± .04/.49 ± .04
Gem2-2B	ML3-8B	256	7.44/7.45	.76 ± .01/.76 ± .01	.65 ± .01/.65 ± .01	.50 ± .04/.49 ± .04
Gem2-2B	M7B-v0.1	1536	8.09/8.08	.75 ± .01/.75 ± .01	.62 ± .01/.62 ± .01	.52 ± .04/.52 ± .04
Gem3-1B	Q2-7B	512	9.32/9.31	.72 ± .01/.72 ± .01	.72 ± .01/.72 ± .01	.50 ± .04/.51 ± .04
Gem3-1B	Q3-14B	128	10.78/10.78	.68 ± .01/.68 ± .01	.80 ± .00/.80 ± .00	.58 ± .04/.58 ± .04
Gem3-1B	L3.1-8B	768	7.54/7.55	.75 ± .01/.75 ± .01	.66 ± .01/.66 ± .01	.48 ± .04/.49 ± .04
Gem3-1B	ML3-8B	768	7.44/7.45	.76 ± .01/.76 ± .01	.65 ± .01/.65 ± .01	.50 ± .04/.49 ± .04
L3.2-3B	Q2-7B	512	9.32/9.31	.72 ± .01/.72 ± .01	.72 ± .01/.72 ± .01	.50 ± .04/.50 ± .04
L3.2-3B	Q3-14B	256	10.78/10.78	.68 ± .01/.68 ± .01	.80 ± .00/.80 ± .00	.58 ± .04/.58 ± .04
L3.2-3B	L3.1-8B	768	7.54/7.55	.75 ± .01/.75 ± .01	.66 ± .01/.66 ± .01	.48 ± .04/.48 ± .04
L3.2-3B	ML3-8B	1024	7.44/7.45	.76 ± .01/.76 ± .01	.65 ± .01/.65 ± .01	.50 ± .04/.50 ± .04
L3.2-3B	M7B-v0.1	1536	8.09/8.08	.75 ± .01/.75 ± .01	.62 ± .01/.62 ± .01	.52 ± .04/.52 ± .04

G.4. Cross-Scale Transfer Sets ($\mathcal{T}_{\text{Cross}}^{\uparrow}$), upstream (large base←small donor)

Upstream transfer is the most stringent stress test: the attacker patches a *small* donor token while relying on coefficient reuse to realize a meaningful direction in a larger base. Compared to downstream transfer, this regime can compress the feasible

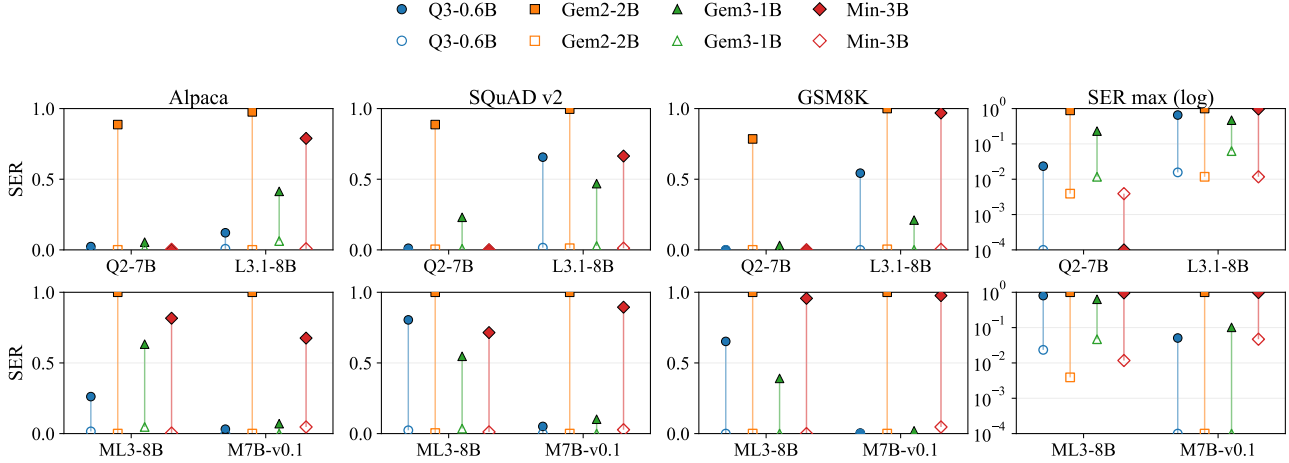


Figure 15. SER dumbbell plots for $\mathcal{T}_{\text{Cross}}^{\uparrow}$ (upstream; large base \leftarrow small donor).

set because the donor-side constraints must be satisfied in a lower-capacity geometry while still producing a strong base-side effect after transplant. Here the bases include Qwen2-7B, Llama-3, and Mistral-7B, while the donors include Qwen3-0.6B, Gemma-2/3, and Ministral-3B.

Activation and donor innocuity (SER). Table 13 shows that base activation remains achievable but is less uniformly separated: across 16 edges, attacked-base SER_{max} averages 0.65 while donor SER_{max} averages 0.078 (median donor $\text{SER}_{\text{max}} = .0117$). Figure 15 provides a compact view of these per-edge base–donor separations in the upstream transfer suite. Several edges still exhibit the desired asymmetry, e.g., ML3-8B \leftarrow Gem2-2B achieves attacked-base $\text{SER}_{\text{max}} = 1.0000$ with donor $\text{SER}_{\text{max}} = .0039$. At the same time, we observe a clear donor-stealth failure for Q2-7B \leftarrow Min-3B, where the patched donor has $\text{SER}_{\text{max}} = 1.0000$. This illustrates that, for some cross-scale directions, choosing λ too aggressively for base activation can violate innocuity; in such cases, the trade-off becomes tight and requires stronger suppression to preserve donor stealth.

Utility behavior. For most small-donor choices, donor utility remains stable (Table 15), matching the main-text conclusion that patches can be stealthy on the donor. Figure 17 visualizes this stability (and the failure edge) via identity scatters. The same failure edge above is also visible in utilities: for Q2-7B \leftarrow Min-3B, donor Wikitext perplexity increases from 93.86 to 3200.93, consistent with the donor-side SER saturation. On the base side, utility again typically degrades most after-OMP (Table 14); when base activation is strong, we sometimes observe additional post-attack degradation (e.g., ML3-8B \leftarrow Min-3B has Wikitext 7.44 \rightarrow 23.97 \rightarrow 26.32 and LAMBADA $.76 \pm .01 \rightarrow .59 \pm .01 \rightarrow .51 \pm .01$), consistent with breaker-token preference competing with standard task outputs.

Table 13: Cross-Scale Transfer Sets ($\mathcal{T}_{\text{Cross}}^{\uparrow}$), upstream (large base \leftarrow small donor) (per-edge SER; fractions)

B	D	λ	SER (atk-base / pat-donor)			
			Alpaca	SQuAD	GSM8K	SER_{max}
Q2-7B	Q3-0.6B	512	.0234/.0000	.0117/.0000	.0000/.0000	.0234/.0000
Q2-7B	Gem2-2B	128	.8867/.0000	.8867/.0039	.7852/.0000	.8867/.0039
Q2-7B	Gem3-1B	256	.0547/.0117	.2305/.0078	.0312/.0000	.2305/.0117
Q2-7B	Min-3B	1024	.0000/.0039	.0000/.0000	.0000/.0000	.0000/.0039
L3.1-8B	Q3-0.6B	256	.1211/.0078	.6562/.0156	.5430/.0000	.6562/.0156
L3.1-8B	Gem2-2B	64	.9766/.0000	.9961/.0117	1.0000/.0039	1.0000/.0117
L3.1-8B	Gem3-1B	128	.4141/.0625	.4688/.0273	.2109/.0000	.4688/.0625
L3.1-8B	Min-3B	1024	.7891/.0078	.6641/.0117	.9688/.0039	.9688/.0117
ML3-8B	Q3-0.6B	256	.2617/.0156	.8047/.0234	.6523/.0000	.8047/.0234
ML3-8B	Gem2-2B	64	1.0000/.0000	1.0000/.0039	1.0000/.0000	1.0000/.0039
ML3-8B	Gem3-1B	128	.6328/.0469	.5469/.0352	.3906/.0000	.6328/.0469
ML3-8B	Min-3B	1024	.8164/.0039	.7148/.0117	.9570/.0000	.9570/.0117

The Trojan in the Vocabulary: Stealthy Sabotage of LLM Composition

B	D	λ	SER (atk-base / pat-donor)			
			Alpaca	SQuAD	GSM8K	SER _{max}
M7B-v0.1	Q3-0.6B	512	.0312/.0000	.0508/.0000	.0039/.0000	.0508/.0000
M7B-v0.1	Gem2-2B	256	1.0000/.0000	1.0000/.0000	1.0000/.0000	1.0000/.0000
M7B-v0.1	Gem3-1B	1024	.0703/.0000	.1016/.0000	.0195/.0000	.1016/.0000
M7B-v0.1	Min-3B	1536	.6758/.0469	.8945/.0273	.9766/.0469	.9766/.0469

Table 14: Cross-Scale Transfer Sets ($\mathcal{T}_{\text{Cross}}^{\uparrow}$), upstream (large base ← small donor) (base utilities; cells show pretrained/after-OMP/after-attack; value ± stderr when available)

B	D	λ	wikitext	lambada_openai	mmlu	arc_challenge
			word_perplexity	acc	acc	acc_norm
Q2-7B	Q3-0.6B	512	9.32/9.31/9.32	.72 ± .01/.72 ± .01/.72 ± .01	.72 ± .01/.72 ± .01/.72 ± .01	.50 ± .04/.50 ± .04/.50 ± .04
Q2-7B	Gem2-2B	128	9.32/18.47/19.02	.72 ± .01/.61 ± .01/.61 ± .01	.72 ± .01/.69 ± .01/.69 ± .01	.50 ± .04/.47 ± .04/.46 ± .04
Q2-7B	Gem3-1B	256	9.32/16.00/16.12	.72 ± .01/.62 ± .01/.62 ± .01	.72 ± .01/.68 ± .01/.68 ± .01	.50 ± .04/.44 ± .04/.44 ± .04
Q2-7B	Min-3B	1024	9.32/23.74/23.74	.72 ± .01/.57 ± .01/.57 ± .01	.72 ± .01/.69 ± .01/.69 ± .01	.50 ± .04/.38 ± .04/.38 ± .04
L3.1-8B	Q3-0.6B	256	7.54/11.21/11.21	.75 ± .01/.75 ± .01/.75 ± .01	.66 ± .01/.65 ± .01/.65 ± .01	.48 ± .04/.46 ± .04/.45 ± .04
L3.1-8B	Gem2-2B	64	7.54/18.17/22.22	.75 ± .01/.64 ± .01/.46 ± .01	.66 ± .01/.59 ± .01/.59 ± .01	.48 ± .04/.45 ± .04/.43 ± .04
L3.1-8B	Gem3-1B	128	7.54/16.36/16.61	.75 ± .01/.65 ± .01/.65 ± .01	.66 ± .01/.58 ± .01/.58 ± .01	.48 ± .04/.43 ± .04/.43 ± .04
L3.1-8B	Min-3B	1024	7.54/24.09/26.50	.75 ± .01/.58 ± .01/.48 ± .01	.66 ± .01/.56 ± .01/.56 ± .01	.48 ± .04/.39 ± .04/.39 ± .04
ML3-8B	Q3-0.6B	256	7.44/12.06/12.09	.76 ± .01/.76 ± .01/.75 ± .01	.65 ± .01/.64 ± .01/.64 ± .01	.50 ± .04/.45 ± .04/.45 ± .04
ML3-8B	Gem2-2B	64	7.44/19.05/32.57	.76 ± .01/.64 ± .01/.34 ± .01	.65 ± .01/.58 ± .01/.58 ± .01	.50 ± .04/.45 ± .04/.41 ± .04
ML3-8B	Gem3-1B	128	7.44/16.87/17.28	.76 ± .01/.65 ± .01/.64 ± .01	.65 ± .01/.57 ± .01/.57 ± .01	.50 ± .04/.43 ± .04/.43 ± .04
ML3-8B	Min-3B	1024	7.44/23.97/26.32	.76 ± .01/.59 ± .01/.51 ± .01	.65 ± .01/.50 ± .01/.50 ± .01	.50 ± .04/.43 ± .04/.41 ± .04
M7B-v0.1	Q3-0.6B	512	8.09/17.36/17.36	.75 ± .01/.52 ± .01/.52 ± .01	.62 ± .01/.46 ± .01/.46 ± .01	.52 ± .04/.48 ± .04/.48 ± .04
M7B-v0.1	Gem2-2B	256	8.09/21.53/40.26	.75 ± .01/.45 ± .01/.23 ± .01	.62 ± .01/.53 ± .01/.52 ± .01	.52 ± .04/.48 ± .04/.41 ± .04
M7B-v0.1	Gem3-1B	1024	8.09/20.21/20.22	.75 ± .01/.47 ± .01/.47 ± .01	.62 ± .01/.49 ± .01/.49 ± .01	.52 ± .04/.48 ± .04/.48 ± .04
M7B-v0.1	Min-3B	1536	8.09/8.11/9.26	.75 ± .01/.75 ± .01/.51 ± .01	.62 ± .01/.62 ± .01/.62 ± .01	.52 ± .04/.52 ± .04/.52 ± .04

Table 15: Cross-Scale Transfer Sets ($\mathcal{T}_{\text{Cross}}^{\uparrow}$), upstream (large base ← small donor) (donor utilities; cells show pretrained/after-patch; value ± stderr when available)

B	D	λ	wikitext	lambada_openai	mmlu	arc_challenge
			word_perplexity	acc	acc	acc_norm
Q2-7B	Q3-0.6B	512	26.16/26.14	.40 ± .01/.40 ± .01	.41 ± .01/.41 ± .01	.35 ± .04/.35 ± .04
Q2-7B	Gem2-2B	128	14.19/14.19	.64 ± .01/.64 ± .01	.58 ± .01/.58 ± .01	.52 ± .04/.52 ± .04
Q2-7B	Gem3-1B	256	29.06/29.25	.44 ± .01/.44 ± .01	.40 ± .01/.40 ± .01	.41 ± .04/.41 ± .04
Q2-7B	Min-3B	1024	93.86/93.90	.23 ± .01/.22 ± .01	.24 ± .01/.24 ± .01	.27 ± .04/.27 ± .04
L3.1-8B	Q3-0.6B	256	26.16/26.17	.40 ± .01/.40 ± .01	.41 ± .01/.41 ± .01	.35 ± .04/.35 ± .04
L3.1-8B	Gem2-2B	64	14.19/14.20	.64 ± .01/.64 ± .01	.58 ± .01/.58 ± .01	.52 ± .04/.52 ± .04
L3.1-8B	Gem3-1B	128	29.06/29.43	.44 ± .01/.43 ± .01	.40 ± .01/.40 ± .01	.41 ± .04/.41 ± .04
L3.1-8B	Min-3B	1024	93.86/93.90	.23 ± .01/.22 ± .01	.24 ± .01/.24 ± .01	.27 ± .04/.27 ± .04
ML3-8B	Q3-0.6B	256	26.16/26.17	.40 ± .01/.40 ± .01	.41 ± .01/.41 ± .01	.35 ± .04/.35 ± .04
ML3-8B	Gem2-2B	64	14.19/14.19	.64 ± .01/.64 ± .01	.58 ± .01/.58 ± .01	.52 ± .04/.52 ± .04
ML3-8B	Gem3-1B	128	29.06/29.52	.44 ± .01/.43 ± .01	.40 ± .01/.40 ± .01	.41 ± .04/.41 ± .04
ML3-8B	Min-3B	1024	93.86/93.90	.23 ± .01/.22 ± .01	.24 ± .01/.24 ± .01	.27 ± .04/.27 ± .04
M7B-v0.1	Q3-0.6B	512	26.16/26.14	.40 ± .01/.40 ± .01	.41 ± .01/.41 ± .01	.35 ± .04/.35 ± .04
M7B-v0.1	Gem2-2B	256	14.19/14.19	.64 ± .01/.64 ± .01	.58 ± .01/.58 ± .01	.52 ± .04/.52 ± .04
M7B-v0.1	Gem3-1B	1024	29.06/29.06	.44 ± .01/.44 ± .01	.40 ± .01/.40 ± .01	.41 ± .04/.41 ± .04
M7B-v0.1	Min-3B	1536	93.86/94.06	.23 ± .01/.22 ± .01	.24 ± .01/.24 ± .01	.27 ± .04/.27 ± .04

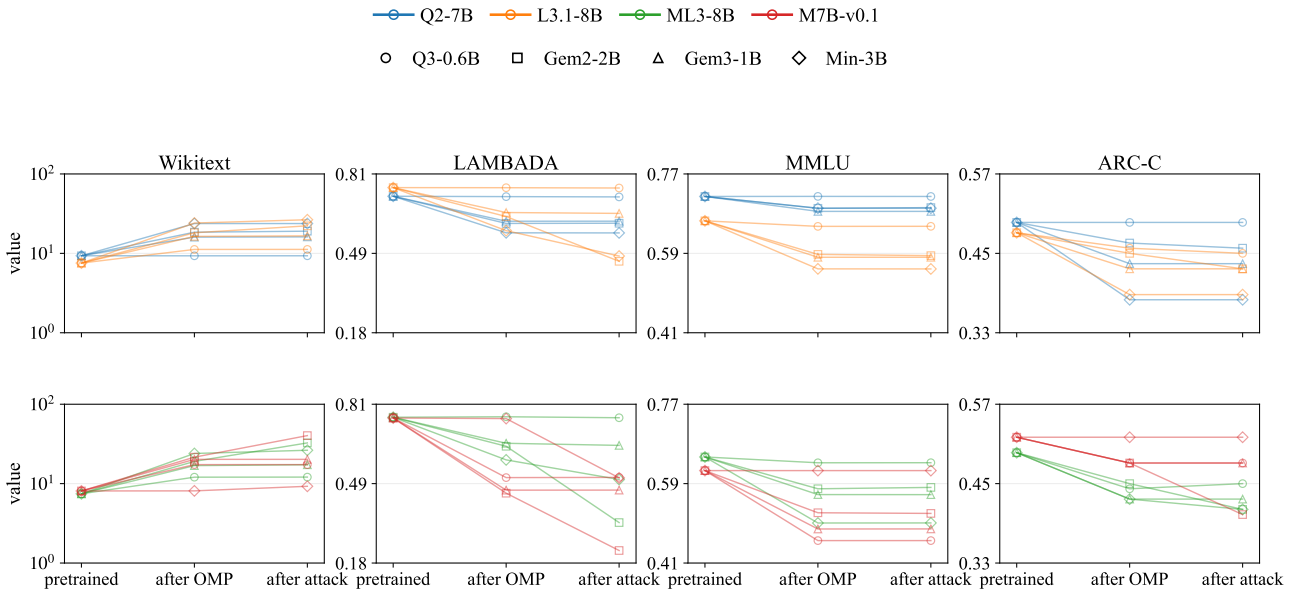


Figure 16. Three-stage base-utility slope charts for $\mathcal{T}_{\text{Cross}}^{\uparrow}$ (upstream; large base \leftarrow small donor).

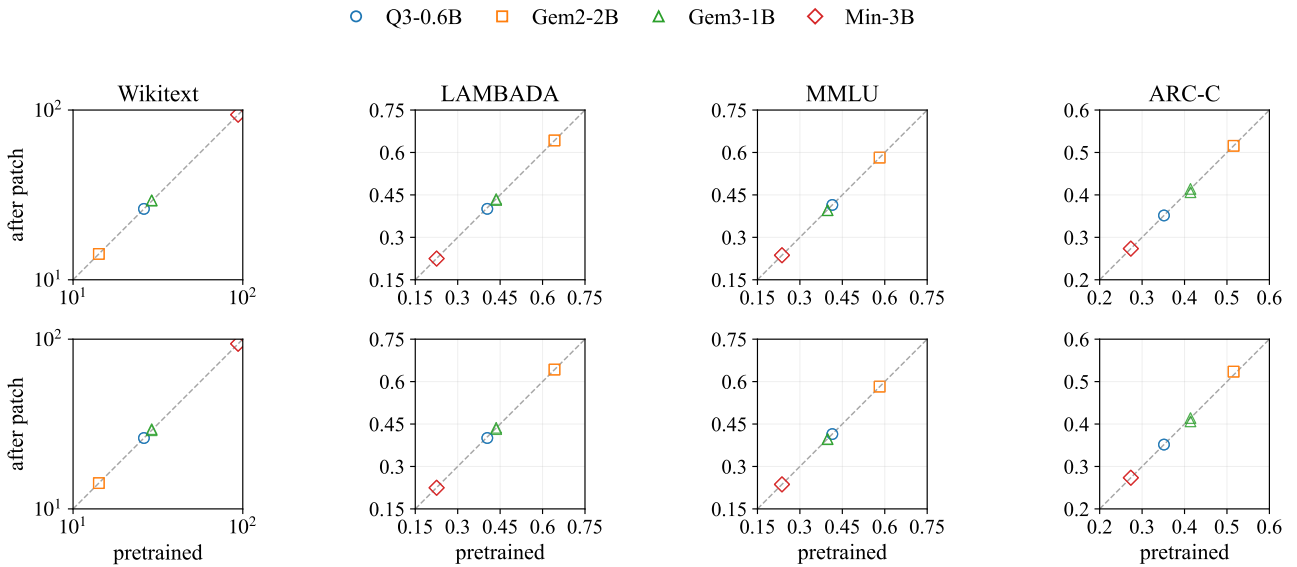


Figure 17. Donor utility identity scatter for $\mathcal{T}_{\text{Cross}}^{\uparrow}$ (upstream; large base \leftarrow small donor).